Optimization and Application of Synthetic High-Density Lipoprotein (sHDL) System in Atherosclerosis and Glioma Therapy.

by

Dan Li

A dissertation submitted in partial fulfillment
of the requirements for the degree of
Doctor of Philosophy
(Pharmaceutical Sciences)
in the University of Michigan
2018

Doctoral Committee:

Assistant Professor Anna Schwendeman, Chair
Professor Maria G. Castro
Assistant Professor Yang Chen
Professor David Smith
Professor Duxin Sun

Dan Li

dansmile@umich.edu

ORCID iD: 0000-0001-5512-8712

Dedication

To my family with all my love and gratitude

Acknowledgements

First, I would like to thank my research advisor Dr. Anna Schwendeman for her guidance and support. She has encouraged me to pursue my research interest, cope with challenges, and has given me plenty of invaluable suggestions on both my research and life. Under her guidance, I gradually become an independent scientist. She also offered me opportunities to collaborate with outstanding scientists both inside and outside her lab and gave me chances to present my research outcomes. The skills and confidence obtained through presentation and communication practice will help me through the rest of my career. I will always be grateful for her support on all my decisions and plans for career development. To me, she is not only an advisor but also a close friend who is always optimistic and proactive. I am also very thankful to Dr. David Smith for all his guidance and advice on my research. It was my pleasure to be his GSI and do rotation in his lab. I learned a lot from him both in and out of his classes. I would also like to thank Dr. Duxin Sun for his patience and helpful insights on my research. As my temporary advisor in my first year, he helped me get used to the study at Umich, which I am very grateful. I am glad to have Dr. Maria Castro on my committee who is very knowledgeable and helped me a lot on our collaborative project. I also want to thank Dr. Steven P. Schwendeman, Dr. Y. Eugene Chen, Dr. Yang Chen, for their time and comments on my research.

Working in this great lab with so many excellent lab members, past and present, has really made my time in graduate school enjoyable. I would like to specifically thank Karl Olsen for his help with all my animal studies, Rose Ackermann for her technical help and expertise, and Dr. Jie Tang, Dr. Wenmin Yuan, Dr. Rui Kuai and Dr. Yayuan Liu for their help with my projects. I would also like to thank Padma in Dr. Maria Castro's lab Dr. Yanhong Guo from Dr. Y. Eugene Chen's group for their efforts put in our collaborative projects. My fellow graduate students in the Schwendeman group always made the lab a lovely place and they have helped me tremendously: Emily E. Morin, Sang Y. Kim, Jukyung Kang, Maria V. Fawaz, Minzhi Yu, Lindsay Scheetz, Alexander Benet, Brittany Bailey, J. Maxwell Mazzara, Karthik Pisupati, Rae Sung Chang, Amy

Doty, Kari Nieto, Morgan Giles, Jia Zhou, Jennifer Walker, Jason Albert, Justin Hong. Thank you all for creating a wonderful work environment that I will miss very much.

Second. I cannot thank my family enough for their constant encouragement, including my parents, my parents in law, my husband and my dear little daughter. It is their love that gives me strength to overcome obstacles and pursue my career goals. Whenever it is and wherever I am, they are always by my side. They are the most important and meaningful part of my life. I'm grateful for my parents for raising me up, providing me the best education and giving all their love to me. It is them that make me who I am today. In addition, I would like to express my appreciation for my parents in law for their support and help to balance my study and life. There is one person of great importance who accompanied me to get through all hard time and share all happy moments, my husband Yilin Zheng. Thank you for trusting me without any doubts and giving me the courage to become the best of myself. I feel fortune to have my daughter, Eleanor, during my graduate study. Although she is very young, her smile is always the best rewards for my work and effort. I hope we can grow up together and I could set a good example for her to become an independent person with her own thoughts and career.

Finally, I do not know how it would be possible to go through graduate school without the amazing friends I have been lucky enough to make in Michigan. There are too many to name individually, but I would like to especially thank Yuchen Fan, Kai Wang, Emily E. Morin, Zhilin Chen, Alex Yu, Sang Y. Kim, Dr. Jie Tang, Dr. Wenmin Yuan and Shuai Hu. Thank you all for making this experience so enjoyable and memorable. I am blessed to have met you all and looking forward to staying connected with you as we progress in our careers. It is both a short and long journey to pursue a PhD degree. I feel very lucky to see all the sceneries during the journey, bitter and sweet, all of which are very precious to me and will become the most memorable experience in my whole life.

GO BLUE!

Table of Contents

List of Tables

List of Figures

Abstract

Overwhelming evidence indicates that higher levels of high-density lipoprotein cholesterol (HDL-C) correlate with reduced risk of coronary heart disease (CHD). HDL can efflux excess cholesterol by reverse cholesterol transport (RCT). Hence, reducing acute plaque accumulation by direct infusion of cholesterol-free synthetic HDL (sHDL) has generated considerable interest. sHDL consists of a phospholipid bilayer held together by apolipoprotein A-I (ApoA-I). Due to the high manufacturing cost of recombinant ApoA-I, ApoA-I mimetic peptides complexed with a variety of lipids have been studied as treatments for various pathologies. However, the best methods of administration and formulation remain controversial. For sHDL products consisting of ApoA-I mimetic peptides like ETC-642, rapid elimination can limit their clinical application and subsequent development. Thus, prolonging the circulation time of sHDL can potentially improve its anti-atherosclerosis effect. In addition, designing novel nanoparticles mimicking sHDL can eliminate the need for the ApoA-I protein/peptide component in sHDL while preserving the core pharmacological activity of sHDL.

We first studied the influence of administration route and lipidation of ApoA-I mimetic peptide 22A on plasma peptide levels, cholesterol mobilization, and lipoprotein remodeling *in vivo*. The mean circulation half-life for 22A-sHDL ($T_{1/2}$ = 6.27 h) was longer than for free 22A ($T_{1/2}$ = 3.81 h). The amount of 22A absorbed by the vascular compartment after intraperitoneal (IP) dosing was ~50% for both 22A and 22A-sHDL. The strongest pharmacologic response was observed after intravenous (IV) injection of 22A-sHDL compared to IP injection and administration of free peptide. Both the route of administration and the formulation of 22A significantly affected the peptide's pharmacokinetic and pharmacodynamic properties. Following this study, sHDL surface modification with polyethylene glycol (PEG) was investigated for its potential to extend sHDL circulation *in vivo*. The circulation half-life of sHDL was extended both by adding more PEG or using PEG of longer chain lengths. Addition of PEG also increased the AUC for the phospholipid component of sHDL, leading to higher mobilization of free cholesterol in plasma due to prolonged circulation and increased stability.

To extend this research into biomimetic nanomaterial development, we formulated nanomicelles (NanoMCLs), structural nano-mimetics of sHDL with small particle size (12-14 nm) and a hydrophobic core and hydrophilic exterior. NanoMCLs were shown to be functionally similar to sHDL and exhibited up to 14-fold more efficient inhibition of inflammatory cytokine release *in vitro* compared to sHDL. When administered as a 6-week treatment to $ApoE^{-/-}$ mice fed a high-fat diet, sHDL and NanoMCL reduced atheroma by 21% and 40%, respectively. In addition, NanoMCL treatment significantly depleted atheroma macrophages.

Lastly, the application of sHDL as an anti-cancer drug delivery system was explored for treatment of glioma. Chemotherapeutic agent docetaxel (DTX) and immune-stimulatory toll-like receptor-9 (TLR-9) agonist cholesterol-CpG1826 (cholCpG) were co-incorporated in sHDL nanoparticles. The sHDL composition was optimized to maximize DTX retention in plasma. In a murine glioma model, intracranial injection of DTX-sHDL-cholCpG system exhibited significant anti-tumor efficacy with 20% of animals surviving past 90 days.

In summary, this thesis systemically studied the effect of sHDL lipid composition on cholesterol mobilization and established sHDL-PEG and NanoMCL systems to improve the anti-atherosclerosis effect of sHDL. In addition, DTX-sHDL-CpG nanoparticles were developed and applied in glioma therapy. We have shown that sHDL is a versatile nanoparticle with utility in atherosclerosis treatment and drug delivery.

.

Chapter 1 : Introduction

1.1 High density lipoprotein (HDL)

1.1.1 HDL structure and metabolism

High-density lipoproteins (HDL) are small, natural nanoparticles circulating throughout the body, and are best known for their anti-atherosclerosis function and anti-inflammatory effect by facilitating reversal cholesterol transport (RCT) from vascular cell macrophages. Their size ranges from 7 to 13 nm in diameter.[1] Plasma levels of HDL cholesterol are negatively correlated with the risk of developing atherosclerosis, and, because of this, HDL is known as "good cholesterol".[2] HDL consists of a phospholipid- bilayer held together by the amphipathic, alpha-helical protein, apolipoprotein A-I (ApoA-I). Human ApoA-I is a 243 amino acid protein with an average molecular weight of 28.1 kDa.[3-4] It is the main protein associated with HDL and constitutes about 70% of the protein content in HDLs.[5] Other apolipoproteins associated with HDLs include apoA-II, apoE and others.[6]

The lipid species present in HDL are important, not only because they provide the overall structure to HDL, but also because they act as substrates for a variety of receptors and enzymes associated with HDL and its metabolic properties. There are more than 200 different identified lipid species contained in HDLs, notably phospholipids, unesterified (free) sterols, cholesteryl esters, and triglycerides. Phospholipids together with sphingomyelin (SM) make up 40-60 wt% of total HDL lipids and they constitute the surface lipid monolayer of HDL.[7] Among all the phospholipids, phosphatidylcholines (PC) are by far the largest population of HDL lipids, making up 33-45 wt% of total HDL lipids. Other phospholipids present in HDL include lysophosphatidylcholines (lyso PC), phosphatidylethanolamines (PE), phosphatidylinositols (PI), phosphatidylserines (PS), phosphatidylglycerols (PG), plasmologens, cardiolipin, and phosphatidic acids. In addition to PCs, sphingolipids including sphingomyelin (SM), ceramides, sphingosylphosphorylcholine, and sphingosine-1-phosphate make up roughly 5-10 wt% of total HDL lipids. [7] SM accounts for 5-10 wt% of total lipids in HDL and is essential for determining the surface pressure in lipid membranes. Lecithin cholesterol acyltransferase (LCAT) is a

glycoprotein that has both a phospholipase A2 and an acyltransferase action. It is essential for the normal maturation, interconversion and rearrangements of all lipoprotein classes and is involved in reverse cholesterol transport process of HDL. SM has been found to inhibit the LCAT reaction in discoidal HDL.[8] The low abundance of SM and free cholesterol in small, dense HDL may elevate the fluidity of surface lipids.[9] These lipids vary in structure, molecular weight, and transition temperature as a result of their different physical and biological properties. The lipidome of HDL can be altered under pathophysiological conditions, such as low HDL-cholesterol hypertriglyceridemic states, acute phase, and Niemann-Pick disease type B.[10]

HDLs can be classified into different subclasses by density, size, shape, composition and surface charge. Based on particle shape and gel electrophoresis, HDLs are subdivided into discoidal pre-β HDL with β-mobility on electrophoresis and the α subfraction of HDL with α-mobility on electrophoresis, which can be further classified into four categories from α-1 (large, spherical) to α-4 (small, discoidal) HDL.[6] Based on density, HDLs are divided into large, lipid-rich HDL2 and smaller HDL3, which can be further divided into five subpopulations with decreasing size: HDL2b, HDL2a, HDL3a, HDL3b, and HDL3c.[5]

HDL is able to carry cholesterol from peripheral cells to the liver though reverse cholesterol transport (RCT) process. The intravascular metabolism of HDL is shown in Fig. 1.1.[11] Briefly, lipid-free ApoA-I, the major structural protein of HDL is synthesized in the liver and small intestine in humans. ApoA-I associates with cholesterol and phospholipids after its secretion in the blood to form discoidal nascent pre-β HDL. Unesterified cholesterol and phospholipids from peripheral cells, as well as from liver and intestine, are effluxed by ATP-binding cassette subfamily A member 1 (ABCA1) transporter. Pre-β HDL is lipidated by the cholesterol and lipids to form discoidal α-4 HDL. The cholesterol in HDL is then esterified by lecithin-cholesterol acyl transferase (LCAT). The movement of more hydrophobic cholesterol ester (CE) to the core of the HDL particle converts the α-4 HDL into larger, spherical HDL3. This process is known as maturation of HDL. The spherical HDL3 can further pick up cholesterol from peripheral tissues by ATP-binding cassette transporter G1 (ABCG1) and Scavenger receptor class B type 1 (SR-BI) and convert it to the cholesterol ester with the help of LCAT to form HDL2. Both HDL2 and HDL3 can also exchange their cholesterol ester for triglycerides (TG) from TG-rich lipoproteins, such as LDL and VLDL. This process is mediated by cholesterol ester transfer protein (CETP), resulting in the formation of HDL with a hydrophobic core composed of cholesterol ester and

triglycerides. Some of this HDL will directly return back to the liver and deliver the HDL cargoe to hepatocytes for metabolism through HDL receptors. Other HDL will be hydrolyzed by plasma enzymes, such as hepatic lipase (HL), endothelial lipase (EL), and secretory phospholipase A2, which results in the removal and recycling of phospholipids and ApoA-I protein contained in HDL and reversely transforms the spherical HDL to discoidal HDL. The liver then takes up CE released from these HDLs through a SR-BI-mediated process. The whole process is also accompanied by the catabolism of free ApoA-I and pre-β HDL by the kidney which are excreted in the urine.

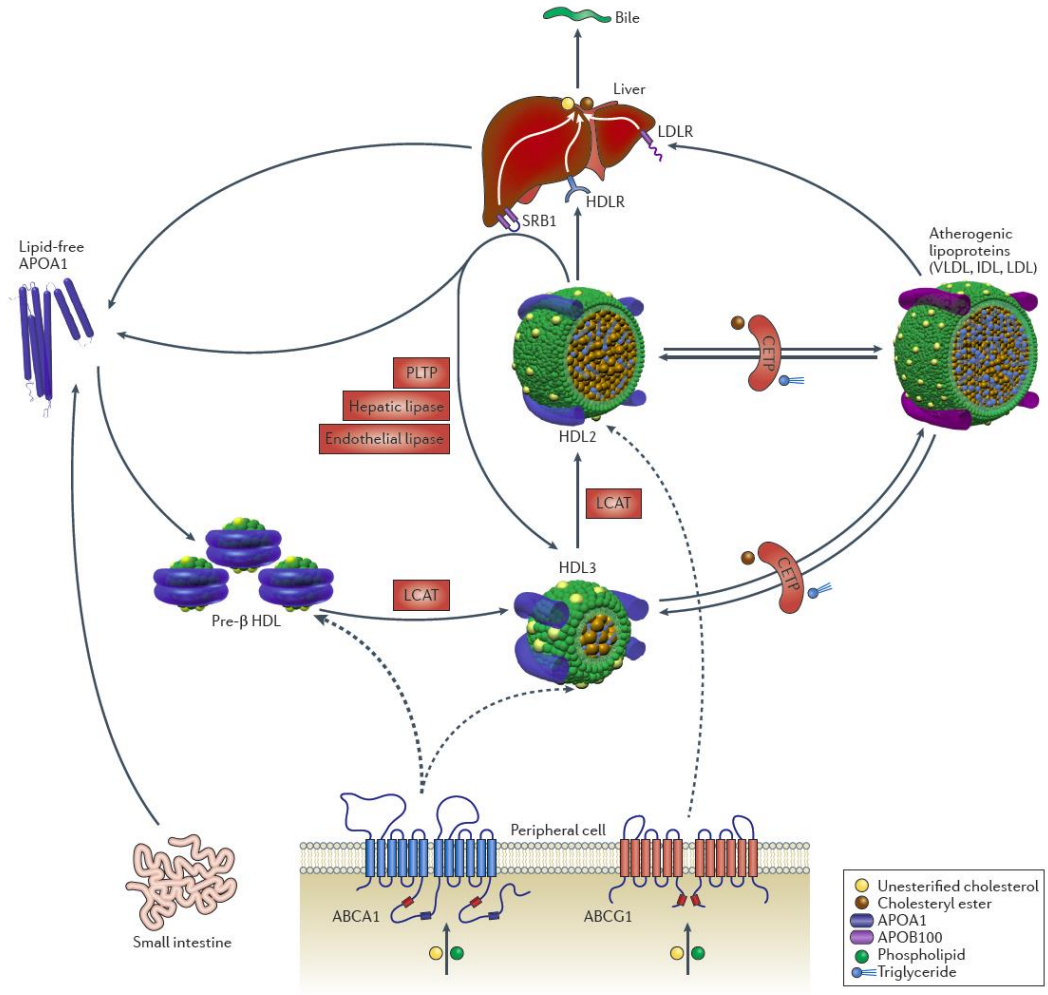

Figure 1.1: Metabolism of HDL in vivo.[11]

1.1.2 HDL function

HDLs are reported to play multiple roles in various diseases due to their unique interactions with different target sites. The most well-known function of HDL is its effect on atherosclerosis and cardiovascular diseases by facilitating reverse cholesterol transport (RCT), which is a multi-

step process resulting in the net movement of cholesterol from peripheral tissues back to the liver via the plasma compartment as described in section 1.1.1. [12] In addition, HDLs also achieve anti-atherosclerosis effects through other cardio-protective mechanisms. For instance, HDLs can reduce inflammation at the site of atherosclerotic lesions. [13] Due to the intrinsic targeting capability for the atherosclerotic plaques, HDL can facilitate targeted delivery of anti-inflammatory therapeutics to plaques. [14-15] Also, HDLs can be used to deliver certain imaging reagents to plaques for early diagnosis. Moreover, HDLs possess antioxidant and antithrombotic effects, which can help with endothelial integrity and repair. [13, 16] HDLs inhibit the accumulation of peroxidation products on the surface of LDLs which reduce oxidative stress, a risk factor associated with cardiovascular disease. The antithrombotic activity of HDL is achieved by activating endothelial-derived nitric oxide (NO) synthesis, which plays an important role in vasodilation and vascular endothelial integrity. [17]

1.2 Current development of synthetic HDL

A number of reconstituted HDL products have advanced to different stages of clinical trials.[18] These reconstituted HDL products (rHDL) are intended for administration following an initial cardiovascular event in patients with acute coronary syndrome (ACS) to remove excess cholesterol from arterial plaques and reduce the chance of a secondary event. Since rHDL is amied to remove cholesterol from peripheral tissues or macrophages, in clinical trials, one of the biomarker for successful cholesterol efflux or mobilization is the transient increase of plasma cholesterol levels including total cholesterol (TC) or free cholesterol (FC). But along with the further elimination of HDL-cholesterol, the TC and FC level return back to baseline normally. [19-20] The summary of clinical trials examining the doses, routes of administration, molecular composition, pharmacokinetic parameters, and safety profiles of HDL products is provided in **Table 1.1**. At least seven different HDL products have been evaluated in clinical trials, including (a) HDL based on ApoA-I purified from human plasma, such as SRC-rHDL, CSL-111 and CSL-112; (b) HDL based on recombinant ApoA-I and its variants, such as proApoA-I-liposomes, ETC-216, and CER-001; and (c) rHDL based on synthetic ApoA-I mimetic peptides, such as ETC-642. The maximum tolerated doses of HDL in human patients vary depending on the composition of each product and their respective impurities. In general, the HDL products have been reported to be safe when administered once per week by prolonged intravenous infusion at up to 80 mg/kg for SRC-rHDL (~ 6.5 g of ApoA-I/dose or 33 g of total HDL/dose), 135 mg/kg for CSL-112 (~ 10 g

of ApoA-I/dose or 35 g of total HDL/dose), 45 mg/kg for CER-001 (~ 4 g of ApoA-I/dose or 15 g of total HDL/dose), and 30 mg/kg for ETC-642 (~ 3 g of ApoA-I peptide/dose or 9 g total HDL/dose). Potential safety concerns associated with HDL products include transient elevation of liver transaminases (ALT and AST) along with other minor liver toxicities. These concerns arise as a result of the hyper-pharmacology of HDL products, as a significant amount of cholesterol is rapidly mobilized from peripheral organs and delivered to the liver for metabolism. The half-life of ApoA-I in plasma following HDL administration ranges between 6 and 24 hours, depending on the dose and product composition. Overall, various Phase I and II clinical trials performed to date in over 800 patients and healthy volunteers have demonstrated that HDL products are well tolerated without any major complications or severe side effects.

Table 1.1: Summary of clinical pharmacokinetics and safety profiles of HDL infusions.

Drug	Composition*	Clinical Study	Dose of ApoA-I protein or peptide	Pharmacokinetics	Safety	Ref.
SRC-rHDL (ZLB)	ApoA-I/sPC (1:4.2)	Phase 1 Single dose in healthy subjects (n = 7)	15 and 40 mg/kg	$T_{1/2}$ of ApoA-I> 24hr; $T_{1/2}$ of total PL ~ 8hr	No data reported	21-22
		Phase 1 Single dose in hypercholestero-lemic men (n = 24)	80 mg/kg	No data reported	No data reported	23
		Phase 1 Single dose in ABCA-1 heterozygotes and control subjects (n = 9)	80 mg/kg	No data reported	No data reported	24
CSL-111 (CSL Behring)	ApoA-I/sPC (1:4.2)	Phase 1 Single dose in type 2 diabetes patients (n = 7)	80 mg/kg	ApoA-I increased from 1.2 (baseline) to 2.8 g/L and returned to baseline on day 7	No data reported	25
		Phase 1 Single dose in patients with vascular disease (n = 20)	Placebo and 80 mg/kg	The level of HDL cholesterol increased by 20% after infusion of rHDL	No liver function changes	26
		Phase 1 Single dose in type 2 diabetes patients (n = 17)	Placebo and 20 mg/kg	$T_{1/2}$ of ApoA-I~ 72 hr No report	No data reported	27
		Phase 2 Multiple doses in ACS patients (n = 183)	4 weekly infusions of placebo, 40 and 80 mg/kg	No report	Liver function abnormalities in 80 mg/kg group; 40 mg/kg is well tolerated	28
CSL-112 (CSL Behring)	ApoA-I/sPC (1:1.5)	Phase 1 Single dose in healthy subjects (n = 57)	Placebo, 5, 15, 40, 70, 105 and 135 mg/kg	T_{max} of ApoA-I = 2 hr; For doses >70 mg/kg; $T_{1/2}$ of ApoA-I=14.7 ~ 99.5 hr.	No safety issues	20, 29
		Phase 1 Multiple doses in healthy subjects (n = 36)	Four weekly infusion of placebo, 3.4 and 6.8 g/dose Eight bi-weekly of 3.4 g/dose	T_{max} of ApoA-I = 2hr; $T_{1/2}$ of ApoA-I = 19.3 hr ~ 92.8 hr	Safe and well tolerated	20, 30-31
		Phase 2a Single dose in patients with stable atherothrombotic disease (n = 45)	Placebo, 1.7, 3.4 and 6.8 g/dose	T_{max} of ApoA-I ≈ 2 hr; $T_{1/2}$ of ApoA-I ≈ 12 hr.	Good safety	32
		Phase 2b (AEGIS-I) Patients with acute myocardial infarction (n = 1258)	Four weekly infusions Placebo, 2 and 6 g/dose		Well-tolerated, no significant alterations in liver or kidney function or other safety concern	33-34
		Phase 3 (AEGIS-II) Patient with acute coronary syndrome (ACS) (n=17,400)	Currently recruiting	Currently recruiting	Currently recruiting	35

ProApoA-I-liposome (UCB)	rProApoA-I/sPC (1:1.25)	Phase 1 Single dose in patients with low HDL cholesterol (male, n = 4)	IV infusion for 1hr or 10 min 1.6 g proApoA-I	$T_{1/2}$ of ApoA-I < 24 hr	No adverse events	36
		Phase 1 Single dose in FH patients (n = 4)	4g by IV infusion over 20 min ~ 40-50 mg/kg	Plasma ApoA-I levels increased transiently during the first 24 hr. C_{max} 64% and 35% above the baseline at 1 hr, respectively.	No safety issues	37
ETC-216 (Esperion)	rApoA-I/POPC (1:1)	Phase 1 Single dose in healthy subjects (n = 32)	IV infusion of doses 0-100 mg/kg (males) and 0-50 mg/kg (females)	T_{max} of HDL free cholesterol level ≈ 30 min at 15 mg/kg and higher	Safe and well tolerated at all doses.	38
		Phase 2 Multiple doses in ACS patients (n = 57)	Five doses; once per week by IV infusion; Placebo, 15 and 45 mg/kg.	No report	Minor gastrointestinal adverse effects in 3 groups. Two adverse events in high-dose group deemed possibly drug related.	38-39
CER-001 (Cerenis)	rApoA-I/SM/DPPG (1:2.7:0.1)	Phase 1 Single dose in healthy volunteers (n = 32)	IV infusion of escalating doses of 0.25, 0.75, 2, 5, 10, 15, 30, 45 mg/kg.	T_{max} of ApoA-IApoA ≈1-2 hr; $T_{1/2}$ ≈ 10 hr; C_{max} is dose-dependent and up to 0.9 mg/dL at 45mg/kg;	Safe and well tolerated at all doses;	40-41
		Phase 2 (CHI SQUARE) Multiple doses in patients with ACS (n = 507)	6 weekly infusions of 0, 3, 6, and 12 mg/kg.	No PK data	Generally well tolerated	42-43
		Phase 2 Multiple doses in patients with HoFH (n = 23)	12 biweekly infusions at 8 mg/kg.	ApoA-I increased by 13% from 114.8 mg/dL to 129.3 mg/dL during first hour after infusion.	One serious adverse event reported to be drug related	44-45
		Phase 2 Multiple doses in patients with FPHA (n = 7)	IV infusion for 1hr; 20 infusions at 8 mg/kg for 6 months.	T_{max} of ApoA-I ≈ 4 hr; $T_{1/2}$ ≈ 12 hr	No serious adverse events	46-47
ETC-642 (Esperion)	ApoA-I peptide/DPPC /SM (1:1:1)	Phase 1 Single dose in patients with stable atherosclerosis (n = 28)	IV infusion of placebo and 0.1, 0.3, 1, 3 and 10 mg/kg	Dose proportional rise in the levels of peptide after infusion; $T_{1/2}$ = 8.3 ~ 12.8 hr.	Safe and well tolerated	48-49
		Phase 1 Single dose in patients with stable cardiovascular disease (n = 24)	IV infusion; 10, 20, 30 mg/kg	Dose proportional rise in the levels of peptide; $T_{1/2}$ of peptide = 10.2 ~13.8 hr.	Asymptomatic elevations of liver function in one patient at 30 mg/kg	50
		Phase 1 Multiple doses in patients with stable cardiovascular disease (n = 32)	4 weekly IV infusions of placebo 10, 20 and 30 mg/kg	No data reported	No data reported	51

Abbreviations: sPC: soybean phosphatidylcholine; rApoA-I: recombinant ApoA-I; ACS: acute coronary syndrome; POPC: palmitoyloleoylphosphatidyl choline; SM: and sphingomyelin; DPPG: dipalmitoylphosphatidyl-glycerol; FH: familial hypercholesterolimea; HoFH: heterozygous familial hypercholesterolemia; FPHA: familial primary hypoalphalipoproteinemia; DPPC: dipalmitoylphosphatidylcholine. * Indicates weight ratio, literature reported molar ratios were converted to weight ratios

1.2.1 HDL Based on ApoA-I Purified from Human Plasma

The first rHDL product tested in a clinical trial was SRC-rHDL developed by ZLB Central Laboratory, Switzerland. ApoA-I was isolated from human plasma and reconstituted with soybean phosphatidylcholine (sPC) using the cholate dialysis process described below.[22] Nanjee *et al.* evaluated the effect of a single infusion of SRC-rHDL at 40 mg/kg in healthy volunteers.[21] The dose, up to 40 mg/kg, was safe and well tolerated.[23-24] Following ZLB acquisition by CSL Behring, Australia in 2000, SRC-rHDL was renamed as CSL-111. The product was tested in a large (183 patients) Phase II safety and efficacy (ERASE) clinical trial in 2005.[28] Patients with ACS were administered with four infusions of CSL-111 at 40 mg/kg or 80 mg/kg or placebo at weekly intervals. The high-dose CSL-111 treatment at 80 mg/kg was discontinued early due to abnormalities in liver functions, but CSL-111 was well tolerated at the 40 mg/kg dose. Due to the safety issue, CSL-111 was reformulated into CSL-112 by reducing the lipid to protein ratio, resulting in a homogenous particle size of 13 nm.[18] Safety of CSL-112 was evaluated in healthy volunteers following single and multiple administrations.[20] CSL-112 was found to be much safer than its predecessor, CSL-111, as higher doses up to 135 mg/kg were well tolerated. In addition, ApoA-I levels remained above the baseline for 3 days following a single infusion of CSL-111.[31] A largest-to-date clinical trial with HDL has been completed for CSL-112 in 1200 patients with acute myocardial infarction.[33] Among patients with acute myocardial infarction, 4 weekly infusions of CSL112 are feasible, well tolerated, and not associated with any significant alterations in liver or kidney function or other safety concern. The ability of CSL112 to acutely enhance cholesterol efflux was confirmed. The potential benefit of CSL112 to reduce major adverse cardiovascular events is being assessed in an adequately powered 17,400 patient Phase 3 trial. [35]

1.2.2 HDL Based on Recombinant ApoA-I

The first rHDL product synthesized with recombinant ApoA-I was proApoA-I-liposome developed by UCB (Belgium). Pro-ApoA-I, a recombinant protein produced in E. coli, has an additional 6 amino acid pro-sequence attached to native ApoA-I.[52] Pro-ApoA-I liposomes administered at 1.6 and 4 g per dose were well tolerated, and ApoA-I levels remained elevated for over 24 hrs. ApoA-I Milano is a naturally occurring variant of ApoA-I with Arg-173 to Cys substitution. ApoA-I Milano is produced by a recombinant process in E. coli.[53] In 1998, Esperion acquired the rights to ApoA-I Milano and produced a new rHDL product, termed ETC-216, which

is composed of ApoA-I-Milano and 1-palmitoyl-2-oleoyl-sn-glycero-3-phosphocholine (POPC).[38] After 5 weekly infusions at 15 mg/kg and 45 mg/kg, ETC-216 significantly reduced coronary plaque volume (an average of 4.2%) in treated patients measured by IVUS.[39] ETC-216 was safe and well tolerated at all doses tested. CER-001 is another rHDL product under development by Cerenis. CER-001 is composed of dipalmitoylphosphatidyl-glycerol (DPPG), sphingomyelin (SM), and recombinant human ApoA-I, which is produced in a mammalian expression system in CHO cells.[42] In a Phase I clinical trial in healthy volunteers, subjects were administered with escalating doses of CER-001 up to 45 mg/kg.[41] The AUC, C_{max}, and $T_{1/2}$ for ApoA-I increased with each increased dose.[41] CER-001 was also tested in a multiple-dose efficacy trial with 3, 6 and 12 mg/kg doses given once weekly for 6 weeks.[42] CER-001 was also shown to be safe and well tolerated at all the doses tested in these trials.

1.2.3 HDL Based on ApoA-I Mimetic Peptide

In addition to recombinant ApoA-I protein-based rHDL as described above, new rHDL systems composed of ApoA-I mimetic peptides and phospholipids have been developed. Utilization of ApoA-I mimetic peptides is expected to reduce the manufacturing cost and facilitate industrial scale-up of rHDL. ETC-642 was the first ApoA-I mimetic peptide to reach clinical evaluation.[48, 50] A Phase I clinical study, performed in 2002, examined a single-dose infusion of ETC-642 in 28 patients with stable atherosclerosis.[48] Study participants were monitored for 4 weeks following a single drug administration at 0.1, 0.3, 1, 3, and 10 mg/kg. As expected, the pharmacokinetics parameters, such as AUC and ETC-642 elimination half-life, increased with higher doses.[48] The second Phase I trial was conducted with stable cardiovascular patients at higher doses of 10, 20, and 30 mg/kg.[50] At the highest dose level tested, evidence of asymptomatic elevations of liver functions was observed in a single patient, suggesting identification of a maximum tolerated dose. Overall, these two clinical trials have demonstrated the safety and tolerability of single infusion of ETC-642 up to 20 mg/kg dose. A multiple dose safety study with ETC-642 was also conducted at 10, 15, and 20 mg/kg doses administered once weekly for four weeks;[51] however, the results of this study have not yet been made public.

1.2.4 Synthesis of sHDL based on ApoA-I mimetic peptide

Apolipoprotein mimetic peptides, which have similar Class A-type amphipathic α-helical structures to ApoA-I, were initially used to investigate the structural features of the full-length ApoA-I protein [54]. Due to their ability to recapitulate the biological functions of full-length protein

in vivo, they were then applied to produce mimetic HDL particles. [55-57] Several ApoA-I mimetic peptides have been synthesized to date and are designed based on sequences that are homologous to the native protein [58]. These peptides are generally optimized to maximize different functional outputs, such as cholesterol efflux capacity and lipid binding affinity, [55, 58] and have been the focus of many recent clinical trials. Examples of such mimetic peptides and their applications are described in Table 1.2.

Table 1.2: Mimetic peptides of ApoA-I: sequences and desired clinical applications.

Peptide	Sequence	Company	Optimized Functional Output	Ref
ESP24218	P-V-L-D-L-F-R-E-L-L-N-E-L-L-E-A-L-K-Q-K-L-K	Esperion	Lipid binding LCAT activation RCT	56
D4F	Ac-D-W-F-K-A-F-Y-D-K-V-A-E-K-F-K-E-A-F-NH2	Novartis	Same as L4F Chemical stability	59
L4F	Ac-D-W-F-K-A-F-Y-D-K-V-A-E-K-F-K-E-A-F-NH2	Novartis	RCT Lipid binding Inflammation reduction	60
Reverse 4F	K-L-K-Q-K-L-A-E-L-L-E-N-L-L-E-R-F-L-D-L-V-Inp Ac-F-A-E-K-F-K-E-A-V-K-D-Y-F-A-K-F-W-D-NH2 (reverse 4F)	Kos pharmaceuticals	Lipid binding Cholesterol mobilization	61-62
5A	D-W-L-K-A-F-Y-D-K-V-A-E-K-L-K-E-A-F-P-D-W-A-K-A-A-Y-D-K-A-A-E-K-A-K-E-A-A	KineMed Inc.	ABCA1 activation Low hemolysis Lipid binding	57
18A	Ac-EWLEAFYKKVLEKLKELF-NH2	N/A	RCT	63
ATI-5261	Ac-E-V-R-S-K-L-E-E-W-F-A-A-F-R-E-F-A-E-E-F-L-A-R-L-K-S-NH2	Roche	Anti-oxidant properties Promote ABCA1 dependent cholesterol efflux	64

There are several different methods for the preparation of HDL *in vitro*. The method to make ApoA-I reconstituted HDL is known as the sodium cholate dialysis method. This method involves the addition of detergents, such as cholate, followed by several days of dialysis to remove the detergent. The main drawbacks to use of this procedure are time consumption, incomplete detergent removal, endotoxin contamination of ApoA-I, and particle heterogeneity which limit the application of this method. Another method that utilizes sonication of peptide and lipid mixtures has also been employed to prepare HDL. Briefly, the lipid mixture in chloroform is dried under nitrogen flow to form lipid film and is then placed under vacuum oven. PBS buffer is added to the film, and the mixture is vortexed and sonicated under nitrogen. Apo A1 mimetic peptide in PBS

buffer is added to the mixture, which becomes transparent immediately. The resulting heterogeneous HDL needs to be filtered and purified by gel filtration chromatography to obtain homogeneous HDL. [65] However, this method also has similar drawbacks in that highly homogenous particles are difficult to make, especially in large scale. [66] Preparation of synthetic HDL particles by co-lyophilization, a technique developed and patented by Esperion Therapeutics,[66] circumvents many of the issues described above. The process involves co-dissolving peptide and lipid constituents in organic solvent, freeze-drying, and subsequent hydration with an isotonic, neutral buffer. The mixture is then repeatedly heated and cooled to form homogenous HDL particles without further purification.

1.2.5 Lipid component play important role in sHDL RCT process.

In most research and clinical trials, the pharmacokinetics of ApoA-I protein or mimetic peptides were thought to be the driving force for cholesterol efflux and mobilization, so the influence of lipid components was always overlooked. However, lipids play an important role in receptor binding and particle stability, and they can affect the biological properties of rHDL as evidenced by research results both *in vitro* and *in vivo*. When ApoA-I mimetic peptide, 5A, was combined with either SM or POPC, 5A-SM exhibited higher ABCG1- and SR-BI-mediated cholesterol efflux relative to 5A-POPC. Injection of 5A-SM in rats resulted in 3-fold higher mobilization of plasma cholesterol than for 5A-POPC. 5A-SM exhibited more potent anti-inflammatory properties and significant reduction of plaque area in ApoE$^{-/-}$ mice. [67] These findings extend to humans as well. Among rHDL products in clinical trials as mentioned above, CER-001 and CSL-112 have similar compositions including ApoA-I protein and phospholipids but differ in lipid amount and lipid species. The lipid composition of CSL-112 is soy PC only, and CER-001 is sphingomyelin with only 3% DPPG 1:2.7 (wt/wt). In phase I clinical trials, these two products were administered at various dose level for pharmacokinetics, pharmacodynamics, and safety evaluation. When the pharmacokinetics of ApoA-I protein were plotted at the same dose level of 15 mg/kg for these two rHDLs, a major difference in half-life was observed with 68 hrs for CSL-112 versus 37 hrs for CER-001(Figure 1.1A). Additionally, the cholesterol mobilization profiles were significantly different as shown in Figure 1.1B and 1.1C. CER-001 achieved higher total HDL-cholesterol, greater HDL-cholesterol ester change, and more rapid elimination as compared to CSL-112 after a single infusion. We next plotted the E_{max} values of total or free cholesterol increase versus ApoA-I dose levels for the two products (Figure 1.1D and 1.1E). The plot indicates

that, to achieve same maximum cholesterol concentration, higher doses of CSL-112 are needed. The cholesterol mobilization effect plateaus at 30 mg/kg for CER-001 while E_{max} values keep increasing as dose levels escalate for CSL-112. All these dissimilarities may result from the altered dose levels and type of lipids in the rHDL. CER-001 appears to be more potent in activating cholesterol efflux but easily causes side effects due to the narrow therapeutic window. From Figure 1.1F, CSL-112 is able to efflux more cholesterol as compared to CER-001 when subjects' plasma after rHDL administration was incubated with macrophage cells. This is because SM and saturated fatty acid-containing lipids like DPPC have superior cholesterol binding capacity relative to unsaturated POPC and soyPC which is incorporated in CER-001. [67] Therefore, CSL-112 is more capable of accepting, or binding, cholesterol and interacting with LCAT to be esterified.

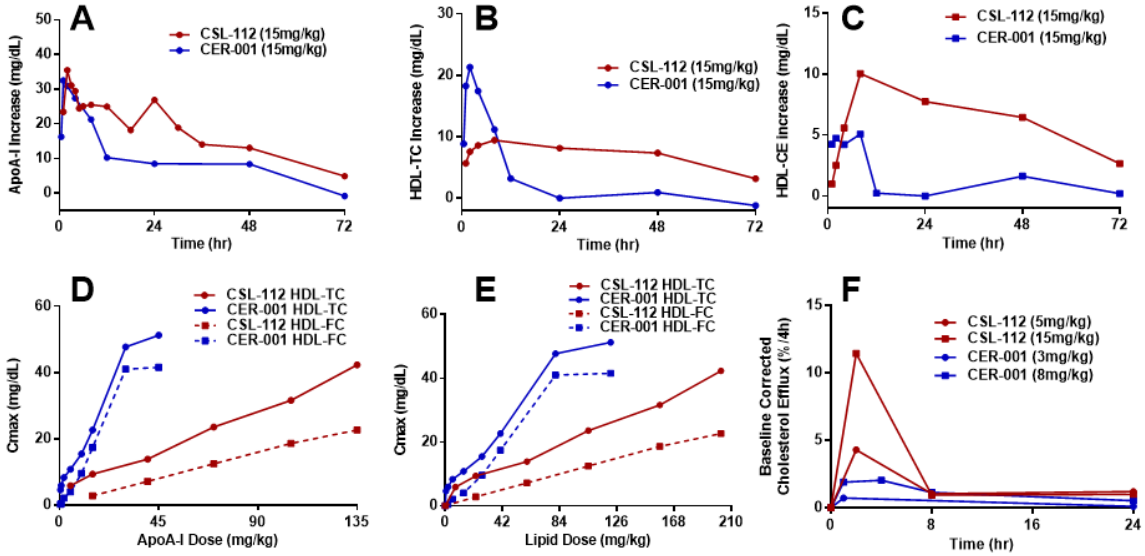

Figure 1.2: Comparision of pharmacokinetic and pharmacodynamic properties of CER-001 and CSL-112 at 15mg/kg in clinical trials. ApoA-I concentration-time profile after IV administration of CER-001 or CSL-112 at 15mg/kg (Panel A); HDL-TC and HDL-CE increase after administration (Panel B and C); Relationship between maximum concentration of HDL-TC/HDL-FC and ApoA-I or lipid dose (Panel D and E); Ex vivo cholesterol efflux ability of plasma (Panel F).

1.3 Limitations and biomimetics of sHDL

Current sHDL products in clinics are mostly composed of lipids and ApoA-I protein either isolated or purified from human plasma. The doses required to elicit clinical effect is 40 mg/kg[20], meaning that a large amount of protein is required to meet patients' needs, which is very expensive due to the complicated manufacturing process. Thus, ApoA-I mimetic peptides were introduced as substitutes for ApoA-I protein to form sHDL and achieve similar effects. However, the half-life

of sHDL composed of ApoA-I mimetic peptide is 8-12 hours, which is much shorter than endogenous protein with a half-life of 3.3 days. This rapid elimination necessitates more frequent dosing, which is inconvenient for patients using an intravenous product, or administration of high doses, which can lead to off-target toxicity. Thus, prolonging the circulation time of sHDL can be a potential strategy to improve its cholesterol efflux effects while avoiding possible side effects. Polyethylene glycol (PEG) has been widely used to coat or "PEGylate" nanoparticle surfaces to archive "stealth-like" characteristics, which can be influenced by PEG density, molecular weight, and structure. It can be considered a method for slowing sHDL nanoparticle elimination by the reticuloendothelial system. [68]

Several other investigators have developed biomimetic HDLs for not only for treatment or imaging of atherosclerosis but also for drug delivery purposes.[69-77] For example, Marrache *et al.* reported the construction of a synthetic, biodegradable HDL-NP platform for detecting vulnerable plaques by targeting the collapse of the mitochondrial membrane potential that occurs during apoptosis.[77] The particle has an average size of approximately 120 nm and contains a poly(lactide-co-glycolide) (PLGA) polymer, cholesteryl oleate, and phospholipid with triphenylphosphonium (TPP) decorated with ApoA-I mimetic peptide 4F. In addition, quantum dots (QDs) were incorporated into the PLGA matrix for imaging purposes. *In vitro* evaluation of this technique showed a promising detection sensitivity and also therapeutic potential as well as favorable biodistribution and pharmacokinetics. Sanchez-Gaytan *et al.* developed a hybrid polymer/HDL nanoparticle composed of a lipid/apolipoprotein coating that encapsulated a PLGA core.[75] This PLGA-HDL was 30-90 nm in size and displayed some characteristics of endogenous HDL, including preferential uptake by macrophages and an effective *in vitro* cholesterol efflux capacity. The presence of a PLGA core also enabled incorporation and sustained release of therapeutic agents for atheroma-targeted delivery. These PLGA-HDL nanoparticles accumulated in atherosclerotic plaques and co-localized with atheroma macrophages in an $ApoE^{-/-}$ mouse model. Thaxton *et al.* synthesized a spherical HDL nanoparticle with a gold NP core-shell structure in which the gold NP core served as a size- and shape-controlling scaffold for constructing an HDL-like particle through surface attachment of phospholipids and ApoA-I. The nanoparticles were designed to have a similar size to endogenous HDL and to mimic the general surface composition of HDL to enable physical binding of cholesterol and cellular cholesterol efflux *in vitro*.[69, 78] Biomimetic HDL nanoparticles discussed here have demonstrated the ability to accumulate in the

atheroma and, in some instances, had local anti-inflammatory effects.[79-80] However, to the best of our knowledge, the ability of these biomimetic HDL to reduce atheroma in diseased animals has not been confirmed, and none of these nanoparticles have been compared head-to-head with the sHDLs that have been tested in clinical trials. In addition, most biomimetic HDL nanoparticles have a larger particle size and density compared to endogenous HDL, which likely results in differences in biodistribution, HDL receptor interaction, and hepatic uptake of mobilized cholesterol. Thus, there is an urgent need to design a sHDL mimetic product that is easy to prepare affordably.

1.4 HDL as drug delivery system for brain tumor therapy

In addition to the role HDL plays in cardiovascular and liver disease, the utility of HDLs extends to tumor therapy as well due to the interaction between HDLs and cancer cells. Glioblastoma multiformes (GBM) are the most aggressive primary tumors within the central nervous system. Even after surgery, chemotherapy, and radiotherapy, the prognosis of patients with GBM remains dismal. GBMs always recur, and often result in the death of the patient. Therefore, the development of effective treatment strategies to control the progression and survival of these gliomas is in high demand. Because of the shortcomings of chemotherapy like low solubility, non-specificity and toxicity of drugs, nanoparticles have been used to deliver chemotherapeutic or immunotherapeutic molecules.

An ideal brain tumor-targeted delivery system should at least meet the following requirements: efficient penetration through the BBB, efficient penetration/diffusion within tumor regions, and efficient intracellular delivery. HDL is a promising brain tumor-targeted delivery system because many of its features allow it to meet the above requirements.

First, lipoproteins, such as HDL, are reported to circulate in the blood for an extended period of time,[81] which can increase the possibility of HDLs penetrating the BBB and enables them to accumulate in the tumor regions by the enhanced permeability and retention (EPR) effect. HDL therapies show a long circulation time, and the half-life of ApoA-I can be up to 92.8 hours. [20, 27, 30-31] These half-lives are comparable to some of the best-modified (PEGylated) long-circulating liposomes. Differing from certain other nanoparticles whose components may cause severe side effects, reconstituted HDLs are safe and well tolerated in the human body as a delivery system due to their endogenous nature, therefore they will not trigger immune reactions or be recognized by the reticuloendothelial system (RES). [32, 82] Second, the BBB tight junction and extracellular matrix

of tumors can prevent the diffusion of nanoparticles within the tumor regions due to the small opening space which is less than 40 nm.[83] Conventional nanoparticles, such as liposomes, are normally larger than 60 nm, which may limit the diffusion of the nanoparticles within the tumor tissue. HDL has ultra-small sizes, with diameters of about 10 – 20 nm, depending on the composition, and therefore can penetrate deeply and diffuse efficiently with in the tumor regions. Third, it has been reported that natural human HDL was effective in inhibiting human glioblastoma cell (SNB-19 cell line) growth in a nontoxic, dose-dependent manner.[84] The LD50 was 10-fold lower than that for normal rat astrocyte growth *in vitro*. One possible mechanism for this study's findings was the interaction between oxidized lipids from HDL with the plasma membranes of the GBM cells.

Many malignant cells have been shown to overexpress SR-BI in order to scavenge cholesterol-rich HDLs so that a high level of growth can be maintained. This provides a good marker for HDL to target due to its recognition by SR-BI.[85] Among 50 human ovarian epithelial cancers, SR-BI is overexpressed on 96% of the tumors.[86] Further, prostate cancer cells have been shown to take up cholesterol-rich HDLs through SR-BI for the biosynthesis of endogenous androgen.[87] It was demonstrated that the uptake of HDL cholesterol esters is not dependent on the internalization and degradation of the particle, and SR-BI localized in cholesterol- and sphingomyelin-rich caveolae is the HDL receptor which mediates the selective uptake of cholesterol esters.[2] Both discoidal and spherical HDLs are able to deliver drugs and interact with SR-BI, however, discoidal HDL has higher binding affinity than spherical HDLs.[88] This evidence supports the idea that cancer cells have increased uptake of cargo loaded in HDLs via SR-BI. Thus, the caveolae domain and SR-BI expressed on both GBM and BBB endothelial cell membranes will be receptors for drug-loaded sHDL and achieve the selective and targeting interaction with HDL particles and uptake of the loaded cargo. In addition, by decorating HDL with different targeting ligands, such as EGF [89], RGD [90], and folate [91 92], HDL can be targeted to tumor cells that do not express SR-BI, which will further improve the targeting efficiency and decrease the side effects. Considering these advantages, sHDL can be considered as a novel therapeutic delivery platform for GBM to effectively deliver chemotherapeutic agents combined with immune-stimulatory molecule.

1.5 Research scope and impact

sHDL has been investigated for years as an urgent treatment to for heart attack patients to reduce the risk of second event. A number of sHDL products have advanced to different stages of clinical trials.[18] These sHDL products are intended for administration following an initial cardiovascular event in patients with acute coronary syndrome (ACS) to remove excess cholesterol from arterial plaques that may cause a secondary event. However, the ApoA-I protein component in most sHDL products is purified or isolated from human plasma, which is a very costly and complicated process. Though ApoA-I mimetic peptide with a similar structure to ApoA-I protein was introduced as surrogate component, the half-life of sHDL with ApoA-I mimetic peptide was relatively short and required frequent dosing, which may limit its future development. Thus, understanding the impact of ApoA-I mimetic peptide lipidation on its biological function can further optimize current sHDL formulations to address these concerns. By modifying the lipid composition of sHDL, the circulation time of sHDL can be prolonged for durable removal of excess cholesterol. In addition, establishing a lipid-based nanoparticle mimicking both structure and function of sHDL without peptide will create a novel substitute for sHDL in ACS therapy and other indications. Based on evaluation of the nanoparticles, researchers are able to potentiate its effect with additional modifications. Because sHDL has amphipathic properties, it has been employed as drug delivery system for insoluble drugs. Our formulation of the DTX-sHDL-CpG system provides a new, generalizable framework for using sHDL-based chemoimmunotherapy for glioma treatment.

1.6 Thesis overview

The overall goal of this thesis was to investigate the impact of lipid composition of sHDL on its cholesterol efflux effect and to determine whether sHDL can be modified to extend its circulation time and amplify cholesterol removal with sufficient safety. This can provide a possible approach to improve current or future sHDL products regarding their stability and efficacy. This idea is simple but attractive due to lower costs and easier preparation processes compared to conventional sHDL-like nanoparticles. Ultimately, the DTX-sHDL-CpG platform can broaden the application of sHDL in chemo-immunotherapy for other cancers.

In Chapter 2 of this thesis, we studied the impact of formulation and administration route of ApoA-I mimetic peptide, 22A, on its biological activity *in vivo* including plasma peptide levels, cholesterol mobilization, and lipoprotein remodeling. The mean circulation half-life was longer

for 22A-sHDL ($T_{1/2}$ = 6.27 h) than for free 22A ($T_{1/2}$ = 3.81 h). The amount of 22A absorbed by the vascular compartment after IP dosing was ~50% for both 22A and 22A-sHDL. The strongest pharmacologic response was observed after IV injection of 22A-sHDL—specifically, a 5.3-fold transient increase in plasma free cholesterol (FC) level compared to 1.3-fold and 1.8-fold FC increases for 22A-IV and 22A-sHDL-IP groups. Addition of either 22A or 22A-sHDL to rat plasma caused lipoprotein remodeling and appearance of a lipid poor apoA-I. Using a PK-PD model, we found that lipid components in sHDL were more predictive of cholesterol level changes in serum than were any other components. Hence, both the route of administration and the formulation of ApoA-I peptide significantly affected its pharmacokinetics and pharmacodynamics. These findings also provided the information that was applied in Chapter 3.

In Chapter 3, sHDL surface modification with polyethylene glycol (PEG) was investigated for its potential to extend sHDL circulation *in vivo*. Various amounts (2.5, 5 and 10%) and different chain lengths (2 and 5 kDa) of PEG-modified lipids were incorporated in sHDL's lipid membrane. *In vitro* characterization, cell uptake, and cholesterol efflux effects of sHDL and sHDL-PEG were evaluated. *In vivo* experiments were conducted to study impact of PEG on sHDL pharmacokinetics and pharmacodynamics. This work showed a comparable cholesterol efflux ability between sHDL and sHDL-PEG *in vitro*. Adding more PEG or using PEG of longer chain lengths extended the circulation half-life of sHDL. Addition of PEG also increased the area under the curve for the phospholipid component of sHDL ($p < 0.05$), reflecting a greater mobilization of plasma free cholesterol.

Chapter 4 introduces nano-micelle (NanoMCL), a structural nano-mimetic of sHDL with a small particle size (12-14 nm) and a hydrophobic core and hydrophilic exterior. It shows that NanoMCLs are functionally similar to sHDL with the capacity to efflux cholesterol from macrophages and deliver cholesterol to hepatocytes for elimination. The NanoMCLs also have a better ability to inhibit inflammatory cytokine release *in vitro* compared to sHDL. More importantly, when administered *in vivo*, NanoMCLs exhibited improved cholesterol mobilization from peripheral tissues compared to sHDL, followed by elimination from the body within 48 hours. When administered as a 6-week treatment in an animal model of atherosclerosis, sHDL and NanoMCL reduced atheroma by 21% and 40%, respectively. Based on these encouraging results, NanoMCL could prove to be a valuable alternative to sHDL in treatment of cardiovascular disease and other inflammatory diseases.

Chapter 5 discusses the application of sHDL as a delivery vehicle for anti-cancer drugs with the co-delivery of immuno-stimulatory molecule CpG for glioma treatment. After examining SR-BI receptor expression on different cancer cells, GL26 was selected to build tumor model. Chemotherapeutic agent docetaxel (DTX) was selected as model drug. DTX and immune-stimulatory TLR-9 agonist cholesterol-CpG (cholCpG) were co-incorporated into sHDL nanoparticles. sHDL composition was optimized to maximize DTX retention in plasma. The resulting DTX-sHDL-CpG nanoparticles exhibited characteristically ultra-small ~10-12 nm size and discoidal shape. Nanoparticles were uptaken successfully by tumor cells, and sHDL was able to penetrate through the BBB *in vitro*. However, systemic administration of free DTX, DTX-sHDL, or DTX-sHDL-CpG did not make a difference in the mean survival of animals. Though, all three groups demonstrated longer survival than the saline-treated group. Compared to intravenous administration, intracranial injection of DTX-sHDL-CpG led to notable tumor growth inhibition, which extended the mean survival of mice from 34 days to 55 days with 20% long-term survivors. Thus, DTX-sHDL-CpG can be applied as a promising platform for cancer treatment.

The conclusions of this work and implications for future studies are discussed in Chapter 6. Chapter 2 is originally published in *Journal of Lipid Research*. Chapter 3 is published in *Molecular Pharmaceutics*. Chapter 4 is under review for publication in *ACS Nano*. Chapter 5 will be submitted for publication once manuscript is completed.

Chapter 2 : Impact of administration route and lipidation on pharmacokinetic and pharmacodynamics properties of sHDL

This research was originally published in the *Journal of Lipid Research*. Tang J, Li D, Drake L, Yuan W, Deschaine S, Morin EE, Ackermann R, Olsen K, Smith DE, Schwendeman A. Influence of route of administration and lipidation of apolipoprotein A-I peptide on pharmacokinetics and cholesterol mobilization. J. Lipid Res. 2017 Jan;58(1):124-136.

2.1 Abstract

Apoliprotein A-I (apoA-I), apoA-I mimetic peptides and their lipid complexes or reconstituted high-density lipoprotein (HDL) have been studied as treatments for various pathologies. However, consensus is lacking about the best method for administration - by intravenous (IV) or intra-peritoneal (IP) routes, and formulation - as an HDL particle or in a lipid-free form. The objective of this study was to systematically examine peptide plasma levels, cholesterol mobilization and lipoprotein remodeling *in vivo* following administration of lipid-free apoA-I peptide (22A) or phospholipid reconstituted 22A-sHDL by IV and IP routes. The mean circulation half-life was longer for 22A-sHDL ($T_{1/2}$ = 6.27 h) than for free 22A ($T_{1/2}$ = 3.81 h). The percent of 22A absorbed by the vascular compartment after the IP dosing was ~50% for both 22A and 22A-sHDL. The strongest pharmacologic response came from IV injection of 22A-sHDL - specifically a 5.3-fold transient increase in plasma free cholesterol (FC) level compared to 1.3 and 1.8-fold FC increases for 22A-IV and 22A-sHDL-IP groups. Addition of either 22A or 22A-sHDL to rat plasma caused lipoprotein remodeling and appearance of a lipid poor apoA-I. Hence, both the route of administration and the formulation of apoA-I peptide significantly affect its pharmacokinetics and pharmacodynamics.

2.2 Introduction

The therapeutic use of apolipoprotein A-I (apoA-I), its mutants, and peptide mimetics for the treatment of atherosclerosis has been studied in a variety of animal models and clinical trials.[93-94] However, there is a lack of consensus regarding whether the apoA-I protein or peptide should be administered in a lipid-free form or bound to phospholipids as a reconstituted HDL particle.

Early clinical trials showed that infusion of lipid-free apoA-I failed to increase circulation level of HDL cholesterol (HDL-C) and resulted in shorter circulation time than that for endogenous apoA-I. [95] Consequently, the majority of clinically developed apoA-I products have been administered as reconstituted HDL particles: apoA-I/soybean phosphatidylcholine (CSL-111 and CSL-112), apoA-I-Milano/palmitoyl-oleoyl-phosphotidylcholine (ETC-216), and apoA-I/sphingomyelin/dipalmitoyl-phosphorylglycerol (CER-001). [94, 96-97] In contrast, many preclinical studies have been performed using infusions of lipid-free proteins, and apoA-I peptides have been optimized for their pharmacological activity in lipid-free form. [98]

There is also an uncertainty concerning the mechanism(s) by which reconstituted HDL infusions elicit pharmacological effects and whether such mechanism(s) differ(s) from that used by lipid-free apoA-I. The ability of lipid-free apoA-I to efflux lipids through interaction with the ATP-binding cassette transporter (ABCA1) and its capacity to form de novo functional pre-β HDL particles are considered to be critical for cholesterol efflux *in vivo*. [99-100] However, infused apoA-I peptides or proteins do not remain in the lipid-free form. Rather, they bind and remodel endogenous HDL, improving its functionality and thereby eliciting a pharmacological effect. [101-102] In contrast, when apoA-I is dosed in the form of an HDL particle, the magnitude of its pharmacological effect, measured by the degree of cholesterol mobilization from tissues to plasma, depends on the HDL's phospholipid composition. [103-104]

In a similar fashion, there is a lack of consensus surrounding the optimal route of administration for apoA-I and its mimetic peptides. For long term dosing in rodents, intraperitoneal (IP) administration is preferred for a technical reason, namely the difficulty of repeated dosing in the tail vein. [105] However, in many acute studies, apoA-I and HDL are administered intravenously (IV) specifically because these compounds act in the vascular compartment through either remodeling endogenous lipoproteins or direct efflux of the excess of cholesterol from foam cells in atheroma. [106-107] The effective dose of apoA-I or reconstituted HDL that reaches circulation is likely lower following IP administration in comparison to IV administration due to loss occurring during absorption from tissue to the vascular compartment. Yet, the fraction of apoA-I or HDL that is actually capable of reaching the vasculature following IP dose has not been experimentally determined yet.

With growing interest around the potential therapeutic roles of administered reconstituted HDL and apoA-I in the treatment of sepsis, diabetes, rheumatoid arthritis, lupus, and other diseases

[103, 108-109], it is important to develop a basic understanding of HDL/apoA-I pharmacokinetics in order to select the proper dose, dosing intervals, and route of administration. In addition, the ability to measure basic HDL-related biomarkers of pharmacological effect in order to understand how these biomarkers relate to the dose, dosing interval, and administration route is important. Having this information at hand will allow investigators to select pharmacologically relevant doses and avoid obtaining false negative results. Pharmacokinetic-pharmacodynamic (PK/PD) modeling is a scientific tool to relate PK models (describing the relationship between dose, systemic drug exposure and time) to PD models (describing the mathematical relationship between exposure level and the pharmacological effect). [110] By establishing PK/PD modeling, the relationship between the PK and PD profile can be quantified, providing an assessment of effect onset/duration relative to the plasma PK profile. [111]

In this study, we selected a "two by two" experimental design to compare the administration of apoA-I peptide and apoA-I peptide reconstituted HDL following IV and IP administrations in normal adult male rats. We selected the synthetic peptide 22A, or ESP24218, as a model apoA-I mimetic peptide. This peptide was the first apoA-I mimetic peptide to reach clinical development, which has been administered clinically in both single and multiple-dose trials, and its human pharmacokinetic data is available. [112-113] We determined peptide and phospholipid pharmacokinetics and measured cholesterol mobilization in plasma, distribution of mobilized cholesterol among HDL, low-density lipoprotein (LDL), and very-low-density lipoprotein (VLDL) particles, plasma efflux capacity, and lipoprotein remodeling following free 22A and 22A reconstituted HDL dosing.

2.3 Materials and methods

2.3.1 Materials

ApoA-I mimetic peptides 22A, PVLDLFRELLNELLEALKQKLK, and 5A, DWLKAFYDKVAEKLKEAFPDWAKAAYDKAAEKAKEAA, were synthesized by Genscript Inc. (Piscataway, NJ). The purities of peptides were determined to be over 95% by reserve phase HPLC. Phospholipids 1-palmitoyl-2-oleoyl-sn-glycero-3-phosphocholine (POPC) and 1,2-dipalmitoyl-sn-glycero-3-phosphocholine (DPPC) were generously donated by Nippon Oils and Fats (Osaka, Japan). All other materials were obtained from commercial sources.

2.3.2 Preparation and characterization of 22A-sHDL particles

Synthetic HDL particles were prepared by the thin film-hydration method. Briefly, DPPC and POPC were dissolved in chloroform at 20 mg/mL. 22A peptide was dissolved in methanol: water (1:1 volume ratio) at 10 mg/mL. DPPC, POPC, and 22A were mixed in a 4 mL glass vial at different weight ratios and vortexed for 5s. The mixture was dried by nitrogen gas flow and then placed in the vacuum oven overnight to remove residual solvent. The resulting lipid film was hydrated with PBS (pH 7.4) (final concentration of 22A = 15 mg/mL) and vortexed. The suspension was homogenized in a bath sonicator for 5 min and then with a probe sonicator intermittently (50 W×10 S×12 cycles) to form a clear or translucent 22A-sHDL solution.

2.3.3 Analysis of 22A-sHDL particles

The purity of 22A-sHDL was analyzed by gel permeation chromatography (GPC) with UV detection at 220 nm using Tosoh TSK gel G3000SWx 7.8mm x 30cm column (Tosoh Bioscience, King of Prussia, PA) on a Waters Breeze Dual Pump system. The HDL samples were diluted to 1 mg/mL peptide concentration and an injection volume of 10 □L was used. The samples were eluted with PBS (pH 7.4) at a flow rate of 1 mL/min. The sHDL hydrodynamic diameters were determined by dynamic light scattering (DLS), using a Zetasizer Nano ZSP, Malvern Instruments (Westborough, MA). Samples were diluted to 1.5 mg/mL peptide concentration. The volume intensity average values were reported.

2.3.4 Rat pharmacokinetics and cholesterol mobilization

Male Sprague-Dawley rats (300 ~ 350 mg) were purchased from Charles River Laboratories (Wilmington, MA) and acclimated for one week. The animals were maintained on a chow diet. Prior to dosing, the animals were fasted overnight and received either 22A peptide or 22A-sHDL particles at 75 mg/kg by either intraperitoneal (IP) or intravenous injection (IV). Four groups of rats (n = 4/group) were dosed as follows: IV dose of 22A solution group; IP dose of 22A solution group; IV dose of 22A-sHDL group and IP dose of 22A-sHDL group. Blood (300 - 500 μL) was drawn from the jugular vein into BD microtainer (TM) tubes (BD, Franklin Lakes, NJ) for capillary blood collection at pre-dose and 0.25, 0.5, 1, 2, 4, 8 and 24 after dosing. The animals were fed following the 8 h time-point and fasted again prior to the 24 h bleed. Serum was isolated immediately from the whole blood by centrifugation at 14,000 rpm for 10 min at 4 °C. Serum was aliquoted into multiple tubes and stored at -80°C prior to analysis.

2.3.5 LC-MS analysis of peptide plasma levels

Immediately after serum separation, 10 μL of 5A peptide (3 mg/mL) was added to 10 μL of serum as an internal standard (IS), peptides were extracted with 100 μL of methanol containing 0.1% acetic acid. After vortexing for 30 s, the mixture was centrifuged at 14,000 rpm for 10 min at 4°C. The top layer was drawn off and used for quantifying peptide levels in the serum, using Agilent 6520 Accurate-Mass Q-TOF LC/MS equipped with a dual electrospray ionization source (Dual-ESI) (Agilent Technologies, CA). The HPLC separation was performed using the Agilent 300SB-C18 column (2.1 mm × 50 mm, 3.5 μm). The mobile phase consisted of (A) water containing 0.1% (v:v) formic acid and (B) methanol (pH 2.2) containing 0.1% (v:v) formic acid using a gradient elution of 10% to 60% B at 0-3.5 min, and 60% to 95% B at 3.5-8 min. The flow rate was 0.4 mL/min with an injection volume of 10 μL. Mass spectra were acquired in negative ion mode with the mass range set at m/z 100-3200. The conditions used for the ESI source included a capillary voltage of 3500 V, a drying gas temperature of 332 °C, a drying gas flow of 5 L/min, and a nebulizer pressure of 45 psi as well as a fragmentor voltage of 225 V. MassHunter Workstation software (Agilent Technologies, CA) was used for data acquisition and processing. The extracted ion chromatogram (EIC) of 22A was exported from the total ion chromatogram (TIC) by monitoring the key fragment of 22A at m/z 656.6. Analogously, the EIC of 22A (-)Lys metabolite and IS 5A was extracted at m/z 832.5 and m/z 844.4, respectively. The total integral area of 22A peak and 22A (-)Lys metabolite peak was used to calculate concentration.

2.3.6 Measurement of plasma lipids

The levels of serum phospholipids (PL), total cholesterol (TC), and unesterified or free cholesterol (FC) were determined by enzymatic analysis using commercially available kits (Wako Chemicals, Richmond, VA). The cholesterol ester level (CE) was calculated as the difference between TC and FC levels at each time point. Briefly, serum samples were diluted with PBS (pH 7.4) 10-fold for TC detection and 3 fold for FC detection and with Milli Q water 10 times for PL detection. Defined amounts of standards or diluted samples were transferred into 96-well plate (50 □L, 60 □L and 20 □L for TC, FC and PL, respectively). Color reagents were added according to manufacturer instructions. The plates were gently shaken using an orbital shaker and incubated at 37 ˚C for 5 min The UV absorbance at 600 nm was measured by a Synergy NEO HTS Multi-Mode Microplate Reader (Bio-Tek).

2.3.7 Pharmacokinetic parameters calculation and PK-PD modeling

Pharmacokinetic (PK) and pharmacodynamic (PD) analyses of the data were performed by least-squares regression analysis, weighted by the inverse of the fitted value, using Phoenix© WinNonlin® (Pharsight Corporation, Mountain View, CA, USA). Serum 22A and phospholipids (PL) PK parameters were estimated using a one-compartment disposition model for IV bolus administration, and a one-compartment disposition model with first order absorption and no lag time for IP administration. The PK parameters included time to reach maximum serum concentration (Tmax), maximum serum concentration (C_{max}), area under the serum concentration-time curve (AUC), first-order absorption rate constant after IP injection (k_{01}), first-order elimination rate constant (k_{10}), elimination half-life ($T_{1/2}$), apparent total clearance (CL or CL/F, where F is bioavailabiliy) and apparent volume of distribution (Vd or Vd/F). The goodness of fit was determined by diagnosis plots and quantified by sum of squared residuals and model was selected using Akaike Information Criterion (AIC). The coefficient of variation (%CV) for each fitted parameter was also reported. The resulting pharmacokinetic parameters of 22A or phospholipids were then used as constants in the integrated PK-PD model.

The PK-PD model was established by relating serum concentrations of either 22A or the phospholipid components of 22A-sHDL to FC levels as the PD endpoint using indirect pharmacodynamic response models (19). Fig. 2.6 shows the indirect response model described by Jusko et al. for PK-PD modeling in this study. [114] The pharmacologic response (free cholesterol mobilization) is controlled by a zero order rate constant for generation of response (k_{in}) and a first order rate constant for loss of response (k_{out}). The response compartment can be modulated by stimulating kin using a sigmoidal infinite model. Steepness of the sigmoidal curve (γ) and the serum concentration needed to achieve a 50% maximum stimulation of response of a dosed agent (EC_{50}) were calculated. After the PK parameters were obtained by fitting to compartmental models, they were regarded as fixed values and then used to estimate PD parameters (i.e. k_{in}, k_{out}, EC_{50} and γ). The final models were chosen based on best fit in terms of sum of squared residuals, diagnosis plots and AIC values.

2.3.8 Distribution of mobilized cholesterol in lipoproteins

The rat sera samples were analyzed to assess cholesterol distribution between VLDL, LDL, and HDL lipoprotein fractions. Separation of lipoproteins was performed on Waters HPLC system equipped with Superose 6, 10/300 GL column (GE Healthcare, Piscataway, NJ) and on-line

detection of cholesterol by post-column enzymatic reactions [115]. Rat sera prior to dosing, 0.25, 2 and 24 h post-injection were analyzed. Sera aliquots (50 □l) were injected and eluted with a 154 mM sodium chloride/0.02% sodium azide solution at 0.8 ml/min. The post column reaction was done using a 5 mL reaction coil at 37°C and detected by UV at 490 nm. The cholesterol detection enzymatic reagents were delivered at 0.2 ml/min flow rate and mix-in with separated lipoprotein post column. The enzymatic reagent solution was composed of 100 mM phosphate buffer (pH 7.0), 4 M sodium chloride, 0.2% triton X-100, 10 mM sodium cholate, 2.5 mM 4-aminoantipyrine, 7.54 mM 2-hydroxy-3,5 dichlorobenzene, 0.0625 U/ml cholesterol oxidase, 1.25 U/ml peroxidase, 1.25 U/ml lipase and 0.1U/ml cholesterol ester hydrolase. All enzymatic reagents were purchased from Sigma.

2.3.9 Remodeling of endogenous plasma lipoprotein

Remodeling of endogenous lipoproteins in serum was assessed after incubation of 22A peptide or 22A-sHDL with human sera. Solutions of 22A peptide or 22A-sHDL at 0.1, 0.5, 1.5 and 3 mg/mL peptide concentration in sera were incubated at 37°C for 1 h with shaking at 300 rpm. The various sub-classes of HDL were separated by size and charge by one-dimensional native polyacrylamide gel electrophoresis (PAGE) and visualized by western blot. Samples were subjected to electrophoresis using 10-well Tris-Borate-EDTA gradient (3-25%) acrylamide native gels (Jule, Inc., Milford, CT) [116]. For each well, 5 µl of human sera after incubation with PBS, 22A peptide or 22A-sHDL was mixed with 5 µl of 2X TBE sample buffer and 6 µl of the resulting mixtures were loaded per well. Gels were run at 200 V until the sample dye was 2.5 cm away from the bottom of the gel. Proteins were visualized by western blot by transfer onto PVDF membrane and incubation overnight with anti-human apoA-I -HRP conjugated antibody (Meridian Life Science, Memphis, TN). Bands were visualized using SuperSignalTM West Pico Chemiluminescence Substrate (Thermo Fisher) and images were acquired on a FluorChem M Imager (Protein Simple, San Jose, CA) and Image J was used for spot densitometry.

2.3.10 Statistical analyses

Statistical analyses of the data were performed by Student's t-test for comparing two treatment groups or by one-way ANOVA/Dunnett's test for comparing multiple treatment groups with 22A-sHDL/IV serving as the control. Data are expressed as mean ± standard deviation of at least three independent experiments. $P < 0.05$ was considered to be statistically significant.

2.4 Results

2.4.1 Composition optimization, assembly and characterization of 22A-sHDL particles

HDL composition was optimized using an apoA-I mimetic peptide, 22A, and phospholipids to match the size of endogenous pre-□ HDL particles. The 22A peptide was previously clinically tested in dyslipidemia patients as ETC-642. [117] The composition of ETC-642 is approximately 1:1:1 weight ratios of 22A peptide, DPPC and sphingomyelin, combined to form homogeneous pre-□ HDL-like discs [117]. In this study we replaced sphingomyelin with POPC in order to increase sHDL interaction with lecithin-cholesteryl acyltransferase (LCAT). Unsaturated phospholipids like POPC are preferred substrates for LCAT, while sphingomyelin is not a substrate of the enzyme. [118] In order to optimize 22A-sHDL particle size and purity, we varied the weight ratio of 22A to total phospholipids varied between 1:0.5 to 1:4 (Table 2.1). Gel permeation chromatography was used to examine the purity and the size distributions of newly generated 22A-sHDL particles. As shown in Fig. 2.1A, the retention times of different 22A-sHDL particles were between 7 and 10 min, the peak of unbound or lipid-free peptide appeared at around 11.5 min. The amount of lipid-free peptide was less than 0.48% for all formulations. The retention time of sHDL decreased with the increase of lipid to peptide ratio, indicating formation of larger sHDL particles.

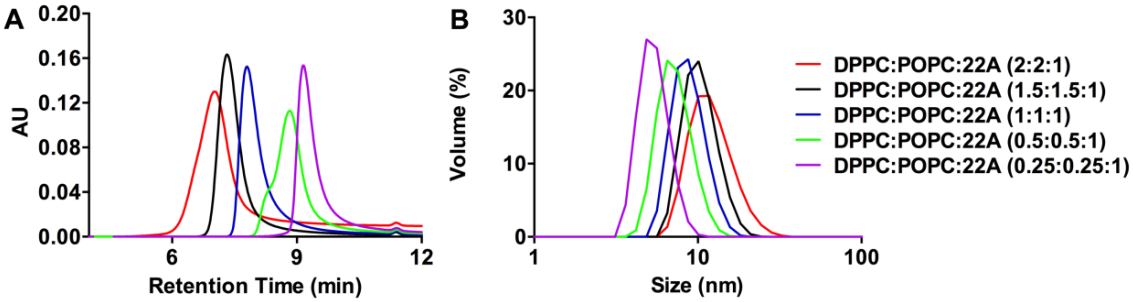

Figure 2.1: Characterization of 22A reconstituted sHDL particles. Gel permeation chromatography (A), dynamic light scattering (B).

Dynamic light scattering (DLS) analysis confirmed the increase of particle size from 5.5 nm to 12.5 nm with the increase of lipid:peptide ratio (Fig. 2.1B), which was consistent with the GPC results. The particle polydispersity index (PDI) for 0.5:1, 1:1 and 4:1 formulations were high, indicating heterogeneity of particle size (Table 2.1). Large PDI and small size for 0.5:1 and 1:1 formulation indicates insufficient amount of lipids for complete peptide binding and perhaps presence of peptide aggregates in the solution. [119] Increasing the ratio to 4:1 resulted in larger PDI

as well, indicating the presence of large lipid vehicles due to phospholipid excess. The optimal lipid to peptide weight ratio for 22A peptide appears to be between 2:1 and 3:1. The 1:1:1 weight ratio of 22A: DPPC: POPC was selected for future examination. These 22A-sHDL particles had almost no impurities and a homogeneous size of 9.0 ± 0.1 nm. Many other studies verified that the size of natural human HDL ranges from 8.5 - 12.0 nm. [120] To further confirm similarity of size for selected 22A-sHDL with endogenous HDL, purified human HDL was analyzed by GPC (supplemental Fig. 2.8). The retention time for endogenous human HDL was 7.35 min, demonstrating a size similarity to the selected 22A-sHDL.

Table 2.1: The characterization summary of different 22A-sHDL particles.

sHDL formulations (wt/wt/wt ratio)	**Retention time (min)**	**Particle size (nm)**	**Polydispersity index**
DPPC:POPC:22A (2:2:1)	7.02	12.5 ± 0.1	0.29 ± 0.07
DPPC:POPC:22A (1.5:1.5:1)	7.32	10.5 ± 0.1	0.17 ± 0.06
DPPC:POPC:22A (1:1:1)	7.80	9.0 ± 0.1	0.16 ± 0.03
DPPC:POPC:22A (0.5: 0.5:1)	8.83	7.4 ± 0.1	0.23 ± 0.04
DPPC:POPC:22A (0.25:0.25:1)	9.16	5.5 ± 0.1	0.56 ± 0.09

2.4.2 Validation of LC-MS method for peptide quantification in serum

A new LC-MS method capable of accurate and sensitive detection of 22A and its main metabolite was developed. For this, we used a different apoA-I-mimetic peptide, 5A, as an internal standard. We have compared solid-state extraction of peptide from serum using Oasis® HLB extraction cartridges (Waters, Miford, MA) and organic solvent precipitation methods for sample preparation prior to LC-MS analysis. Product recovery using the solid-state extraction method was less than 30% (data was not shown). Using methanol to precipitate proteins, the peptide recovery was greater than 90%. [121] The LC-MS analysis indicated a rapid decrease in 22A peak area in serum and the appearance of a terminal lysine-truncated metabolite (22A(-)Lys). The 22A(-)Lys metabolite was stable in plasma for up to 48 h. For the pharmacokinetic evaluation, a sum of serum concentrations of 22A and 22A (-)Lys was plotted as a function of time.

A limited validation was performed for serum extraction of peptide and LC-MS analysis. Linearity of the LC-MS analysis was observed for the peptide concentration range of 5 and 200 μg/mL, with $r^2 = 0.995$ (supplemental Fig. 2.9). The limit of quantification was determined to be 5 μg/mL. The extraction recovery of 22A ranged between 92 - 112 %. The accuracy of

concentration determination for serum samples spiked with 22A at 6, 50, 160 μg/mL ranged from 7.8 to 12.0% of the target concentrations with precision (n = 6) ranging between 2.3% and 1.5%. The inter-assay precision (n = 3) was between 3.8 - 4.3% (shown in supplemental Table 2.6). Based on the analysis of percentage of 22A Lys (-) peptide in serum for the first four time points, metabolism appears to occur in a similar rapid manner for all four groups (as shown in supplemental Fig. 2.10).

2.4.3 Pharmacokinetic evaluation of apoA-I peptide

This experiment evaluated the dependence of apoA-I peptide's pharmacokinetics on its formulation and administration route. We found that following IV administration of either 22A solution of 22A-sHDL, peptide elimination followed first-order kinetics (Fig. 2.2A and B). As shown in Table 2.2, after IV dosing the clearance (CL) of 22A was more rapid when administered as free peptide than as 22A-sHDL particles (CL = 0.025 vs. 0.014 dL/h). Given the same volume of distribution between IV formulations (Vd = 0.13-14 dL), a similar increase was observed for the 22A elimination rate constant (K_{10} = 0.18 vs. 0.112 h^{-1}) with a concomitant decrease in the elimination half-life of 22A ($T_{1/2}$ = 3.81 vs. 6.27 h). As a result of the slower clearance, area under the 22A serum concentration-time curve (AUC) was 1.79-fold higher for 22A-sHDL than for the 22A peptide. This PK difference is significant and it is possibly due to peptide proteolysis *in vivo* or potentially different organs responsible for elimination of lipid-free peptide – kidney and sHDL particles – liver [122-123]. Following IP administration of 22A and 22A-sHDL, a first order absorption was observed from the injection site into the systemic circulation. The plasma peptide levels following IP administration were lower compared with IV administration and peaked at 4 h. The AUC of 22A, after IP dosing of 22A and 22A-sHDL, were only 52.0% and 54.1% of the IV administration, respectively. Since the vascular compartment is a target organ for most HDL therapeutics, dose adjustment appears to be critical since only about half of dose reaches the systemic circulation following IP administration.

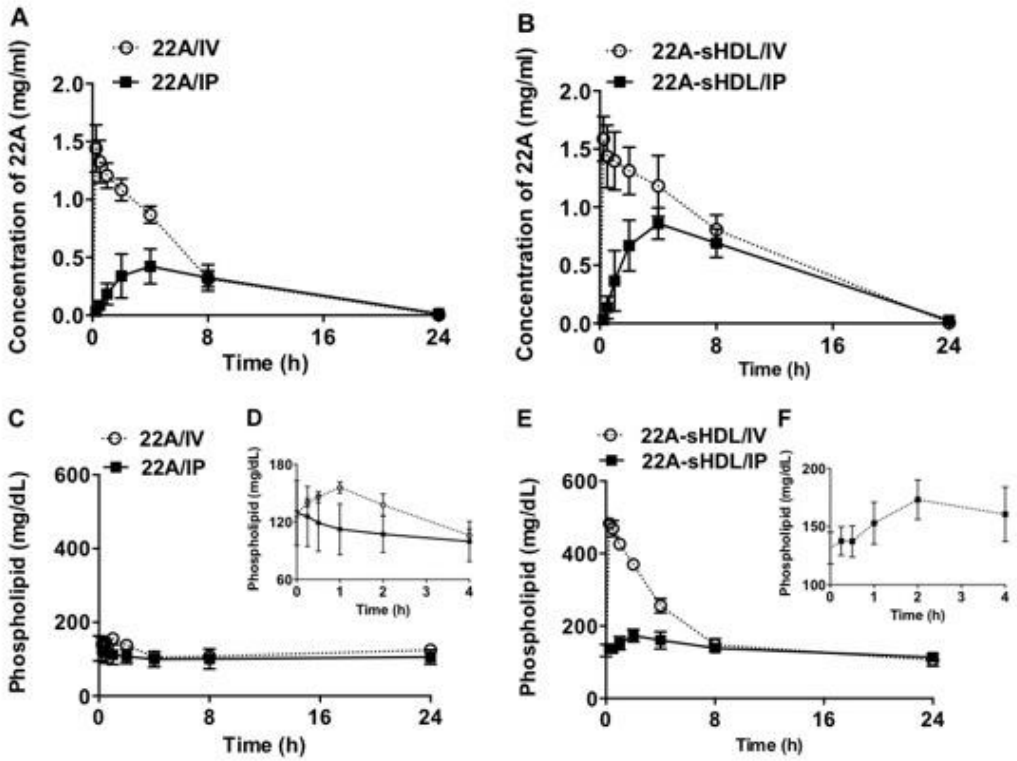

Figure 2.2: Pharmacokinetics of 22A peptide and phospholipids after administration of lipid-free 22A peptide or 22A-sHDL.Pharmacokinetics of 22A peptide after administration of lipid-free 22A peptide (panel A) or 22A-sHDL (panel B). The kinetics of phospholipid mobilization and elimination following administration of lipid-free 22A peptide (panel C and insert D) or 22A-sHDL (panel E and insert F). Sprague-Dawley rats received 75 mg/kg of 22A or 22A-sHDL by either IV or IP injection. For 22A-sHDL a dose of 75 mg/kg of peptide corresponded to a 150 mg/kg dose of phospholipids. Serum peptide concentrations were determined by LC-MS and total choline containing phospholipids was measured by a commercial choline oxidase assay.

No difference was observed when comparing the volume of distribution (Vd) of 22A after IV and IP administrations of 22A (i.e., 0.14 for IV and 0.16 dL [Vd/F × F or 0.30 × 0.52] for IP). Likewise, the clearance (CL) of 22A did not change between these two dosing routes (i.e., 0.025 for IV and 0.025 dL [CL/F × F or 0.048 × 0.52] for IP). As a result, the elimination rate constants (K) and half-lives ($T_{1/2}$) of 22A were very similar following IV and IP administrations. In contrast, the Vd of 22A was about 40% lower when administered as 22A-sHDL/IP (0.081 dL [Vd/F × F or 0.15 × 0.54]) as compared to 22A-sHDL/IV (0.13 dL). The reason for this difference is unclear but may be related to partial dissociation of 22A and phospholipid during absorption into systemic circulation following IP administration and peptide degradation/tissue binding during absorption. Since there was no difference in the CL of 22A after IV and IP treatments of 22A-sHDL (i.e., 0.014 for IV and 0.014 dL/h [CL/F × F or 0.026 × 0.54] for IP), the 22A elimination rate constant

(K) was higher (0.17 vs. 0.11 h^{-1}) and the 22A half-life ($T_{1/2}$) lower (4.14 vs. 6.27 h) following IP administration as compared to IV dosing.

Table 2.2: Pharmacokinetic parameters (% CV) of 22A peptide after 75 mg/kg doses of 22A by four different treatments.

Parameters	Groups			
	22A/IV	**22A/IP**	**22A-sHDL/IV**	**22A-sHDL/IP**
T_{max} (h)	–	4.27 (15.3)	–	4.04 (21.5)
C_{max} (mg/dL)	152.16 (5.0)^{ns}	34.83 (14.0)****	165.23 (7.6)	68.87 (19.9)****
AUC (mg*h/dL)	836.3 (7.8)***	434.5 (17.3) ****	1495.5(13.9)	809.4 (24.6)***
K_{01} (h^{-1})	–	0.33 (34.3)	–	0.35 (47.7)
K_{10} (h^{-1})	0.18 (9.6)**	0.16 (10.9)*	0.11 (16.6)	0.17 (14.4)*
$T_{1/2}$ (h)	3.81 (9.6)***	4.43 (10.9)**	6.27 (16.6)	4.14 (14.4)**
CL (dL/h)	0.025 (7.8)^{ns}	0.048 (17.4)****	0.014 (13.9)	0.026 (24.6)*
Vd (dL)	0.14 (5.0)^{ns}	0.30 (26.1)**	0.13 (7.6)	0.15 (36.16)^{ns}
AIC	15.48	12.35	23.36	7.00

Mean ± S.D. (n = 3), $^{*}p<0.05$, $^{**}p<0.01$, $^{***}p<0.001$, $^{****}p<0.0001$, ns: no significant difference compared with 22A-sHDL/IV treatment. T_{max}: Time at which the C_{max} is observed; C_{max}: the maximum plasma concentration of 22A; AUC: the area under the curve in plot of concentration of 22A against time; k_{01}: the first-order absorption rate constant; k_{10}: the first order elimination rate constant; $T_{1/2}$: the half-life of elimination; CL: apparent total clearance for 22A (CL for IV and CL/F for IP, where F is bioavailability); V_d: apparent volume of distribution for 22A (Vd for IV and Vd/F for IP, where F is bioavailability); AIC: Akaike Information Criterion.

2.4.4 Phospholipid kinetics

Monitoring lipid plasma kinetics provides indirect information not only about the formation of HDL following administration of naked apoA-I peptide, but also about the *in vivo* stability of administered sHDL and elimination of its lipid component. Administration of apoA-I peptide in sHDL formulation at a dose of 75 mg/kg peptide dose corresponds to administration of 150 mg/kg of phospholipids (PL). The plasma levels of both endogenous and 22A-sHDL administered lipids were measured by choline oxidase assay. The elimination kinetics of total PL following 22A-sHDL injection are shown in Fig. 2.2C-F. After subtracting the pre-dose plasma PL levels, the pharmacokinetic parameters were determined and summarized in Table 2.3. The maximum PL level after IV injection of sHDL reached 483.0 mg/dL and constituted a 2.7-fold

increase over the baseline PL level of 132.2 mg/dL (Fig. 2.2E). The AUC of PL after IV dosing of 22A-sHDL was 1559.6 mg*hr/dL. The AUC after IP administration of 22A-sHDL was 416.2 mg*hr/dL, indicating the bioavailability of lipids into the systemic circulation for IP injection was only 26.7%. Following IP administration of sHDL, the bioavailability of lipids is lower than that of 22A peptide (26.7% versus 54.1%), indicating some degree of dissociation of peptide from sHDL lipids during absorption. Although no exogenous PL was given in the case of peptide injection, it is believed that apoA-I mimetic peptides administered *in vivo* are capable of forming new HDL particles by lipid and cholesterol efflux via ATP-binding cassette transporter ABCA1 or by mobilizing phospholipid directly from cellular membranes [100, 124]. Hence, the slight increase in plasma lipid levels is suggestive of de novo HDL formation. As shown in Fig. 2.2C and D, a small increase in circulating lipids was observed for IV administration of 22A. In contrast, for IP administration of 22A, there was no obvious increase in plasma PL, likely due to tissue binding of peptide and decreased bioavailability to systemic circulation compared to IV dosing of peptide.

Table 2.3: Pharmacokinetic parameters (% CV) of phospholipids after 150 mg/kg doses of phospholipids by two different treatments.

Parameters	**Groups**	
	22A-sHDL/IV	**22A-sHDL/IP**
T_{max} (h)	–	2.33 (14.6)
C_{max} (mg/dL)	420.9 (2.9)	58.3 (10.1)
AUC (mg*h/dL)	1559.6 (3.9)	416.2 (14.2)****
K_{01} (h-1)	–	0.67 (46.9)
K_{10} (h-1)	0.27 (4.9)	0.25 (40.2)
$T_{1/2}$ (h)	2.57 (4.9)	2.74 (40.2)^{ns}
CL (dL/h)	0.027 (3.9)	0.10 (14.2)**
Vd (dL)	0.10 (2.9)	0.40 (35.1)*
AIC	13.51	19.34

Mean ± S.D. (n = 3), $^{*}p<0.05$, $^{**}p<0.01$, $^{****}p<0.0001$, ns: no significant difference compared with 22A-sHDL/IV treatment. ***T_{max}***: Time at which the C_{max} is observed; ***C_{max}***: the maximum plasma concentration of phospholipid; ***AUC***: the area under the curve in plot of concentration of phospholipid against time; ***k_{01}***: the first-order absorption rate constant; ***k_{10}***: the first order elimination rate constant; ***$T_{1/2}$***: the half-life of elimination; ***CL***: apparent clearance for phospholipid (*CL* for IV and *CL*/*F* for IP, where *F* is bioavailability); ***V_d***: apparent volume of distribution for phospholipid (*Vd* for IV and *Vd*/*F* for IP, where *F* is bioavailability); ***AIC:*** Akaike Information Criterion.

2.4.5 Cholesterol mobilization and esterification

To investigate the impact of lipidation and route of administration on apoA-I peptide ability to elicit pharmacological response, we examined the kinetics of plasma cholesterol biomarkers. Both free apoA-I peptide and sHDL infusions are capable of facilitating reverse cholesterol transport (RCT) by enhancing cholesterol efflux. Therefore, transient increases in plasma levels of cholesterol following treatment are expected. The kinetic changes in plasma total and unesterified cholesterol levels were measured directly by plate assays and the cholesterol ester levels were calculated (Fig. 2.3). Administration of 22A-sHDL by IV resulted in a rapid two-fold increase in total cholesterol (TC) within 0.5-1 h post-dose (Fig. 2.3A and B). The TC levels also increased slightly following IV administration of lipid-free 22A peptide ($p<0.05$ 0.25-2 h post-dose). In contrast, no statistically significant increase in TC was observed for administration of both lipid-free 22A and 22A-sHDL by IP route (Fig. 2.3A and B).

The mobilized cholesterol for 22A-sHDL infusions was predominantly unesterified or free cholesterol (Fig. 2.3C and D). Normal pre-dose levels of rat plasma free cholesterol (FC) were approximately 11.7 mg/dL, and increased to 91.0 mg/dL within 1 h for IV dosing. The IP dosing of 22A-sHDL or IV dosing of lipid-free 22A also generated an increase in FC, but the effect was much smaller than that caused by IV injection of 22A-sHDL. There was no FC increase detected after IP peptide solution administration (Fig. 2.3C and D). For 22A-sHDL IV administration, limited conversion of mobilized free cholesterol into cholesterol ester (CE) was observed (Fig. 2.3E). It is possible that mobilized free cholesterol overwhelmed the esterification capacity of circulating LCAT, or that 22A-sHDL was not a good activator of rat lecithin cholesterol acyltransferase. Cholesterol seemed to be predominantly eliminated from plasma in its unesterified form following mobilization, and returned to the baseline levels 24 h post-dose. Hence, the pharmacological effect of apoA-I peptide was remarkably affected by the formulation and administration route, in which the IV dose of 22A-sHDL generated the strongest cholesterol transfer and mobilization efficacy.

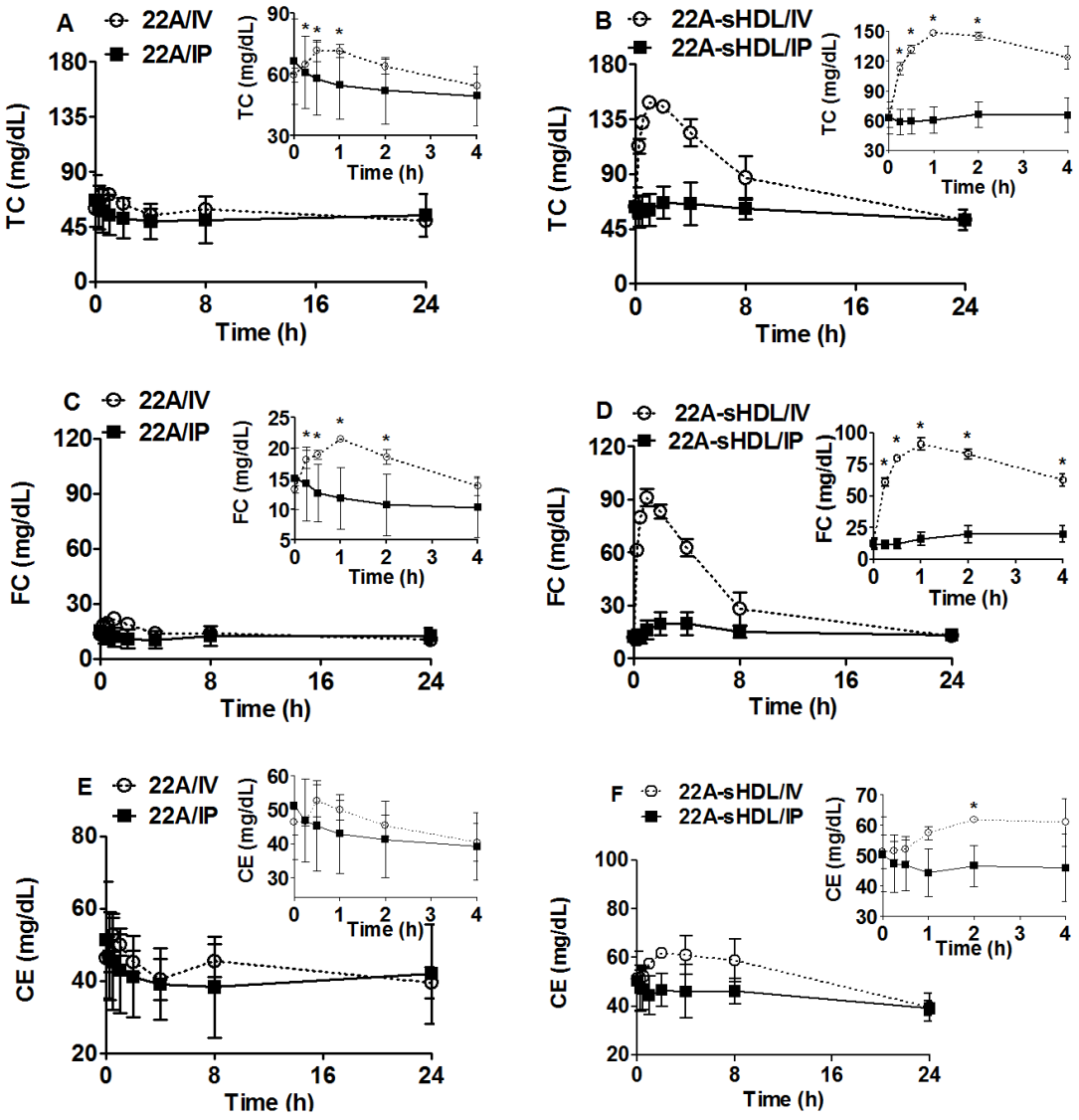

Figure 2.3: Pharmacodynamic assessment of sHDL therapeutics after IV or IP administration of lipid-free 22A peptide or 22A-sHDL.Mobilization of total TC (A and B), FC (C and D) and CE (E and F) after injection of 75 mg/kg of 22A peptide solution (A, C and E) and 22A-sHDL (B, D and F). (*) denotes statistical significant differences of TC, FC or EC changes compared with their pre-dose levels with p-values of at least < 0.05.

2.4.6 Lipoprotein Distribution of Mobilized Cholesterol

In order investigate in greater detail the mechanism of cholesterol mobilization and elimination following apoA-I peptide or sHDL administrations, we determined the relative distribution of mobilized cholesterol in the HLD, LDL and VLDL fractions. Serum lipoproteins were separated by gel permeation chromatography and total cholesterol was detected following post-column enzymatic reaction (Fig. 2.4). Again, for the 22A-sHDL IV group, drastic but

transient changes in lipoprotein profiles were observed over 24 h. Cholesterol was mobilized by injected HDL-sized particles, causing a rapid increase in particle size upon free cholesterol uptake. Since sHDL are prepared with a short, single-helical peptide, the size of the nanoparticle is not constrained by the length and structure of lipid bound full-length apoA-I, a major protein component of endogenous HDL. Therefore, we saw a rapid transition of cholesterol-carrying particles from HDL to LDL size (15 min post-dose, with the maximum increase in cholesterol levels associated with LDL-sized particles detected by 2 h post-dose). While mobilization of FC was significant, the increase in levels of CE was disproportionally lower, indicating that cholesterol is likely to be taken up by the liver in its unesterified form (Fig. 2.3D and F). At 2 h post-dose we also observed a significant increase in cholesterol levels in VLDL-sized lipoproteins. The VLDL-C increase could be due to saturation of liver receptors and enzymes that internalize, metabolize and secrete large amount of mobilized FC. However, the cholesterol changes were transient and lipoprotein-cholesterol distribution returned to a pre-dose profile 24 h post-dose. In contrast to 22A-sHDL IV group, only limited lipoprotein changes were observed for all other groups. A small transient increase in LDL-cholesterol level was observed for the 22A peptide group at 0.25 and 2 h post-dose, returning to baseline by 24 h post-dose. Due to limited cholesterol mobilization for all groups except for 22A-sHDL, it was difficult to assess differences in *in vivo* mechanisms of cholesterol efflux, mobilization, lipoprotein transfer and elimination for both lipid-fee peptide administrations and IP dosing of sHDL.

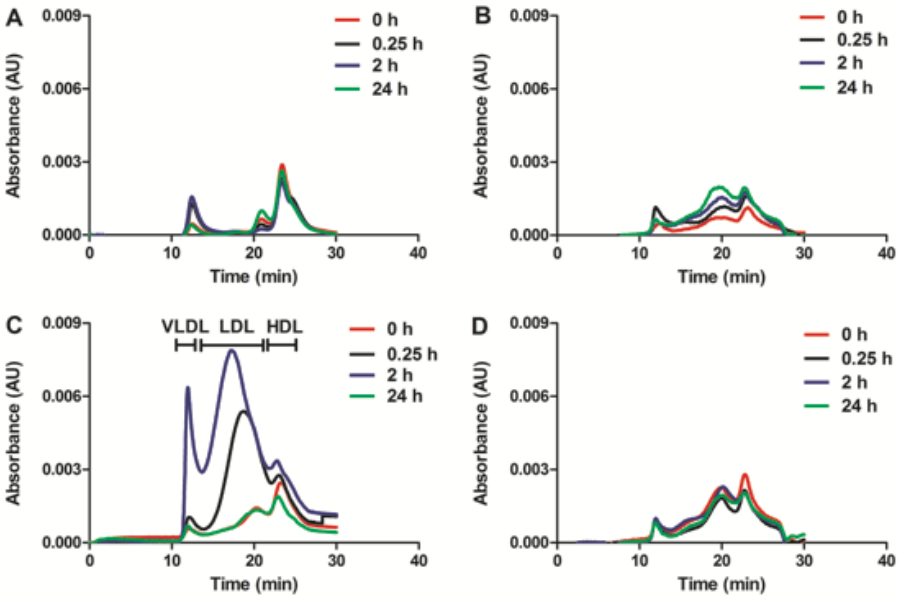

Figure 2.4: The cholesterol distribution between VLDL, LDL and HDL lipoprotein fractions following IV (A) or IP administration (B) of 22A peptide solution or IV (C) or IP administration (D) 22A-sHDL.

2.4.7 Plasma Remodeling

Potential differences in how apoA-I peptide or sHDL induce remodeling of endogenous lipoproteins were examined following *in vitro* incubation of both formulations with human serum. 22A and 22A-sHDL were added at 0, 0.15, 0.5, 1 and 3 mg/ml peptide concentrations, incubated for 30 min and separated by either 1-D native page electrophoresis (Fig. 2.5). The 1-D gels were visualized by western blot, staining for human apoA-I. The incubations were performed with a broad concentration range of 22A peptide, corresponding to *in vivo* concentration ranges of 0-1.5 mg/mL 22A, as measured by LC-MS. Compared to control serum (lane 1), all incubations showed reduction in the apoA-I content of α-HDL, seen by decreased stain intensity between 720 and 200 kDa. Along with this decrease, a 22A-peptide concentration dependent appearance of lipid-free or lipid-poor apoA-I protein was observed. The band of lipid-poor ApoA-I ran around 25-30 kDa and it had slightly higher intensity for 22A-serum incubations, but slightly larger size for 22A-sHDL-serum incubation. Hence, both naked and lipid-bound 22A were capable of associating with endogenous HDL and displacing endogenous apoA-I on HDL particles. Lipoprotein remodeling and release of lipid free apoA-I could potentially be responsible for the therapeutic effect, independent of cholesterol mobilization and RCT.

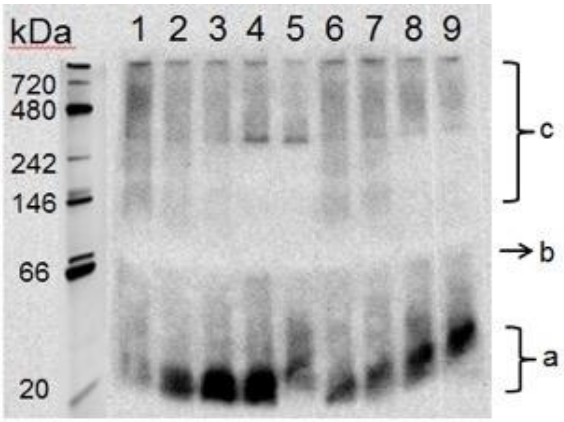

Figure 2.5: Free apoA-I and various subclasses of HDL were separated by 1-D native page electrophoresis and visualized by western blot using anti-apoA-I antibody. Lane 1 was the control serum, lane 2, 3, 4, 5 represented 0.15, 0.5, 1 and 3 mg/ml of 22A and lane 6, 7, 8, 9 represented 0.15, 0.5, 1 and 3 mg/ml 22A-sHDL, respectively. Labels a, b and c refer to the approximate positions of lipid-poor apoA-I, small pre-β HDL particles and large α-HDL particles.

2.4.8 Pharmacokinetics and pharmacodynamics correlation

Based on experimental pharmacokinetic (PK) and free cholesterol mobilization pharmacodynamic (PD) data, the indirect response PK-PD models were developed for 22A and phospholipids (Fig. 2.6). The parameters obtained from PK-PD modeling allow for the prediction of timing and magnitude of FC increase, such that the dosing regimens can be further optimized. The best fit for the PK data was obtained using a one-compartment disposition model, with lowest Akaike Information Criterion (AIC) values for both IV and IP injections without lag time. PD parameters obtained from 22A-FC or phospholipids-FC PK-PD models are listed in Table 2.4. For IP injection of the 22A group, the model failed to fit the data because FC mobilization was limited for this group.

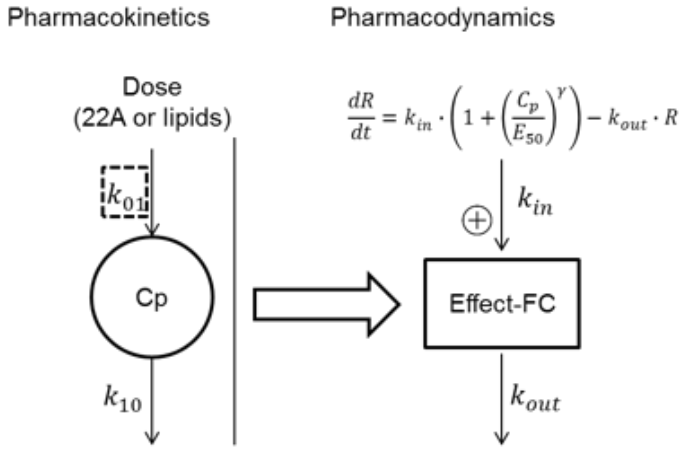

Figure 2.6: Scheme of the pharmacokinetic-pharmacodynamic (PK-PD) model based on a one-compartment PK model. k_{01}: the first-order absorption rate constant for IP groups only; k_{10}: the first order elimination rate constant; k_{in}: the zero-order constant for production of response; k_{out}: the first-order constant for loss of the response; EC_{50}: the serum concentration needed to achieve a 50% of maximum stimulation achieved at the effect site of a dosed agent; γ: steepness of the sigmoidal curve.

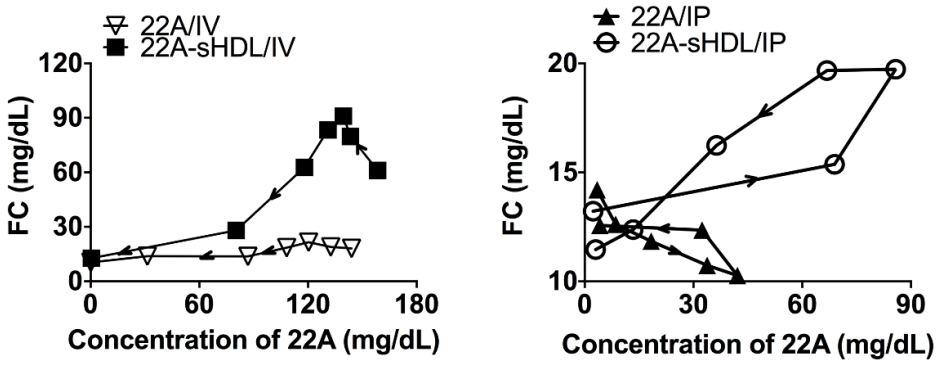

Figure 2.7: Plot of the relationship between 22A serum concentration and FC increase at individual time points following IV (A) or IP (B) administration of 22A peptide solution or 22A-sHDL at dose of 75 mg/kg.

In all four groups, a plot of the relationship between 22A serum concentration and FC levels showed an anticlockwise hysteresis, indicating a significant delay in peak levels of free cholesterol relative to the C_{max} of 22A or phospholipids (Fig. 2.7). This relationship was described by an indirect response model in which serum concentrations of 22A or PL had a stimulatory effect on the production of FC. Under normal physiological condition without HDL injection the endogenous free cholesterol level change can be described by a basic turnover model, which includes a zero-order turnover or synthesis rate constant (k_{in}) and a first-order rate constant for cholesterol elimination (k_{out}). 22A or 22A-sHDL worked as stimulatory factors having an effect on production of the response (Fig. 2.6). Among all stimulation functions, the infinite stimulation model fits the data best, giving the lowest sum of squared residual value. The parameters k_{in} and k_{out} are independent of drug concentration, thus estimated values for all three groups were similar. The free cholesterol baseline level R_0, which is assumed to be constant, can be calculated by $R_0 = k_{in}/k_{out}$ for the three modeled groups. Similar baseline values were observed to be approximately 12 mg/dL, meeting the values detected for pre-dose.

Table 2.4: Estimated pharmacodynamic parameters (with % CV of the estimate) for 22A peptide.

Parameters	**Groups**			
	22A/IV	**22A/IP**	**22A-sHDL/IV**	**22A-sHDL/IP**
k_{in} (mg/(dL*h))	30.38 (53.7)	–	30.48 (18.3)	30.60 (70.4)
k_{out} (h^{-1})	2.65 (61.6)	–	2.61 (10.5)	3.46 (60.1)
EC_{50} (mg /dL)	142.81 (8.6) ***	–	53.77 (21.2)	47.63 (247.8) ns
gamma	2.08 (71.9) ns	–	1.92 (10.6)	0.36 (90.6) ***
LogLik	-9.96	–	-15.97	-11.94

Mean ± S.D. (n = 3), ***p<0.001, ns: no significant difference versus 22A-sHDL/IV group. ***k_{in}***: the zero-order constant for production of response; ***k_{out}***: the first-order constant for loss of the response; ***EC_{50}***: the plasma concentration needed to achieve a 50% of maximum stimulation achieved at the effect site of a dosed agent; ***gamma***: steepness of the sigmoidal curve. **LogLik**: Log-likelihood of best-fitted model.

Table 2.5: Estimated pharmacodynamic parameters (with % CV of the estimate) for phospholipids.

Parameters	Groups	
	22A-sHDL/IV	**22A-sHDL/IP**
k_{in} (mg/(dL*hr))	30.48 (18.2)	22.26 (27.2)
k_{out} (hr^{-1})	2.61 (10.5)	1.85 (27.3)
EC_{50} (mg /dL)	27.11 (51.6)	74.02 (9.93) *
gamma	0.78 (10.6)	1.25 (25.2) ns
LogLik	-15.97	-7.34

Mean ± S.D. (n = 3), *p<0.05, ns: no significant difference versus 22A-sHDL/IV group. k_{in}: the zero-order constant for production of response; k_{out}: the first-order constant for loss of the response; EC_{50}: the plasma concentration needed to achieve a 50% of maximum stimulation achieved at the effect site of a dosed agent; gamma: steepness of the sigmoidal curve. LogLik: Log-likelihood of best-fitted model.

There was no significant difference between the sigmoidicity factor gamma (γ), except in the case of the 22A-PD model for the 22A-sHDL IP group, whose value was much lower than IV group. The EC_{50} represents the plasma concentration needed to achieve a 50% of maximum stimulation achieved at the effect site of a dosed agent. From Table 2.4, 22A peptide had a significantly lower EC_{50} value after IV dosing of 22A-sHDL than after IV dosing of free peptide (53.8 mg/dL versus 142.8 mg/dL), indicating that the sHDL formulation had a more potent effect on cholesterol efflux than did the free peptide. There was no significant difference between the 22A-sHDL IV and IP groups. Combining EC_{50} and γ values, lipidation of 22A increases the potency of peptide whereas altering the administration route can increase the sensitivity of cholesterol efflux towards any 22A concentration change at the effect site. However, the smaller value of phospholipids EC_{50} value for phospholipids in the 22A-sHDL IV group compared to IP groups (27.1 mg/dL versus 74.0 mg/dL) showed that the phospholipids in sHDL triggered higher cholesterol efflux after IV injection compared to IP injection at the same dose, which may result from sHDL particle dis-assembly during the absorption process (Table 2.5).

The log-likelihood value reflects the quality of the fitted model. In the 22A-sHDL IP group, the phospholipid-FC PK/PD model appears to provide a better fit for the data compared to the 22A-FC PK/PD models, as highlighted by the larger LogLik values (Tables 2.4 and Table 2.5). This better fit underscores the notion that FC mobilization is likely elicited by the presence of

cholesterol-free lipid membranes of sHDL in the plasma and to a lesser degree by peptide-mediated cholesterol efflux.

2.5 Discussion and conclusion

We found that both the physical state of the apoA-I peptide (i.e. naked or lipid-bound sHDL) and the route of administration (IV versus IP) profoundly affected its pharmacokinetics and the mechanism of eliciting pharmacological response. Only lipidated 22A-sHDL administered by IV resulted in rapid and massive mobilization of free cholesterol. Additionally, only a partial conversion of FC to CE was observed, and all mobilized cholesterol was subsequently eliminated within 24 h. The difference in plasma-mobilized cholesterol levels did not directly correlate with differences in the pharmacokinetics of apoA-I peptide administered in a lipid-free form or in the bioavailability of apoA-I peptide to systemic circulation following IP dosing. The half-life of peptide administered in lipid-free form was only 0.61-fold shorter relative to 22A-sHDL. However, 1-2 h post-dose the maximum levels of mobilized FC reached 22 mg/dL for 22A and 91 mg/dL for 22A-sHDL (Fig. 2.3C, D, Table 2.2), constituting a 1.3 and 5.3 increase from pre-dose level, respectively. This significant difference in the magnitude of plasma cholesterol mobilization indicated a potential mechanistic difference in how cholesterol efflux is elicited for lipid-free peptide and sHDL *in vivo*. The rapid cholesterol mobilization following IV administration of sHDL was likely caused in part by a physical partitioning of FC from cellular membranes to cholesterol-free lipid bilayers of sHDL. For administration of lipid-free 22A peptide, cholesterol mobilization possibly occurs in a receptor-mediated manner following interaction with peptide or de novo formed HDL following of plasma remodeling of lipoprotein by 22A peptide. Extensive mobilization of FC in serum led to rapid conversion of the injected sHDL particles to LDL-sized, cholesterol-loaded particles, causing a spike in LDL-C levels between 2-8 hours post-dose. These transient increases in LDL-C and triglyceride levels have been observed previously for both free ApoA-I and HDL infusions, and has been attributed to saturating the liver's capacity to excrete free cholesterol and inhibiting hepatic and lipoprotein lipases [125]. While the changes in lipoproteins appeared to be very dramatic following 22A-sHDL IV infusion, they were also transient, as all lipoprotein levels returned to baseline 24-hours post-dose. Similar transient changes in lipoproteins have been observed in clinical settings for infusions of other HDL products, such as CER-001 [126] and ETC-216. [127]

When either lipid-free or lipidated peptide was mixed with serum, each was capable of remodeling of endogenous lipoproteins, leading to the appearance of a lipid-poor apoA-I fraction. The appearance of lipid-poor apoA-I indicates that, upon administration, 22A peptide binds to endogenous HDL particles and causes endogenous apoA-I displacement from HDL. It is unclear how this phenomenon impacts the anti-atherosclerotic activity of apoA-I mimetic peptide as well as how the sequences of various peptides influence endogenous lipoprotein binding. The PK-PD modeling that correlated 22A with an increase in FC, a plasma biomarker of cholesterol efflux, revealed EC_{50} values to be much lower for 22A-sHDL-IV compared with lipid-free-22A-IV (Table 2.4).

The initial decision to use reconstituted HDL particles rather than lipid-free apoA-I in clinical development occurred in the 1990s following the first clinical evaluation by Miller et al. [95, 107] In these studies, prolonged IV infusion and bolus administration of lipid-free apoA-I up to 50 mg/kg dose failed to increase plasma levels of HDL-C. Instead, transient increases in LDL particles were noted and attributed to inhibition of lipoprotein and hepatic lipases. In contrast, infusions of reconstituted HDL particles at 25 and 40 mg/kg of apoA-I resulted in transient increases in HDL unesterified cholesterol levels, followed by cholesterol esterification and elimination. Since these first clinical trials, the elevation of HDL-C levels has become a primary biomarker of sHDL's pharmacological effect. The clinical dose selection and preclinical optimization for many follow-on HDL products (ETC-642, CER-001) were performed based on the HDL-C increase as biomarker. [94, 97] However, it is becoming clear that there are mechanistic differences in how sHDL and free apoA-I elicit cholesterol efflux. Lipid-free apoA-I interacts with ABCA-1 receptors to efflux, forms de novo HDL and remodel existing lipoproteins. In contrast, the cholesterol-free lipid bilayers of sHDL particles are strong acceptors of cholesterol from ABCG1, SR-BI, and via passive efflux from cellular membranes. Indeed, recent studies have shown that SR-BI receptors are largely responsible for free cholesterol elevation following rHDL infusion, and that phospholipids, not ApoA-I, dictate FC efflux. [128-129] Because of these factors, CSL-112 pharmacological efficacy in early clinical trials was monitored by increases in ABCA1 cholesterol efflux capacity of patient plasma following drug administration. [130]

Several studies have directly compared the anti-inflammatory effects of apoA-I and HDL administered by IV infusion in animal models of arthritis and a carotid peri-arterial collar model. [104] When lipid-free apoA-I and reconstituted HDL were administered at a low dose of 8 mg/kg,

they exhibited similar measurable anti-inflammatory activity. This indicates that some of protective mechanisms of apoA-I and sHDL infusions could not be characterized simply by monitoring cholesterol mobilization, and additional biomarkers are needed to establish the PK-PD relationship.

Direct comparisons of the anti-atherosclerotic potency of IP injections of 30 mg/kg of either ATI-5261 peptide or reconstituted HDL were performed in a high-fat diet fed ApoE$^{-/-}$ mouse model of atherosclerosis. [64] While no increase in plasma cholesterol levels was detected, sHDL injections showed slightly better atheroma reduction, however the difference was not statistically significant. In our study, IP administrations resulted in only limited plasma cholesterol mobilization, with slightly higher mobilization for sHDL infusions compared to those using lipid-free peptide. Following IP dosing 52% of lipid-free apoA-I peptide, 54% of lipidated apoA-I peptide and 27% of sHDL phospholipids reached the systemic circulation. In addition, the values for absorption (K_{01}) and elimination (K_{10}) constants differed for PL and 22A following IP administration of 22A-sHDL (Tables 2.2 and 2.3), indicating that some of 22A-sHDL was dissociated prior to absorption. Peptide tissue-binding, proteolysis and disassembly of 22A-sHDL particles are potential reasons for the reduced and different bioavailabilities. Peptide tissue-binding and proteolysis depend on the primary sequence of peptide and, thus, differ for various peptides and full-length apoA-I. Stability of sHDL *in vivo* and extent of endogenous HDL remodeling depend on the lipid binding affinity of amphipathic helixes toward lipid used in sHDL formulation, endogenous lipoproteins and plasma lipid membrane as well as the peptide's tendency to self-associate. [96, 131] Furthermore, lipid formulation of sHDL (peptide-lipid ratio, lipid type and sHDL particle size) affects particle stability, cholesterol affinity and interaction with LCAT. [132] Thus, *in vivo* behavior of apoA-I peptide and sHDL formulation could be distinctly different for various peptide sequences and lipid formulations.

The magnitude of cholesterol mobilization and pharmacokinetic parameters depend on the dose of administered apoA-I peptide. The dose used in this study, 75 mg/kg, was selected to assure the detection of peptide in plasma following IP administration. The selected dose is slightly higher than doses used in animal pharmacology studies for apoA-I and HDL, which range between 1 and 50 mg/kg. [133-134] However, in phase I clinical dosing the infusions were given up to 45 mg/kg for CER-001, 135 mg/kg for CSL-112 and 50 mg/kg for lipid free apoA-I. [94-96] Hence, 75 mg/kg was a reasonable dose for the current study. In addition, our study was conducted in healthy rats

to allow for the multiple blood draws required to determine for PK and PD parameters. However, the cholesterol pool mobilized in healthy rats is likely to be different from that present in human atheromas and, thus it would be beneficial to evaluate how apoA-I lipidation affects cholesterol mobilization in hyperlipidemic disease models.

The results of this study emphasize the criticality of considerations for formulation, route of administration, and dose used in pharmacological studies of apoA-I peptide and sHDL particles. Historic drug development considerations for the selection of HDL dose and formulation were based on measurements of plasma cholesterol level increase, which were primarily observed upon IV administration of sHDL particles. Yet, the increase in plasma cholesterol primarily depends on sHDL lipid composition and particle stability *in vivo*, and is seen upon administration of relatively high doses of sHDL. Thus, endogenous lipoporotein remodeling, anti-inflammatory effects and apoA-I protein mediated ABCA-1 efflux that are exhibited at lower doses are often underemphasized. Consequently, a mechanistic understanding of which therapeutics effects of sHDL are mediated by lipoprotein particles and which are mediated by their apoA-I component, as well as correlating elicited pharmacologic effect *in vivo* with the actual systemic concentrations, AUC and pharmacokinetic parameters for administered apoA-I peptide, will significantly improve clarity around the development of HDL mimetics. Identification of *in vivo* biomarkers indicative of HDL mimetic potency in addition to HDL-C plasma increase and rapid assessment of *in vivo* of PK and biomarker response for novel apoA-I mimetic peptides could improve their development outcomes, as extensive *in vitro* optimization does not account for peptide proteolysis and excessive tissue binding *in vivo*.

2.6 Supplementary information

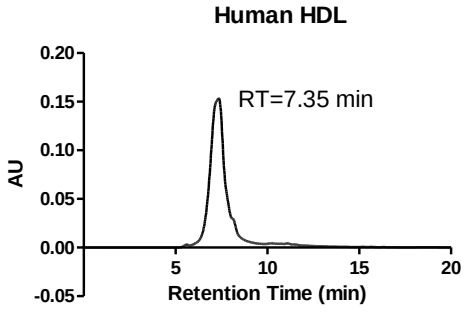

Figure 2.8: The retention time of isolated human HDL analyzed by gel permeation chromatography.

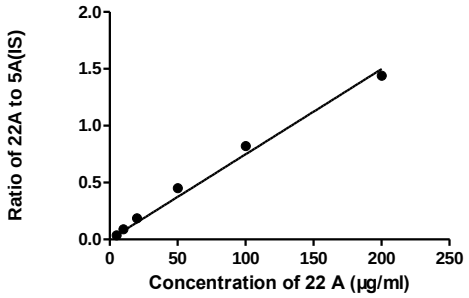

Figure 2.9: Linearity of calibration curve for the determination of 22A concentrations in rat serum (r^2 = 0.995).

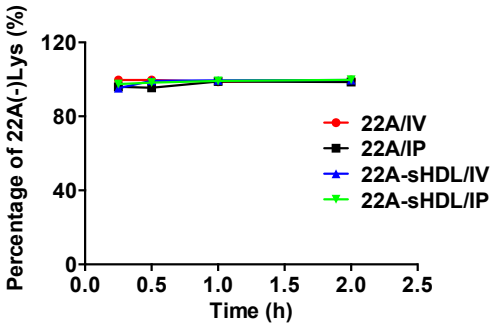

Figure 2.10: The percent of 22A (-) Lys peptide in serum at the first four time points after injection.

Table 2.6: Precision, accuracy and recovery for the determination of 22A in rat serum (n=6).

Concentration (µg/ml)		**RSD (%)**		**RE (%)**	**Recovery (%)**
Added	**measured (mean)**	**intra-assay**	**inter-assay**		
6	6.7	2.29	4.30	12.00	112.0 ± 2.6
50	55.9	2.41	3.92	11.80	111.8 ± 2.7
160	147.5	1.54	3.80	-7.84	92.2 ± 1.4

Chapter 3 : Effect of synthetic high-density lipoproteins modification with polyethylene glycol on pharmacokinetics and pharmacodynamics

This research was originally published in the *Molecular Pharmaceutics*. Li D, Fawaz MV, Morin EE, Ming R, Sviridov D1, Tang J, Ackermann R, Olsen K, Remaley AT, Schwendeman A. Effect of Synthetic High Density Lipoproteins Modification with Polyethylene Glycol on Pharmacokinetics and Pharmacodynamics. Mol Pharm. 2018 Jan 2;15(1):83-96.

3.1 Abstract

Synthetic high density lipoprotein nanoparticles (sHDL) capable of mobilizing excess cholesterol from atherosclerotic arteries and delivering it to the liver for elimination have been shown to reduce plaque burden in patients. Unfortunately, sHDLs have a narrow therapeutic index and relative to the endogenous HDL shorter circulation half-life. Surface modification with polyethylene glycol (PEG) was investigated for its potential to extend sHDL circulation *in vivo*. Various amounts (2.5, 5 and 10%) and different chain lengths (2 and 5 kDa) of PEG-modified lipids were incorporated in sHDL's lipid membrane. Incorporating PEG did not reduce the ability of sHDL to facilitate cholesterol efflux, nor did it inhibit cholesterol uptake by the liver cells. By either adding more PEG or using PEG of longer chain lengths the circulation half-life was extended. Addition of PEG also increased the area under the curve for the phospholipid component of sHDL ($p < 0.05$), but not for the apolipoprotein A-I peptide component of sHDL — suggesting sHDL is remodeled by endogenous lipoproteins *in vivo*. The extended phospholipid circulation led to a higher mobilization of plasma free cholesterol, a biomarker for facilitation of reverse cholesterol transport. The area under the cholesterol mobilization increased about 2 to 4-fold ($p < 0.05$), with greater increases observed for longer PEG chains and higher molar percentages of incorporated pegylated lipids. Mobilized cholesterol was associated primarily with the HDL fraction, led to a transient increase in VLDL cholesterol, and returned to baseline 24 h post-dose. Overall, pegylation of sHDL leads to beneficial changes in sHDL particle pharmacokinetic and pharmacodynamic behaviors.

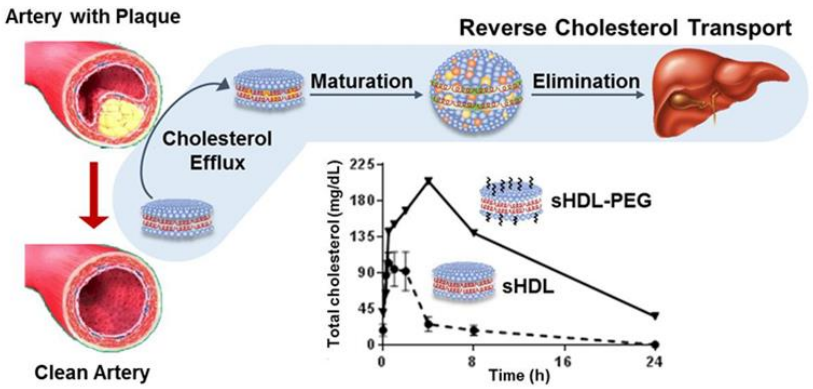

Figure 3.1: Table of Contents/Abstract Graphic.

3.2 Introduction

Cardiovascular disease (CVD) is the leading cause of death in the United States, responsible for 17% of national health expenditures.[135] High-density lipoprotein cholesterol (HDL-C) levels are known to inversely correlate with the risk of CVD.[136] HDL is natural nanoparticle composed primarily of apolipoprotein A-I (ApoA-I) and lipids. One of the key functions of HDL is to maintain cholesterol homeostasis through reverse cholesterol transport (RCT), whereby HDL effluxes free cholesterol from peripheral tissues through ATP-binding cassette transporters (ABCA1 and ABCG1) and then delivers it to liver for excretion by the scavenger receptor B type I (SR-BI) receptor.[137] Thus, the idea of administrating synthetic HDL (sHDL) to facilitate RCT and promote the regression of atherosclerotic plaque has gained significant interest.[18, 138-140] Several sHDL therapeutic products have been developed that consist of either ApoA-I protein purified from human plasma, recombinant ApoA-I, or ApoA-I mimetic peptides.[112, 141] The protein component is usually combined with phospholipids to form sHDL nanoparticles, which are administered intravenously following a cardiovascular event. It was hypothesized that the acute administration of several sHDL infusions could lead to a rapid reduction in plaque volume and prevent the likelihood of subsequent cardiovascular events.[12, 140] A number of sHDL products have been tested in Phase I and II clinical trials and were able to increase HDL-C levels, reduce inflammation and decrease atherosclerotic plaque volume.[141]

Despite initial clinical success, the translation of sHDL nanomedicine into an FDA approved therapy has been difficult. This class of drugs has a unique pharmacokinetic-pharmacodynamic relationship. Administration of sHDL causes rapid mobilization of cholesterol, which is subsequently delivered to the liver for elimination.[11] The amount of mobilized cholesterol

is often several folds higher than pre-dose plasma cholesterol levels, leading to saturation of hepatic receptors and pathways for cholesterol metabolism.[142] Thus, administration of sHDL often results in drug-related toxicity exhibited by transient elevation of liver transaminases (ALT and AST), triglycerides, low and very low-density lipoprotein cholesterol levels (LDL-C and VLDL-C). In addition, the half-life of endogenous ApoA-I protein in humans is only 3.3 days.[143] It is believed that the protein participates in multiple cycles of RCT by forming HDL, effluxing cholesterol, delivering it to the liver, and returning to the peripheral tissues to efflux more cholesterol.[11] In contrast, administration of sHDL results in a protein or peptide half-life of only 8-12 hours.[33, 144]

Due to the rapid elimination of sHDL, the duration of time following administration when sHDL plasma levels remain above the level required to obtain therapeutic effect is quite short. This rapid elimination necessitates either frequent dosing, which is inconvenient for patients especially for an intravenous product, or administration of relatively high doses, which can lead to off-target toxicity. In addition, following administration *in vivo*, sHDL nanoparticles rapidly interact with endogenous lipoproteins by exchanging lipid and protein components. This is a natural phenomenon in lipoprotein metabolism, known as remodeling, that leads to the disassembly of administered sHDL particles, and results in differences in elimination kinetics of ApoA-I and lipid components of sHDL.[31] This remodeling, in turn, affects both the efficacy and safety of administered sHDL. The main hypothesis of this study is that by modifying the sHDL surface with polyethylene glycol, it may be possible to slow down sHDL remodeling by endogenous lipoproteins, thereby reducing sHDL nanoparticle elimination by reticuloendothelial system, increasing its circulation half-life *in vivo* and altering its antiatherogenic properties.

Polyethylene glycol (PEG) has been widely used to coat or pegylate nanoparticle surfaces to archive "stealth-like" characteristics.[68] Pegylated drug delivery systems have been shown to be more physically stable *in vitro* and have longer circulation half-lives *in vivo*, resulting from the ability of PEG to escape uptake by the reticuloendothelial system.[145] Pegylation has been shown to be clinically safe and currently used in several products approved by the Food and Drug Administration.[146] It has been reported that by conjugating PEG to ApoA-I protein, protein *in vivo* circulation was prolonged and anti-inflammatory activity in a murine model of atherosclerosis was improved[147]. The PEG density on the nanoparticle surfaces, PEG molecular weight, and branch structure are all known to affect nanoparticle circulation and efficacy[148], but this has not been

systematically investigated for sHDL. Thus, to test our hypothesis, we incorporated PEG-modified phospholipids in sHDL nanoparticles and examined how the degree of surface modification and PEG chain length affected sHDL pharmacokinetics and pharmacodynamics *in vivo.*

The model sHDL used in this study is a peptide-based sHDL, ETC-642. ETC-642 was previously examined in single- and multiple-dose clinical studies in dyslipidemic patients.[144, 149] It was shown that infusion of ETC-642 increased HDL-C levels at doses as low as 3 mg/kg and was well tolerated by patients at doses up to 30 mg/kg.[149] However, the plasma circulation half-life of 22A-peptide in humans was only ~12 h, which is significantly shorter than the reported half-life of endogenous ApoA-I protein, 68 h.[27, 150] In this study, the abilities of pegylated sHDL to promote cellular cholesterol efflux and facilitate cholesterol uptake *in vitro* were examined. The remodeling of pegylated sHDL by endogenous lipoproteins was also examined *in vitro,* following incubation with human serum, as well as *in vivo* following administration to Sprague-Dawley (SD) rats. Biodistribution of unmodified and pegylated sHDL nanoparticles was examined in mice. The pharmacokinetic properties of both unmodified and pegylated sHDL nanoparticles in addition to their abilities to mobilize, esterify and eliminate cholesterol were also examined in SD rats.

3.3 Materials and methods

3.3.1 Materials

ApoA-I mimetic peptides 22A (PVLDLFRELLNELLEALKQKLK) and 5A (DWLKAFYDKVAEKLKEAFPDWAKAAYDKAAEKAKEAA) were synthesized by Genscript (Piscataway, NJ). The peptide purities were determined to be over 95% by reserve phase HPLC. 1,2-dipalmitoyl-*sn*-glycero-3-phosphocholine (DPPC), N-(Carbonyl-methoxypolyethyleneglycol 2000)-1,2-distearoyl-*sn*-glycero-3-phosphoethanolamine (DSPE-PEG-2k) and N-(Carbonyl-methoxypolyethyleneglycol 5000) -1,2-distearoyl-*sn*-glycero-3-phosphoethanolamine (DSPE-PEG-5k) were purchased from NOF Corporation (White Plains, NY). DSPE-PEG-FITC amd Bodipy-labeled cholesterol were purchased from Avanti Polar Lipids, Inc (Alabaster, AL). All other materials were obtained from commercial sources.

3.3.2 Preparation of sHDL particles

All investigated particles were prepared using a lyophilization method. Briefly, 22A peptide, DPPC, DSPE-PEG2000 (PEG-2k) or DPSE-PEG5000 (PEG-5k) were dissolved in acetic acid at a molar ratio of 1:7.15 for peptide to total lipids. The molar percentage of DSPE-PEG2000 in total lipids was 0, 2.5%, 5% and 10% for sHDL, sHDL-PEG-2k (2.5%), sHDL-PEG-2k (5%),

and sHDL-PEG-2k (10%), respectively. Similarly, HDL-PEG-5k (5%) contained DSPE-PEG5000 at 5% of total lipids. After freeze-drying for over 24 hours, PBS (pH = 7.4) was added to hydrate to a final 22A peptide concentration of 10 mg/mL. The mixture was vortexed briefly, heated to 50°C for 10 min and cooled to 25°C for 10 min, and this cycle repeated three times. sHDL particle concentrations are expressed in terms of 22A peptide concentration.

sHDL and sHDL-PEG particles loaded with DiD fluorescent dye or bodipy-labeled cholesterol were prepared by a freeze-drying method that dissolved DiD or labelled cholesterol in glacial acetic acid together with all other components. The final concentration of bodipy-cholesterol after hydration of lyophilized powder was 30 μg/mL and 20 μg/mL for DiD.

3.3.3 Characterization of HDL and HDL-PEG particles

The purity and particle size of sHDL and sHDL-PEG was analyzed by gel permeation chromatography (GPC), with UV detection wavelength of 220 nm, using a Tosoh TSK gel G3000SWx 7.8mm x 30cm column (Tosoh Bioscience, King of Prussia, PA) on Waters Breeze Dual Pump system. Samples were diluted to 1 mg/ml and 50 μL injection volume was used. The samples were eluted with PBS (pH 7.4). Particle size distribution was also determined by dynamic light scattering (DLS), using a Zetasizer Nano ZSP, Malvern Instruments (Westborough, MA). The samples were diluted to 1 mg/ml prior to analysis.

3.3.4 Cholesterol efflux evaluation

Baby hamster kidney (BHK)-mock and BHK cells transfected with ABCA1 or SR-BI receptors were grown in Dulbecco's modified eagle medium with 10% FBS and 1% pen strep glutamine. 10^5 cells were then seeded into 24-well plates and grown for 24 hours. Cells were washed with PBS (pH 7.4) once at room temperature and labeled with cholesterol for 24 hours in DMEM/BSA/antibiotic media (0.5 mL) containing 1 μCi of [^{3}H] cholesterol/mL of media. Subsequently, labeled cells were washed with PBS (pH 7.4) twice to remove [^{3}H] cholesterol that was not taken up by cells. Tritium-labeled cholesterol was effluxed from cells for 18 hours, using various lipid complex acceptors (5 μM) in duplicate. Finally, all cell media (0.5 mL) was removed into separate Eppendorf tubes and centrifuged at 10,000 rpm for 5 min. Remaining cells were lysed with 0.1%SDS/0.1M NaOH solution for 2 hours. Radioactive counts of media and cell fractions were measured separately, using a Perkin Elmer liquid scintillation counter. Percent cholesterol effluxed from cells was calculated by dividing media counts by the total sum of media and cell counts and then multiplying this number by 100%.

3.3.5 Liver cell uptake of sHDL particles and sHDL cholesterol

HepG2 cell uptake of sHDL and sHDL-PEG loaded either with DiD fluorescent dye or with bodipy-labeled cholesterol was visualized by confocal laser scanning microscopy and quantified by flow cytometry. Briefly, liver hepatocellular carcinoma (HepG2) cells were cultured in Dulbecco's Modified Eagle Medium with 10% FBS and 1% Pen Strep Glutamine and maintained in an incubator at 37℃ and 5% CO_2. On day 0, 10^4-10^5 cells were seeded in a MatTek 35 mm petri dish in DMEM. The next day, media was aspirated and cells were washed with PBS. Fresh media containing sHDL and sHDL-PEG loaded with DiD or bodipy-labeled cholesterol were added at a final 22A concentration of 100 μg/ml. After incubation at 37 °C for 5, 15, 30, 60, and 120 min, cells were washed twice with PBS followed by fixation with 4% paraformaldehyde in PBS for 15 min at room temperature. 1% Triton-X solution was then added to the dish for 15 min and washed with PBS twice. Finally, the cell nuclei were stained with DAPI. The nuclei and bodipy fluorescence images were acquired on a Nikon A-1 Spectral Confocal microscope system (Nikon Corporation, Tokyo), with an excitation wavelength of 644 nm for DiD and 495 nm for bodipy. Quantification of cellular fluorescent signal was performed using a cell sorter (Beckman Coulter FC500 5-colour analyzer).

To understand the effect of sHDL concentration on cholesterol uptake, a similar experiment was conducted in which the bodipy-labelled cholesterol concentration was held constant while the sHDL concentration varied. Briefly, cells were incubated with sHDL or sHDL-PEG2k (10%) particles loaded with bodipy-cholesterol at a concentration of 0.3 μg/mL for 1 hour at 37 °C. The final sHDL concentration was 1 mg /mL, 0.5 mg/mL or 0.1 mg/mL in terms of 22A peptide concentration. Cells were washed twice with PBS and analyzed by flow cytometry.

3.3.6 Particle remodeling in serum

To study the remodeling of sHDL by endogenous lipoproteins, sHDL or sHDL-PEG-2K (5%) particles were incubated with human serum at 1 mg/mL 22A concentration at 37 °C for 1 h with shaking at 300 rpm. To track the exchange of DSPE-PEG 2000 between sHDL and endogenous lipoproteins, sHDL particles were prepared with fluorescent FITC-DSPE-PEG-2K, which has excitation and emission spectrum peak wavelengths of approximately 495 nm and 519 nm respectively. The cholesterol distribution among different lipoproteins in samples after incubation was analyzed using Waters HPLC system equipped with a Superose 6, 10/300 GL column (GE Healthcare, Piscataway, NJ) and on-line detection of cholesterol was achieved via

post-column enzymatic reactions[151]. The post column reaction was done using a 5 mL reaction coil at 37°C by mixing separated lipoprotein and enzymatic reagent whose flow rate was 0.2 mL/min. The UV absorbance of the product was detected at 490 nm. The enzymatic reagent solution was composed of 100 mM phosphate buffer (pH 7.0), 4 M sodium chloride, 0.2% triton X-100, 10 mM sodium cholate, 2.5 mM 4-aminoantipyrine, 7.5 mM 2-hydroxy-3,5 dichlorobenzene, 0.0625 U/ml cholesterol oxidase, 1.25 U/ml peroxidase, 1.25 U/ml lipase and 0.1 U/ml cholesterol ester hydrolase. To examine the distribution of FITC-DSPE-PEG-2K among endogenous lipoproteins, the HPLC fractions of HDL, LDL and VLDL were collected after separation, and fluorescence for each fraction was determined, using a Synergy NEO HTS Multi-Mode Microplate Reader (Bio-Tek).

To determine the effect of sHDL induced remodeling of endogenous HDL subclasses, lipoproteins after incubation were separated by one-dimensional native polyacrylamide gel electrophoresis (PAGE) based on particle size and visualized by western blot for ApoA-I protein. Samples were subject to electrophoresis in 10-well Tris-Borate-EDTA gradient (3-25%) acrylamide native gels (Jule, Inc., Milford, CT). For each line, 5 µl of human serum after incubation with PBS, 22A peptide or 22A-sHDL was mixed with 5 µl of 2X TBE sample buffer and 6 µl of the resulting mixtures were loaded per line. Gels were run at 200 V until the sample dye was 2.5 cm away from the bottom of the gel. Proteins were visualized by western blot by transfer onto PVDF membrane and incubation overnight with anti-human apoA-I-HRP conjugated antibody (Meridian Life Science, Memphis, TN). Bands were visualized using SuperSignal™ West Pico Chemiluminescence Substrate (Thermo Fisher) and images were acquired on a FluorChem M Imager (Protein Simple, San Jose, CA). Image J was used for spot densitometry.

3.3.7 Pharmacokinetic and pharmacodynamic study in rats

The sHDL and sHDL-PEG formulations were prepared at a final 22A concentration of 20 mg/mL in PBS. Sixteen male Sprague-Dawley rats were randomly assigned to four groups: sHDL, sHDL-PEG-2k (5%), sHDL-PEG-2k (10%) and sHDL-PEG-5k (5%), containing four rats each. All rats were fasted overnight before dosing and received different sHDL formulations at the dose of 50 mg/kg based on 22A peptide concentration via tail vein injection. Blood samples of approximately 0.3 mL were collected from the jugular vein in heparinized BD centrifuge tubes (BD, Franklin Lakes, NJ) at pre-dose and 0.25, 0.5, 1, 2, 4, 8, 24 and 48 hours after dosing. Serum

samples were separated immediately by centrifugation at 10,000 rpm for 10 minutes at 4°C and stored at -20°C until further analysis.

3.3.8 Measurement of peptide serum concentration and pharmacokinetic analysis

To determine 22A peptide concentration in serum, 10 μL of 5A peptide (3 mg/mL) was added to 10 μL of each serum sample as an internal standard (IS). The sample was then mixed with 100 μL of methanol containing 0.1% acetic acid and vortexed for 30 seconds. The mixture was centrifuged at 10,000 rpm for 10 minutes at 4°C and supernatant was collected for LC-MS analysis. Samples were injected into the Agilent 6520 Accurate-Mass Q-TOF LC/MS system equipped with a dual electrospray ionization source (Dual-ESI) (Agilent Technologies, CA). An Agilent 300SB-C18 column (2.1 mm × 50 mm, 3.5 μm) was used for separation and the UV detector was set to a wavelength of 220 nm. The flow rate was 0.3 mL per minute, with the initial mobile phase composed of 90% solvent A (water containing 0.1% v/v formic acid) and 10% solvent B (methanol containing 0.1% v/v formic acid). A linear gradient to 40% solvent A and 60% solvent B at 3.5 min, followed by an additional linear gradient to 5% solvent A and 95% solvent B at 8 min was used. Mass spectra were acquired in negative ion mode with the mass range set at m/z 100-3200. The conditions used for the ESI source included a capillary voltage of 3500 V, a drying gas temperature of 332°C, a drying gas flow of 5 L/min, and a nebulizer pressure of 45 psi as well as a fragmentor voltage of 225 V. MassHunter Workstation software (Agilent Technologies, CA) was used for data acquisition and processing. The extracted ion chromatogram (EIC) of 22A was exported from the total ion chromatogram (TIC) by monitoring the key fragment of 22A at m/z 656.6. Since 22A(-)Lys (21A) is the main metabolite of 22A peptide after administration, we also determined 22A(-)Lys levels. The EIC of 22A(-)Lys metabolite and IS 5A was extracted at m/z 832.5 and m/z 844.4, respectively. The total integral area of 22A peak and 22A(-)Lys metabolite peak was used to calculate concentration of 22A. A pharmacokinetic non-compartmental analysis (NCA) was also performed to derive basic pharmacokinetic parameters of peptide using Phoenix© WinNonlin® Version 7.3 (Pharsight Corporation, Mountain View, CA, USA), including maximum serum concentration (C_{max}), area under the serum concentration-time curve (*AUC*), elimination rate constant (K_{10}), elimination half-life ($T_{1/2}$), total clearance (*CL*) and volume of distribution (*Vss*) for each rat using Phoenix© WinNonlin® Version 6.3 (Pharsight Corporation, Mountain View, CA, USA). Coefficient of variation was calculated for each parameter.

3.3.9 Quantification of serum phospholipids and cholesterol

The levels of serum phospholipids (PL), total cholesterol (TC), and unesterified or free cholesterol (FC) were determined by enzymatic analysis, using commercially available kits (Wako Chemicals, Richmond, VA). Cholesterol ester levels (CE) were calculated as the difference between TC and FC levels at each time point. Briefly, serum samples were diluted with PBS (pH 7.4) for TC and FC detection, or with Milli Q water for PL detection. Defined amounts of standards or diluted samples were transferred to 96-well plates (50 μL, 60 μL and 20 μL for TC, FC and PL analyses, respectively), and assay reagents were added per manufacturer's instructions. The plates were gently shaken using an orbital shaker and incubated at 37 ˚C for 5 min. The UV absorbance at 600 nm was measured by a Synergy NEO HTS Multi-Mode Microplate Reader (Bio-Tek). A pharmacokinetic non-compartmental analysis (NCA) was also performed to derive basic pharmacokinetic parameters of phospholipids using Phoenix© WinNonlin® Version 7.3 (Pharsight Corporation, Mountain View, CA, USA). The pharmacodynamic effect in each mouse was determined as the area under the total effect curve (*AUEC*) from dosing time point to 48 hours after dosing, which were calculated by trapezoidal rule. Secondary pharmacodynamic endpoints (maximal effect [E_{max}] and time to E_{max} [$T_{max,\,E}$]) were also analyzed to compare pharmacodynamic effects. The coefficient of variation was calculated for each parameter.

3.3.10 Cholesterol distribution among lipoproteins

To study the effect of sHDL or sHDL-PEG on lipoprotein profiles *in vivo*, cholesterol distribution between lipoprotein fractions was determined for rat serum collected at various post-dose time intervals. Briefly, serum lipoproteins were separated by size using a Waters HPLC system equipped with a Superose 6, 10/300 GL column (GE Healthcare, Piscataway, NJ) and cholesterol distribution between VLDL, LDL, and HDL lipoprotein fractions was determined by post-column enzymatic reactions. Rat serum prior to dosing and 2, 4, 12 and 24 h post-injection was analyzed. Serum aliquots (50 μl) were injected and eluted with 154 mM sodium chloride/0.02% sodium azide solution at 0.8 ml/min. The post column reaction was used to determine cholesterol concentration as described in section 2.6.

3.3.11 In vivo fluorescence imaging

sHDL, sHDL-PEG2k (5%), sHDL-PEG2k (10%) and sHDL-PEG5k (10%) were labelled with fluorescent dye DiR using the same preparation method described in Section 2.2, with the addition of DiR in acetic acid. The final DiR concentration was 20 μg/ml. Twelve 7-week old

male C57BL/6 mice (Harlan Sprague Dawley, Inc. Indianapolis, IN) were randomly divided into four groups of three mice per group. DiR-labelled nanoparticles were intravenously administered at a dose of 100 μg/kg DiR. Whole body optical images were obtained using an IVIS Spectrum Imaging System (Caliper, Fullerton, CA) at 1, 2, 4, 8 and 24 h post-injection. Immediately after the last time point, mice were perfused with PBS and their main organs, including hearts, livers, spleens, lungs, kidneys and brains, were collected and imaged. The average fluorescence intensities were quantified as total photons per centimeter squared per steradian (p s^{-1} cm^{-2} sr^{-1}) using the Living image® software package (Caliper Life Science, Hopkinton, MA).

3.3.12 Statistical Analysis

The significance of difference between data points, calculated Km and Vmax of cholesterol efflux, pharmacokinetic (C_{max}, *AUC*, $T_{1/2}$, K_{10}, *CL*, V_{ss}) and pharmacodynamic parameters (E_{max}, *AUEC*) were determined by one-way ANOVA analysis, with sHDL group as the control. Data are expressed as mean value with CV% of independent experiments. Statistical significance was established at $p < 0.05$, $p < 0.01$, $p < 0.001$ and $p < 0.0001$.

3.4 Results

3.4.1 Preparation and Characterization of PEG Modified sHDL Nanoparticles

The sHDL selected for PEG modification was composed of 22A ApoA-I mimetic peptide and DPPC at 1:2 w/w (1:7.15 mol/mol) ratio of peptide:lipid. This composition was very similar to the composition of ETC-642, a peptide-based sHDL that has been tested in both single- and multiple-dose Phase I clinical trials in dyslipidemic patients[144, 149]. The molar ratio between peptide and phospholipid components of sHDL dictates both the size and purity of the resulting sHDL. For our study, a 1:2 weight ratio resulted in formation of homogeneous preβ-like HDL nanodiscs with average diameter of 8 - 10 nm[152]. Therefore, the ratio between peptide and lipid was kept constant while a portion of DPPC was substituted for DPSE-PEG to achieve surface pegylation of sHDL. Two different molecular weights of PEG were used (2 kDa and 5 kDa) and DSPE-PEG were substituted for DPPC at either 2.5, 5 or 10 molar percent. One unmodified and four pegylated sHDL nanoparticle formulations were prepared and their compositions are summarized in Table 3.1.

The size distributions of sHDL and sHDL-PEG particles were determined by dynamic light scattering (DLS) (Table 3.1, Fig. 3.1A). The average diameter of non-pegylated sHDL was 9.2 ± 0.3 nm, similar to other reported sHDL sizes[152]. The average particle size of sHDL increased

gradually with increasing amounts of surface modifications, from 10.4 ± 0.2, 11.4 ± 0.2 to 13.1 ± 0.1 nm with addition of 2.5, 5 and 10% of PEG-2K, respectively. The size further increased to 14.9 ± 0.1 nm upon surface modification with the longer PEG-5K polymer. The homogeneity of particle size distribution was preserved, as evidenced by the low polydispersity index. Further characterization of sHDL nanoparticle size and purity was performed by gel permeation chromatography (GPC) (Fig. 3.2B). In agreement with our DLS findings, the GPC retention time decreased from 7.89 min to 6.45 min with pegylation, indicating the formation of larger particles.

Table 3.1: The characterization summary of different 22A-sHDL particles.

sHDL Formulations (molar ratio)	RT[a] (min)	Particle size (nm)	PDI[b]
22A: DPPC (1:7.15)	7.89	9.21 ± 0.29	0.36 ± 0.09
22A: DPPC: DSPE-PEG2k (1:6.97:0.18)	7.78	10.44 ± 0.16	0.15 ± 0.06
22A: DPPC: DSPE-PEG2k (1:6.79:0.36)	7.44	11.38 ± 0.22	0.24 ± 0.06
22A: DPPC: DSPE-PEG2k (1:6.43:0.72)	6.92	13.06 ± 0.03	0.23 ± 0.06
22A: DPPC: DSPE-PEG5k (1:6.79:0.36)	6.45	14.91 ± 0.02	0.26 ± 0.02

[a]RT: retention time, [b]PDI: polydispersity index.

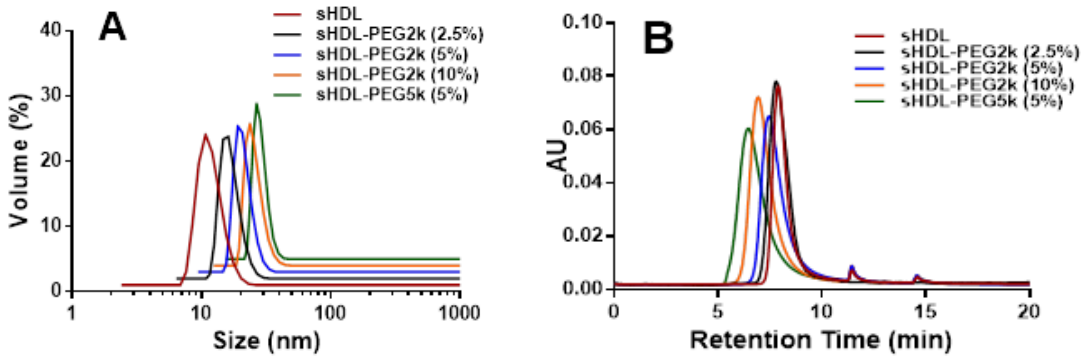

Figure 3.2: Particle size distribution of different 22A-sHDL particles determined by dynamic light scattering (Panel A) and gel permeation chromatography (Panel B).

3.4.2 Impact of PEG modification of sHDL surface on cholesterol efflux capacity

The ability of PEG modified sHDL to facilitate cholesterol efflux was evaluated, using BHK cells stably transfected with either human ABCA1, ABCG1 or SR-BI transporters. Efflux from non-transfected or mock-transfected cells was measured for comparison. The cells were first loaded with ^{3}H- cholesterol and then incubated with sHDL, sHDL-PEG2k (5%), sHDL-PEG2k (10%) or sHDL-PEG5k (5%) for 18 hours at concentrations of 0, 1.25, 2.5, 5, 10 or 20 μM 22A to

obtain dose-response curves (Fig. 3.3). The percent of cholesterol effluxed into the medium by sHDL was determined by counting the radioactivity in the medium and combined radioactivity of medium and lysed cells.

The ABCA1 transporter is one of the major efflux mechanism for removing cholesterol from macrophages in the atheroma, and primarily interacts with the lipid-free and or lipid-poor forms of ApoA-I protein. In contrast, the ABCG1 transporter interacts with larger, more mature HDL to efflux cholesterol. The SR-BI transporter is found in the calveolar regions of macrophage and endothelial cell membranes and is responsible for mediating bi-directional cholesterol efflux and anti-inflammatory signaling induced by HDL. All four formulations showed significant ability to efflux cholesterol passively from the cellular membrane of BHK mock cells (Fig. 3.3D). Induction of ABCA1, ABCG1 and SR-BI transporters slightly increased cholesterol efflux. The amount of effluxed cholesterol reached saturation at 5-10 μM of sHDL in all four cell types and for all sHDL formulations. In summary, pegylation of sHDL does not appear to shield the functional interaction between sHDL and cholesterol transporters.

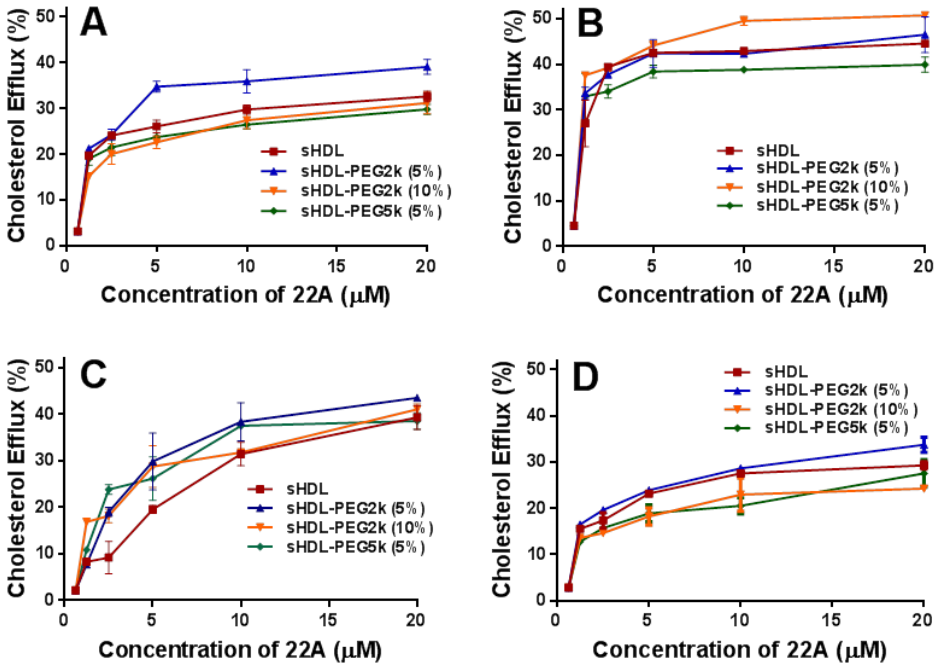

Figure 3.3: Cholesterol Efflux of cholesterol from BHK cells transfected with ABCA1 (Panel A), ABCG1 (Panel B), SR-BI (Panel C) and BHK-mock cell (Panel D) by sHDL particles.

3.4.3 Impact sHDL pegylation on cholesterol uptake by liver cells

After cholesterol is effluxed from peripheral tissues by sHDL, it is taken up by hepatocytes, metabolized and excreted into the bile[12]. To evaluate the effect of sHDL pelygaltion on cholesterol and nanoparticle uptake by hepatic cells, sHDL particles were loaded with bodipy-labeled cholesterol as well as insoluble DiD dye and incubated with HepG2 cells. Following various periods of incubation, cellular uptake of bodipy-cholesterol from both unmodified and pegylated sHDL was visualized by confocal imaging and quantified by flow cytometry (Fig. 3.4A and B). The bottom row shows the channel overlay, with nuclei in blue and bodipy-cholesterol in green. The fluorescence of bodipy appears to distribute throughout cellular membranes and cytosol for all groups and increase with longer uptake time. When bodipy uptake by HepG2 cells was quantified by flow cytometry no statistically significant differences were observed between different sHDL formulations. Thus, HDL nanoparticle pegylation at up to 10% with PEG-2k and up to 5 % with PEG-5K does not prevent cellular uptake of cholesterol by hepatocytes. This lack of cellular uptake difference could be due in part to the mobility of bodipy-cholesterol label. It is possible that bodipy-cholesterol diffused out of sHDL particles and was taken up by the cell as free bodipy-cholesterol leading to a similar apparent cell uptake. To access indirectly the contribution of sHDL-mediated cellular uptake of bodipy-cholesterol, we loaded different amount of bopipy-cholesterol per sHDL particle and performed cell uptake experiment at a constant bodipy-cholesterol concentration (Supplemental Fig. 3.10). At higher sHDL or sHDL-PEG concentrations when less bodipy-cholesterol is loaded per each sHDL particle, lower cellular uptake was observed indicating that at least some cholesterol uptake is mediated by sHDL-receptor interaction.

When sHDL or sHDL-PEG particles were labelled with DiD fluorescent dye within the lipid bilayer, faster accumulation of DiD in HepG2 cells was observed in sHDL groups compared to pegylated sHDL groups (Fig. 3.4C and D). As more PEG was added to sHDL, the uptake of DiD became slower. However, after 2 hours of incubation, the sHDL-PEG2k (5%) group had the same fluorescence intensity as sHDL group, indicating the saturation of DiD uptake. This slower uptake could be caused by PEG shielding the interaction between sHDL particles and cell receptors and the lack of mobility of insoluble DiD label relative to bodipy-cholesterol. The slower HepG2 uptake of pegylated sHDL could result in the increased sHDL circulation *in vivo*.

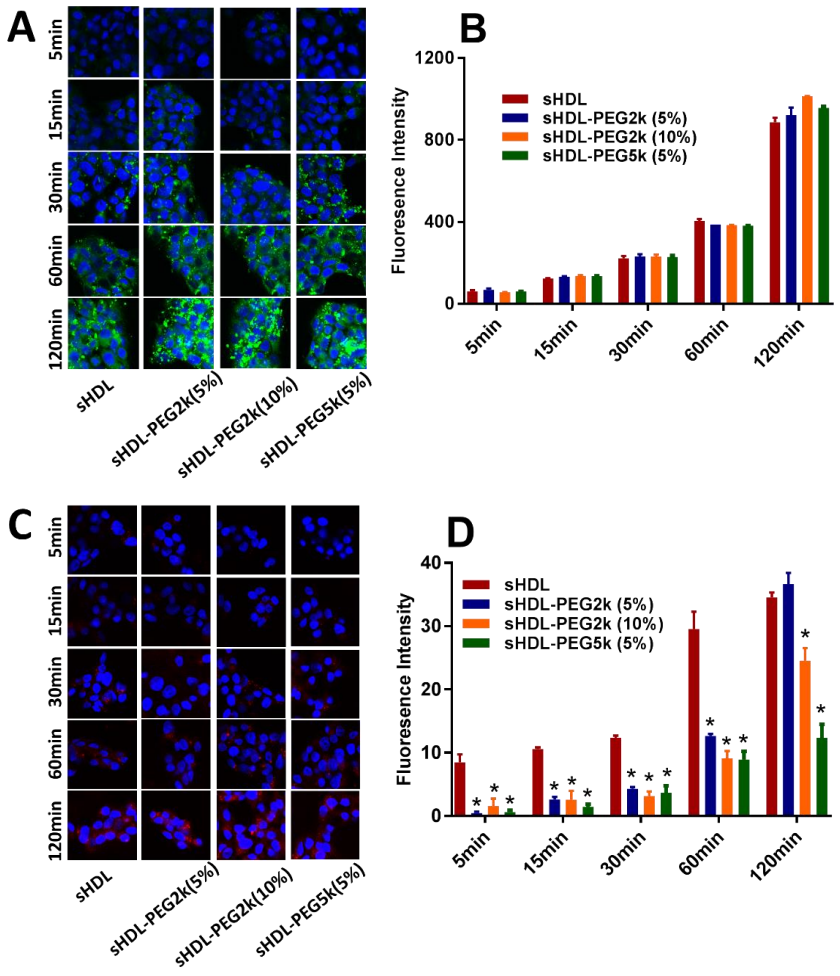

Figure 3.4: Cell uptake of bodipy-labelled cholesterol and DiD fluorescence dye by HepG2 cells at various time points after incubation of sHDL particles containg bodipy-cholesterol (Panel A and B) and DiD (Panel C and D). The fluorescent intensity was quantified by flow cytometry (Panel B and Panel D). (*) denotes statistical significant differences of fluorescence intensities for each group compared with sHDL group with $p < 0.05$.

3.4.4 Effect of sHDL pegylalion on lipoprotein remodeling in vitro

Following *in vivo* administration, sHDL are known to undergo significant remodeling in blood, a process in which both lipid and protein components of sHDL nanoparticle exchange with lipid and protein components of endogenous lipoproteins[153]. The rate of this exchange and how composition of sHDL affects this rate is not well characterized. To examine if pegylation of lipid component of sHDL affects particle remodeling, the sHDL nanoparticles were incubated in serum for 1 h at 37°C. By incorporation of fluorescently labelled DSPE-PEG2k-FITC in sHDL and monitoring fluorescence, we confirmed that pegylated lipid eluted with the HDL fraction before and after incubation with serum (Fig. 3.5B). We used post-column reaction to measure levels of

cholesterol in VLDL, LDL and HDL fractions before and after serum incubations with various sHDLs (Fig. 3.5A). After one hour incubation with non-pegylated sHDL, VLDL cholesterol levels appear to decrease and cholesterol distributes to smaller HDL particles likely due to partitioning to cholesterol-free sHDL. When sHDL-PEG-2K (5%) was mixed with serum, cholesterol redistribution toward HDL appears to be reduced.

Potential differences in how serum incubations with pegylated and non-pegylated sHDL affect re-distribution of endogenous apoA-I between various HDL sub-classes were also examined by 1-D native page electrophoresis. Different free 22A peptide and various sHDLs formulation were added at either 0, 0.3, and 1.0 mg/ml peptide, incubated for 30 min, separated by 1-D native page electrophoresis and visualized by western blot for human ApoA-I (Fig. 3.5C). Compared to control serum (lane 1), addition of all sHDL formulations resulted in the appearance of a lipid-free band of ApoA-I (30 kDa) and in some instances a small pre-β HDL particle or ApoA-I dimer around 60 kDa. For serum incubations with pegylated HDL, increase of ApoA-I signal in larger α-HDL was seen by the decreased intensity between 250 and 720 kDa. The increase in pre-β HDL levels are considered to be a beneficial effect of sHDL infusions as this sub-class of smaller HDL is thought to be responsible for cholesterol efflux from macrophages by the ABCA1 transporter.[154] Thus, serum incubation with non-pegylated sHDL leads to more favorable endogenous HDL remodeling. However, formation of larger alpha-HDL, in case of pegylated sHDL incubations, could be just an artifact of increased hydrodynamic diameter of lipoprotein due to presence of PEG on the surface.

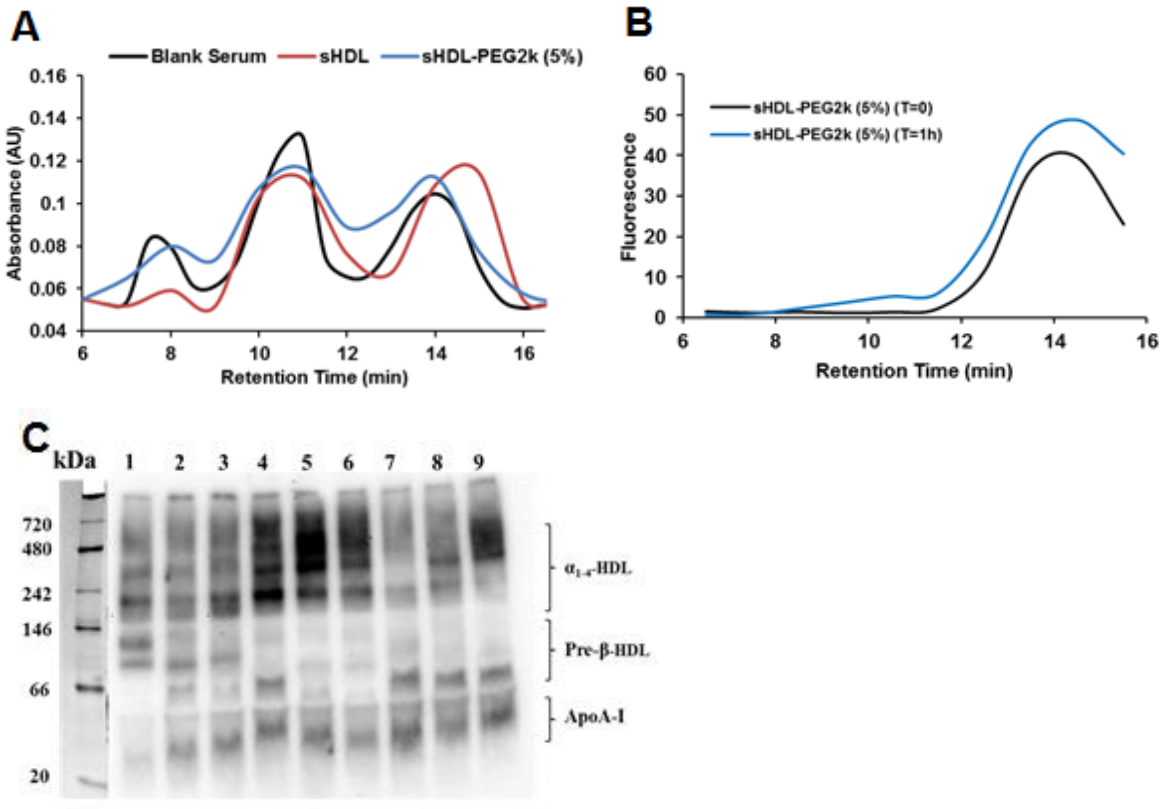

Figure 3.5: The cholesterol distribution between VLDL, LDL and HDL lipoprotein fractions before and at 1 hour after incubation of sHDL and FITC labelled sHDL-PEG2k (5%) with human serum at 37 ºC (Panel A). The distribution of FITC-labelled PEG2k component in sHDL-PEG2k (5%) among lipoproteins after incubation was shown in Panel B. The ApoA-I distribution between various subclasses of HDL after 1 hr incubation was determined by 1-D native page electrophoresis and visualized by western blot using anti-apoA-I antibody (Panel C). Lane 1 was the control serum, lane 2, 3, 4, 5 ,6 represented free 22A, sHDL, sHDL-PEG 2k (5%), sHDL-PEG2k (10%), sHDL-PEG5k (5%) at peptide concentration of 0.3 mg/ml. Lane 7, 8, 9 represented sHDL, sHDL-PEG 2k (5%), sHDL-PEG2k (10%) at peptide concentration of 1.0 mg/ml.

3.4.5 Pharmacokinetics of 22A peptide and phospholipids

The pharmacokinetics of the peptide and phospholipid components of sHDL nanoparticles were examined following IV bolus administration in SD rats (Fig. 3.6). Nanoparticles with different degrees of pegylation were injected at 50 mg/kg dose of 22A peptide. The peptide concentration in serum was detected by LC-MS analysis. The total choline containing phospholipids in serum were measured by plate assay and the pre-dose levels of lipids were subtracted. The serum concentration kinetics data for peptide and lipid components of sHDL were fitted using a non-compartment analysis (NCA) by WinNonlin software (Version 7.3). Pharmacokinetic parameters derived included maximum serum concentration (C_{max}), area under

the serum concentration-time curve (*AUC*), elimination rate constant (K_{10}), elimination half-life ($T_{1/2}$), total clearance (*CL*) and volume of distribution at steady state (V_{ss}).

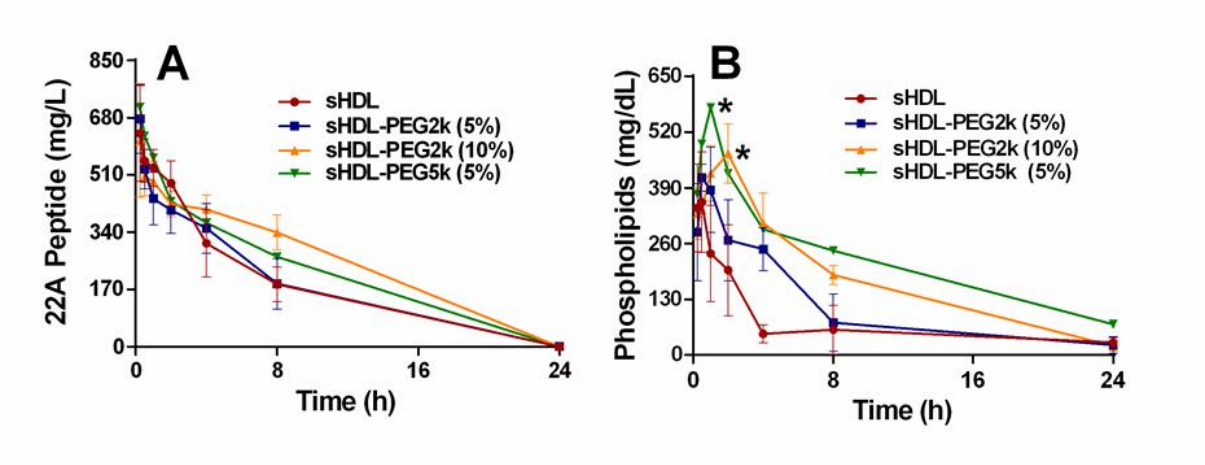

Figure 3.6: Pharmacokinetics of 22A peptide and phospholipids after intravenous bolus of various sHDL to Sprague-Dawley rats at 22A peptide dose of 50 mg/kg corresponding to 100 mg/kg dose of phospholipids. Serum peptide concentrations were determined by LC-MS and total choline containing phospholipids was measured by a commercial choline oxidase assay. (*) denotes statistical significant differences for each PEG-sHDL group compared with sHDL group with $p < 0.0001$.

Similar 22A peptide PK profiles were observed among all treatment groups (Fig. 3.6), indicating that PEG modification had no effect on peptide elimination following sHDL administration *in vivo*. The elimination rate constants obtained from NCA analysis showed no significant difference among all groups and small inter-subject variability for each group. The calculated area under the curve (*AUC*) values were comparable in all groups as well (Table 3.2). Different from 22A peptide, the PK behavior of sHDL's phospholipids was significantly altered by PEG addition. Phospholipids in sHDL-PEG5k (5%) had a higher peak concentration C_{max} (578 mg/dL) relative to the C_{max} of unmodified sHDL (384 mg/dL) ($p < 0.05$). Higher surface density of PEG-2000 led to a longer lipid serum half-life *in vivo* and a higher *AUC* (Fig. 3.6 and Table 3.3). The AUC increased gradually as more PEG was added, from 2071 mg*h/dL for non-pegylated sHDL to 3042 and 4473 mg*h/dL for 5 and 10 mol% PEG-2k, respectively. Similarly, the addition of longer PEG chains at the same surface density of polymer led to a longer half-life and a larger *AUC*, with half-lives of 8.6 h for sHDL-PEG2k (5%) and 12.5 h for sHDL-PEG5k (5%) (NS) and *AUC* of 4473 mg*h/dL for sHDL-PEG2k (5%) and 6108 mg*h/dL for sHDL-PEG5k (5%) ($p < 0.01$).

Table 3.2: Pharmacokinetic parameters (% CV) of 22A peptide after 50 mg/kg doses of sHDL, sHDL-PEG2k (5%), sHDL-PEG2k (10%) and sHDL-PEG5k (5%) treatments.

Parameters	**Groups**			
	sHDL	**sHDL-PEG2k (5%)**	**sHDL-PEG2k (10%)**	**sHDL-PEG5k (5%)**
C_{max} [a] (mg/dL)	633.5 (22.4)	677.1 (15.2)^{ns}	612.3 (27.5)^{ns}	712.0 (15.2)^{ns}
AUC [b] (mg*h/dL)	4185 (19.4)	4150 (22.6)^{ns}	5885 (8.50)*	5163 (10.4)^{ns}
K_{10}[c] (h-1)	0.1521 (7.94)	0.1693 (21.4)^{ns}	0.1071 (33.7)^{ns}	0.1377 (6.46)^{ns}
$T_{1/2}$ [d] (h)	4.588 (8.58)	4.25 (17.4)^{ns}	7.14 (28.8)ns	5.05 (6.34)^{ns}
CL [e] (dL/h)	0.0034 (21.4)	0.0032 (19.9)^{ns}	0.0022 (8.40)*	0.0025 (9.18)^{ns}
V_{ss}[f] (dL)	0.0221 (21.1)	0.0188 (9.84)^{ns}	0.0216 (9.6)^{ns}	0.0179 (13.3)^{ns}

[a]*C_{max}*: the maximum plasma concentration of peptide; [b]*AUC*: the area under the curve in plot of concentration of peptide against time; [c]*K_{10}*: elimination rate constant; [d]*$T_{1/2}$*: the half-life of elimination; [e]*CL*: total clearance for peptide; [f]*V_{ss}*: volume of distribution for peptide at steady state. Data was shown as mean with CV%. Significance: *p<0.05, **p<0.01, ***p<0.001, ****p<0.0001, ns: no significant difference compared with sHDL group.

Table 3.3: Pharmacokinetic parameters (% CV) of total phospholipids after 50 mg/kg doses of sHDL, sHDL-PEG2k (5%), sHDL-PEG2k (10%) and sHDL-PEG5k (5%) treatments.

Parameters	**Groups**			
	sHDL	**sHDL-PEG2k (5%)**	**sHDL-PEG2k (10%)**	**sHDL-PEG5k (5%)**
C_{max}[a] (mg/dL)	383.9 (28.0)	438.1 (9.5)^{ns}	477.0 (27.3)^{ns}	578.0 (4.8)*
T_{max}[b] (h)	0.38 (38.5)	0.88 (28.6)*	1.6 (46.2)*	1.0 (0)***
AUC[c] (mg*h/dL)	2071 (21.7)	3042 (26.2)^{ns}	4473 (11.8)***	6108 (18.5)***
K_{10}[d] (h-1)	0.17 (34.5)	0.11 (54.9)^{ns}	0.072 (19.7)*	0.065 (37.9)*
$T_{1/2}$[e] (h)	4.59 (43.3)	8.62 (46.9)^{ns}	9.96 (18.2)**	12.5 (38.2)*
CL[f] (dL/h)	0.014 (23.6)	0.0088 (20.5)*	0.0057 (10.7)**	0.0044 (30.4)**
V_{SS}[g] (dL)	0.083 (19.7)	0.10 (37.2)^{ns}	0.084 (28.0)^{ns}	0.074 (27.4)^{ns}

[a]*C_{max}*: the maximum plasma concentration of phospholipids; [b]*T_{max}*: the time to observe *C_{max}*; [c]*AUC*: the area under the curve in plot of concentration of phospholipids against time; [d]*K_{10}*: elimination rate constant; [e]*$T_{1/2}$*: the half-life of elimination; [f]*CL*: total clearance for phospholipids; [g]*V_{SS}*: volume of distribution for phospholipids. Data was shown as mean with CV%. Significance: *p<0.05, **p<0.01, ***p<0.001, ****p<0.0001, ns: no significant difference compared with sHDL group.

The dichotomy of how pegylation did not affect pharmacokinetics of ApoA-I peptide component of sHDL but significantly altered elimination of phospholipid component was surprising. It became clear that pegylation of sHDL by insertion of pegylated lipid does not provide stealth properties to the entire nanoparticle, but rather just to the phospholipid bilayer component. This also points to the fact that following *in vivo* administration, sHDL undergoes extensive remodeling. The cholesterol-free lipid bilayers readily accept cholesterol; the ApoA-I peptide

components exchange with endogenous apolipoproteins; and the phospholipid themselves likely exchange with endogenous lipoprotein lipids.

3.4.6 The impact of sHDL pegylation on in vivo pharmacodynamics

To examine the potential therapeutic effect of sHDL pegylation on cholesterol metabolism *in vivo*, the pharmacodynamics biomarkers were measured following administration of nanoparticles to normal SD rats by IV infusion at a dose of 50 mg/kg 22A peptide. sHDL has been reported to facilitate cholesterol efflux from peripheral tissues through RCT, and the level of cholesterol in serum can be used to reflect the transient efflux of cholesterol induced by administration of sHDL. The levels of plasma total cholesterol (TC, Fig. 3.7A) and free cholesterol (FC, Fig. 3.7B) were determined directly, while esterified cholesterol level was calculated by subtracting free cholesterol level from total cholesterol level at each time point (CE, Fig. 3.7C). Pharmacodynamics parameters were calculated and summarized in Table 3.4. The typical pharmacological response following sHDL infusion is a rapid mobilization of free cholesterol into the plasma compartment, followed by a rise in cholesterol ester due to esterification by lecithin-cholesterol acyltransferase (LCAT) and subsequent elimination of cholesterol by the liver. These expected effects were observed for sHDL infusions, with a maximum FC mobilization of 75 mg/dL at 0.5 h followed by a peak in CE (46 mg/dL) at 4 h, and elimination of all mobilized cholesterol by 24 h post-dose. In line with the improvements in phospholipid PK, the pegylated sHDL exhibited greater cholesterol mobilization and longer pharmacodynamic effect relative to non-pegylated sHDLs. Both the higher degree of surface modification by PEG and longer PEG chain lengths resulted in higher maximum effect levels for TC, FC, and CE increases. For example, the maximum mobilized FC levels increased from 75 mg/dL for non-pegylated sHDL, to 110, 125 and 137 mg/dL for sHDL-PEG-2K (5%), sHDL-PEG-2K (10%) and sHDL-PEG-5K (5%). The area under the effect curve also increased for all pegylated formulations: from 422 mg*h/dL (sHDL) to 1241 mg*h/dL (a 1.9-fold increase) for sHDL-PEG-2K (10%) and to 1588 mg*h/dL (a 2.8-fold increase) for sHDL-PEG-5K (5%). Hence, the longer lipid circulation time for pegylated sHDL resulted in greater levels of mobilized cholesterol and a longer duration of the effect.

Table 3.4: Pharmacodynamic parameters (% CV) of total cholesterol (TC), free cholesterol (FC) and cholesterol ester (CE) after 50 mg/kg doses of sHDL, sHDL-PEG2k (5%), sHDL-PEG2k (10%) and sHDL-PEG5k (5%) treatments.

Parameters	sHDL	sHDL-PEG2k (5%)	sHDL-PEG2k (10%)	sHDL-PEG5k (5%)
$T_{max,E}$[a] (h)	0.94 (82.6)	2.0 (70.7)^{ns}	2.0 (0)*	3.3 (46.2)*
E_{max}[b](mg/dL)	114.9 (25.4)	177.8 (8.1)**	181.4 (17.4)*	212.5 (7.7)**

TC	**AUEC[c] (mg*h/dL)**	562.8 (25.9)	1660 (37.2)*	2031 (13.1)****	3171 (25.8)***
FC	**$T_{max,E}$ (h)**	0.56 (55.9)	0.88 (28.6)^{ns}	2.0 (0)****	1.5 (38.5)*
	E_{max} (mg/dL)	74.6 (26.8)	109.6 (7.0)*	125.1 (31.6)^{ns}	136.9 (12.0)**
	AUEC (mg*h/dL)	421.7 (36.5)	740.7 (31.5)^{ns}	1241 (35.6)*	1588 (26.1)**
CE	**$T_{max,E}$ (h)**	1.2 (79.5)	4.3 (67.6)^{ns}	5.0 (40.0)*	7.0 (28.6)**
	E_{max} (mg/dL)	46.4 (43.0)	76.2 (14.6)*	73.5 (39.8)^{ns}	89.9 (33.5)^{ns}
	AUEC (mg*h/dL)	372.9 (21.4)	869.6 (51.8)^{ns}	1034 (41.3)*	1562 (32.1)**

[a]*T_{max}*: time at which the *E_{max}* is observed. [b]*E_{max}*: the maximum plasma concentration of different cholesterol species. [c]*AUEC*: the area under the effect curve. Data was shown as mean with CV%. *p<0.05, **p<0.01, ***p<0.001, ****p<0.0001, ns: no significant difference compared with sHDL group.

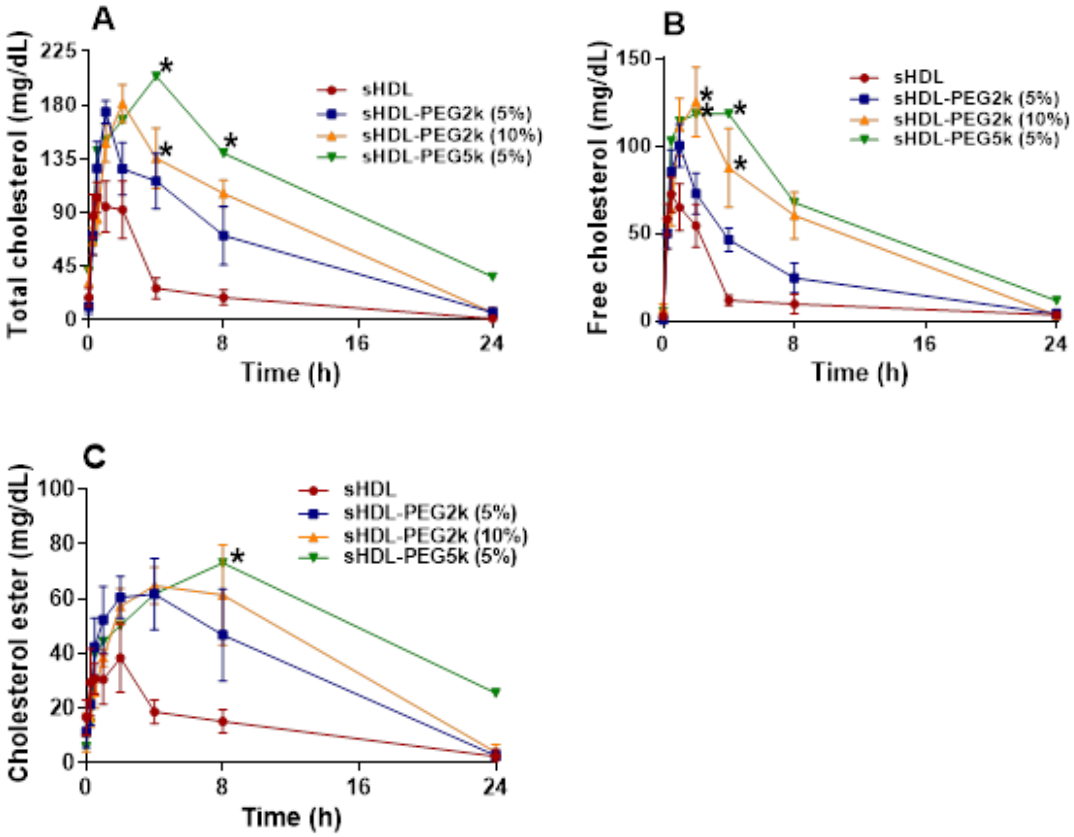

Figure 3.7: Pharmacodynamic assessment after IV administration of sHDL particles from the pharmacokinetic study. The level of total cholesterol (Panel A), free cholesterol (Panel B) and cholesterol ester (Panel C) in rat serum were determined by commercially available kits. (*) denotes statistical significant differences of TC, FC or EC changes for each group compared with sHDL group with p < 0.0001.

3.4.7 Distribution of mobilized cholesterol and lipoprotein remodeling in vivo

In order investigate in greater detail the mechanism of cholesterol mobilization and elimination following administration of pegylated and non-pegylated sHDL particles, we determined the relative distribution of mobilized cholesterol in the HDL, LDL and VLDL fractions by HPLC. The positions of HDL, LDL and VLDL sized particles containing cholesterol are labeled on Fig. 3.8. The infusion of sHDL caused a rapid mobilization of cholesterol in the HDL fraction, with the maximum increase at 0.5 h post-dose (blue line, Fig 3.8A). The increase in HDL-C was accompanied by small increase in VLDL-C, and cholesterol returned to baseline levels by 24 h post-dose. The cholesterol profile changes were different when pegylated sHDLs were administered. Because pegylated sHDLs are slightly larger in size, the mobilized cholesterol appears to elute between HDL and LDL fractions at 0.5, 2 and 4 h post administration (Fig. 3.8B-D). The increase in VLDL-C appears to be higher for all pegylated sHDLs relative to sHDL, especially for sHDL-PEG-2K (10%). It is possible that DSPE-PEG caused inhibition of lipoprotein lipase or stimulation of liver lipogenesis, which both lead to the transient increase in VLDL-C. However, for all formulations cholesterol increases were transient. The cholesterol level and its relative lipoprotein distribution returned to pre-dose levels, indicating completion of the RCT process triggered by administered sHDL. This type of increase in lipoproteins, including VLDL/HDL, has been observed in clinical trials, and the levels returned back to baseline at 24-72 hours post dose.[139, 145, 155-157].

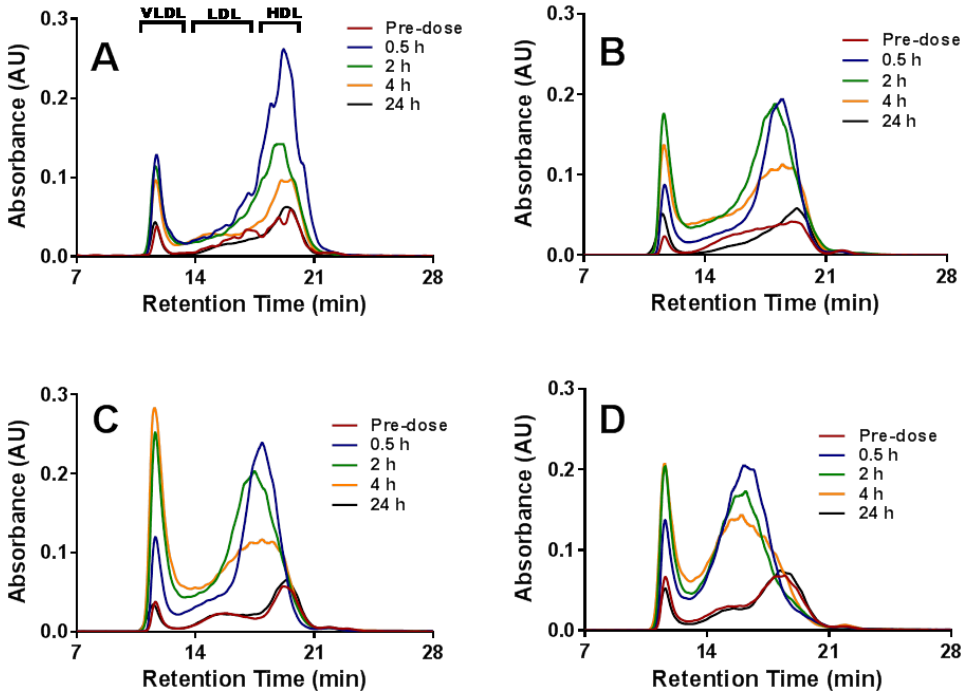

Figure 3.8: The cholesterol distribution between VLDL, LDL and HDL lipoprotein fractions at different time points after IV injection of sHDL (Panel A), sHDL-PEG2k (5%) (Panel B), sHDL-PEG2k (10%) (Panel C) and sHDL-PEG5k (5%) (Panel D) to SD rats.

3.4.8 In vivo distribution of sHDL and sHDL-PEG nanoparticles

A bio-distribution study of sHDL or sHDL-PEG nanoparticles in mice was conducted by labelling particles with DiR. Results are summarized in the supplemental material (Supplemental Fig. 3.9). IThe whole-body mages were obtained at 1, 2, 4, 8, and 24 hours after intravenous injection of nanoparticles and tissues including heart, liver, spleen, lung, kidney and brain were harvested at 24 hours post-dose and imaged. From the whole-body imaging, sHDL-PEG groups have stronger signal than sHDL group at all time points later that 4 hours, and the fluorescence dye DiR mainly accumulated in liver. From the tissue distribution at 24 hours, both sHDL and sHDL-PEG formulations were found to accumulate in the liver and sHDL-PEG groups had much higher fluorescence intensity than sHDL group, indicating that longer circulation of pegylated sHDL results in increased accumulation in major organs.

In this study, we successfully prepared pegylated sHDL with varying PEG surface densities of 5 and 10 mol%, as well as two different molecular weights of PEG, 2 kDa and 5 kDa. Incorporation of PEG resulted in a small increase in the sHDL hydrodynamic diameter, but the

overall size homogeneity was preserved. Owing to the relatively low degree of PEG surface modifications, pegylated sHDL retained their ability to efflux cholesterol by passive uptake and through ABCA1, ABCG1 and SR-BI transporters and facilitate uptake of cholesterol by HepG2 cells. However, when insoluble DiO dye was incorporated in sHDL bilayer, pegylation reduced cellular uptake of sHDL. The differences in HepG2 uptake of bodipy-cholesterol and DiO could be attributed to difference in mobility of two dyes, and, hence different contribution of passive cellular uptake of the dye. The reduced uptake of bodipy-cholesterol with decreased of its loading in sHDL indicated that some of cholesterol uptake is receptor mediated.

Despite high similarity *in vitro*, the performance of pegylated sHDL differed when nanoparticles were examined normal rats. Administration of pegylated sHDL led to greater extent of cholesterol mobilization and longer duration cholesterol elevation relative to non-pegylated sHDL (Fig. 3.7). Administration of pegylated and non-pegylated sHDL led to transient increases in HDL-cholesterol levels, following by increased LDL and VLDL-cholesterol levels and lipoprotein cholesterol profile returned to normal 24-hours post-dose (Fig. 3.8). The transient increase in VLDL cholesterol lasted longer for pegylated sHDLs relative to unpegylated one possibly due to higher levels of cholesterol mobilized by pegylated sHDL. This type of increase in plasma HDL cholesterol levels following by transient increase in LDL and VLDL cholesterol levels has been observed in both pre-clinical and clinical studies for sHDL products (CSL-111, ETC-216, ETC-642, CER-001, CSL-112) and it has been used as biomarker of cholesterol efflux *in vivo* during product development.[19, 149-150, 158-160]. This is based on the fundamental mechanism of the reverse cholesterol transport (RCT) process, where a transient increase in plasma cholesterol should be detected as it is effluxed from peripheral tissues and transported to the liver for elimination. Interestingly, *in vivo* the pharmacokinetic effect appeared to be different from cholesterol mobilization. While some increases phospholipid circulation times and AUCs were observed after administration of pegylated sHDL, the ApoA-I peptide PK parameters remained unchanged (Fig. 3.6). Overall, 22A peptide appears to be eliminated more rapidly than sHDL's lipid components. This indicates that peptide and lipid components of administered sHDL exchange *in vivo* with contents of endogenous lipoproteins and are eliminated independently. Some degree of remodeling was observed *in vitro* following incubation of serum with sHDL, with 22A peptide displacing endogenous ApoA-I proteins from various sub-fractions of HDL (Fig. 3.5).

3.4 Discussion and conclusion

Our intention was to improve the duration of sHDL pharmacologic effect by increasing stability of the entire sHDL nanoparticle in blood and, thus, increasing circulation time. Recent failures of CETP inhibitors brought into question the utility of systemically increasing HDL-C levels.[161-165] CETP inhibition leads to the accumulation of cholesterol-rich HDL particles, while infusion of sHDL provides increased levels of cholesterol-poor HDL which are capable of additional cholesterol efflux from the atheroma.[166-167] It has been reported that naked ApoA-I mimetics have anti-atherogenic activity.[168] However, by administering naked peptide or naked ApoA-I intravenously or orally, lipoprotein changes were not observed.[152, 169-170] Because of this finding ApoA-I and peptides were formulated with phospholipids to form sHDL nanoparticles for clinical trials. There is an emerging evidence that anti-atherogenic effect of ApoA-I mimetic peptides is due to their ability to sequester oxidized lipids in intestine.[171-173] The mechanism is intriguing and we have not investigated the impact of pegylation on this mechanism since in this paper we focus on investigating the impact of pegylation on RCT. Another possible mechanism of ApoA-I peptide or sHDL activity is remodeling of LDL particles and reduction of their accumulation in the arteries.[174-175] This potential mechanism was not examined in detailed in this study, although transient changes in LDL-C were observed (Fig. 3.8).

While extensive pegylation of nanoparticles (20% of lipid) is known to improve their stealth properties[176], we were concerned that 20% pegylation would interfere with sHDL's ability to interact with cholesterol efflux transporters and liver scavenger receptors, leading us to choose modest pegylation levels for our sHDL preparations (5 and 10%). We have previously shown a modest reduction in sHDL internalization by SR-BI receptors expressed by colon carcinoma cells using fluorescently labelled sHDL containing only 5 mol% DSPE-PEG-2K relative to non-pegylated sHDL[177]. When *in vivo* circulation times of fluorescently non-pegylated sHDL and peg-modified sHDL (5 mol% DPPG-PEG2K) were compared by measuring fluorescence intensity by Zhang *et al.*, no differences were observed[178]. Careful examination of how the degree of nanoparticle pegylation influence PK was performed by Liu *et al*[176]. When lipid-calcium phosphate nanoparticles of 30 nm in diameter were modified with DPPE-PEG2K at 5 mol%, no changes in PK or biodistribution were observed. In contrast, modification with 20 mol% lead to a significant improvement in plasma nanoparticle stability and a longer circulation time. Hence, using a higher molar content of PEG on the sHDL surface may lead to a more significant reduction

in sHDL remodeling by lipoproteins *in vivo* and further improvement in PK/PD profiles relative to those observed in the current study.

In this study, the PK parameters of lipid component of sHDL were improved by pegylation, but the half-life of 22A peptide remained unchanged. This result confirms that sHDL particle is not eliminated *in vivo* in its intact form. It is likely that elimination rates of sHDL's protein and lipid components depend on their exchange with endogenous lipoproteins. The signs of this remodeling were confirmed by ex-vivo incubation of sHDL with human plasma (Fig. 3.5), with 22A peptide displacing ApoA-I protein on endogenous HDL, as is evident by the appearance of lipid-free ApoA-I band in western blot (Fig. 3.5). Previously, we observed longer circulation times for sHDL lipid components relative to 22A peptide, as well as extensive displacement of ApoA-I protein from endogenous HDL by 22A peptide.[152] Some differences in elimination rates of protein and phospholipid components were also noticed in clinical studies of sHDL products. Indeed, faster elimination of ApoA-I ($T_{1/2}$ ~ 10 h) was observed relative to phospholipid ($T_{1/2}$ ~ 46 h) following administration of 45 mg/kg of CER-001, ApoA-I-sphingomyelin nanoparticles.[179] The elimination of ApoA-I and lipid components of CSL-112, ApoA-I-soybean phosphatidylcholine nanoparticles, followed an opposite trend to CER-001 with a longer protein half-life of 36.4 h relative to phospholipid half-life of 18.0 h[31]. There are known differences in *in vivo* metabolism of DPPC used in this study to prepare sHDL, soybeanPC (CSL-112) and sphingomyelin (CER-001).[180] In addition, full-length ApoA-I has about 10 amphipathic α-helical segments, resulting in stronger binding to phospholipid relative to the much smaller 22A peptide. Thus, it is possible that ApoA-I-based sHDLs are more stable and less susceptible to the remodeling *in vivo* relative to ApoA-I-peptide-based sHDL.

Various strategies have been used to increase *in vivo* half-life of the ApoA-I component of sHDL. In one study, a trimer of the ApoA-1 protein was produced by recombinant expression[181]. An improvement in residence PK profiles was observed[156, 182], but clinical development of trimeric ApoA-I was halted likely due to high manufacturing cost and immunogenicity concerns. Using a similar concept, crosslinked dimers, trimers and star-like multimers of ApoA-I mimetic peptides were synthesized to improve the *in vivo* stability, circulation time and efficacy of peptide-based sHDL.[183] Having multiple α-helixes to bind phospholipids resulted in longer *in vivo* circulation time and lower plasma cholesterol levels in murine model of atherosclerosis, but a reduction in atheroma volume was not reported.[182] A different chemical approach, termed hydrocarbon

stapling, was employed by Sviridov *et al.* to stabilize peptide α-helices and improve cholesterol efflux, but the impact of stapling on RCT was not fully characterized.[184] Finally, the ApoA-I protein of sHDL was selectively pegylated by attaching a single 20K PEG chain to protein N-terminal by Murphy *et al.*[147] Pegylation of ApoA-I did not reduce its ability to efflux cholesterol, but did improve protein circulation *in vivo* and led to the suppression of bone marrow myeloid progenitor cell proliferation in hypercholesterolemic mice. Pegylation also appeared to improve anti-atherosclerotic properties of HDL as observed by the reduction in atheroma necrotic core area and lipid content of the aortic arch relative to placebo. However, differences between pegylated and unmodified HDL were not significant. This indicates that the composition of pegylated sHDL needs to be further optimized for their plasma stability and pharmacokinetic properties prior to formal efficacy studies.

The focus of this study was to understand how pegylation affects the RCT pathway facilitated by HDL. The impact of pegylation on cholesterol efflux *in vitro* and elevation of cholesterol levels *in vivo* were examined as biomarkers of RCT. However, the impact of pegylation on the anti-inflammatory and anti-thrombotic properties of sHDL has not yet been examined. In addition, the reduction in atheroma volume following HDL administration in animal models of atherosclerosis is the ultimate measure of sHDL's efficacy *in vivo.* In addition, the mechanism by which ApoA-I peptide, sHDL We plan to perform these studies following development of a complete understanding of the impact of pegylation on the pharmacokinetics and *in vivo* stability of sHDL, in addition to selecting the optimal surface-modified sHDL formulation.

The results of our study have broader impact of the field of sHDL design and nanoparticle drug delivery. This study underlines the importance of sHDL remodeling by endogenous lipoproteins *in vivo* in regards to sHDL's PK and pharmacological effect. Hence, strategies for minimizing sHDL *in vivo* remodeling, such as crosslinking ApoA-I or lipid components, could potentially improve sHDL PK properties and efficacy. Similarly, HDL-like nanoparticles used for imaging and drug delivery purposes are likely to remodel *in vivo*, which could lead to rapid cargo release.[141, 155, 157, 178] In the recent years, the formation of protein corona on the surface of nanoparticles used for drug delivery and imaging had emerged as a critical issue for *in vivo* efficacy of nanomedicines.[185-187] Endogenous lipoprotein components were found to be major components of the protein corona.[188] It has been reported that endogenous lipoproteins also rapidly remodel liposomal and micellar nanocarriers and alter cargo release.[189-190] Thus, understanding the forces

driving lipoprotein remodeling *in vivo* and developing strategies to minimize it could lead to the design of more stable and efficacious sHDL based nanomedicines.

3.5 Supplementary information

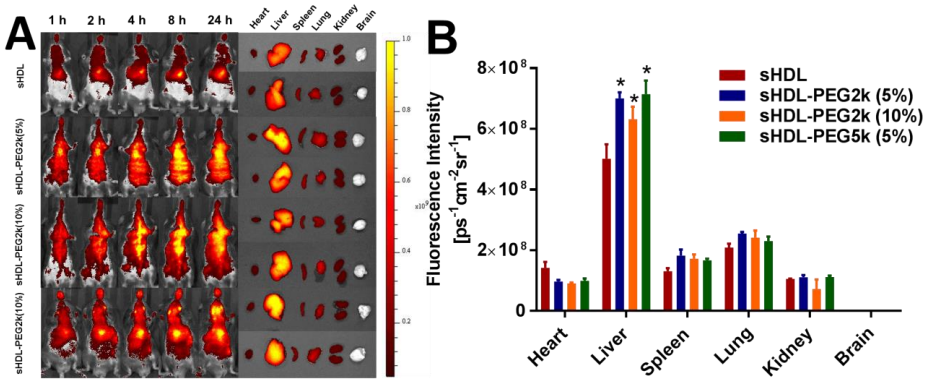

*Figure 3.9: The in vivo imaging of C57BL/6 mice after administration of sHDL, sHDL-PEG2k (5%), sHDL-PEG2k (10%) and sHDL-PEG5k (10%) at 1h, 2h, 4h, 8h, and 24h together with the ex vivo fluorescence images of isolated organs collected at 24 h post-injection (Panel A). The average fluorescence intensities of tissues were analyzed using Living image® software (Panel B). Data represent mean ± SEM (n=3). *: P<0.05 relative to sHDL group.*

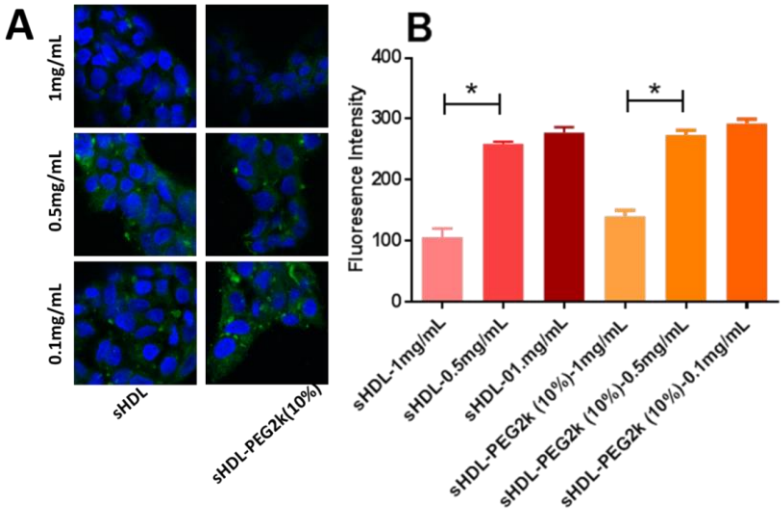

Figure 3.10: Cell uptake of bodipy-labelled cholesterol loaded in sHDL or sHDL-PEG (10%) by HepG2 cells after 1 h incubation. The particle concentrations are 1 mg/mL, 0.5 mg/mL and 0.1 mg/mL (Panel A). The fluorescent intensity was quantified by flow cytometry.

Chapter 4 : Nano-micelles mimicking high-density lipoproteins reverse atherosclerosis and prevent inflammatory response in animals

4.1 Abstract

Administration of high doses of synthetic high-density lipoproteins or "DrainoTM for the arteries" has led to atheroma volume reductions in patients with acute coronary syndrome (ACS). Because there is a high prevalence of cardiovascular disease, commercialization of synthetic high-density lipoprotein (sHDL) treatment will require the manufacturing of metric tons of recombinant apolipoprotein A-I and lipoprotein nanoparticles, which is both technically difficult and costly. Here we introduce nano-micelle (NanoMCL), a structural nano-mimetic of sHDL with a small particle size (12-14 nm) and a hydrophobic core and hydrophilic exterior. We show that NanoMCLs are functionally similar to sHDL with the capacity to efflux cholesterol from macrophages and deliver the cholesterol molecules to hepatocytes for elimination. The NanoMCLs also have a 4-14-fold better ability to inhibit inflammatory cytokine release *in vitro* compared to sHDL. More importantly, when administered *in vivo*, NanoMCLs exhibit 2-fold improved cholesterol mobilization from peripheral tissues compared to sHDL, followed by elimination from the body within 48 hours. When tested in an endotoxemia model, NanoMCL exhibits similar to sHDL ability to inhibit inflammatory cytokine release both in prevention and in treatment settings. When administered as a 6-week treatment to a commonly used animal model of atherosclerosis—ApoE k/o mice fed a high-fat diet, sHDL and NanoMCL induced reduction of atheroma by 21% and 40%, respectively. Further demonstrating superior anti-atherosclerotic efficacy to sHDL, NanoMCL treatment in the mouse model resulted in a reduced area of atheroma macrophages, a landmark of cardiovascular disease. Furthermore, treatments with either sHDL or NanoMCL were well tolerated as neither elevation of plasma toxicity biomarkers nor histological changes in liver tissues were detected. Taken together, we found that NanoMCL a structural and functional mimetic of the sHDL nanoparticle, was effective in relevant animal models. Owing to its simplistic composition and ease of preparation, we propose that NanoMCL could prove to be a valuable alternative to sHDL in treatment of ACS and other inflammatory diseases.

4.2 Introduction

Cardiovascular disease (CVD) is the leading cause of death in the United States, responsible for approximately 17% of national health expenditures.[135] Lipid metabolism imbalance and vascular inflammation lead to an accumulation of macrophages loaded with cholesterol in the sub-intimal space and formation of lipid-rich vulnerable plaques in the arteries that could subsequently rapture and cause cardiovascular infarct which might lead to death.[191-193] While many approved cardiovascular therapeutics inhibit cholesterol synthesis and absorption, thus halting the development of new plaques, there are currently no available therapies that facilitate a reduction in an existing atheroma burden.[194-195] Following a first heart attack, CVD patients are at a significant risk of having a secondary event within 6 to 12 months due to the presence of additional vulnerable plaques.[196-197] Thus, administration of a therapeutic that functions like a "Draino™ for the arteries" by rapidly removing excess lipids from the atheroma might prevent the occurrence of secondary events.

Endogenous high-density lipoproteins (HDLs) facilitate the efflux of excess cholesterol from atheroma macrophages, mobilization of effluxed cholesterol into blood circulation and subsequent delivery of cholesterol to the liver for elimination via the reverse cholesterol transport (RCT) pathway.[198] Endogenous HDLs are 8 to 12 nm nanoparticles with a hydrophilic exterior to promote plasma circulation and a hydrophobic interior to facilitate cholesterol capture.[11] This HDL structure is supported by the helical protein apolipoprotein A-I (apoA-I) that wraps around a bilayer of phospholipids to form a small nanoparticle with a hydrophilic exterior and a hydrophobic core.[141] The small particle size allows HDL to penetrate the endothelial layer into the core of the atheroma and interact with several extracellular receptors on macrophages to efflux cholesterol.[199] However, in individuals with CVD, the number of functional HDL particles capable of cholesterol efflux is reduced.[200] Thus, several synthetic HDL (sHDL) products have been designed and clinically tested for their abilities to reduce patients' atheroma burden. For these sHDLs, apoA-I protein is either produced by a recombinant process or by purification from human plasma. The apoA-I protein is then combined with lipids to form the HDL nanoparticle. In CVD patients, 5 to 6 weekly doses of sHDL are capable of reducing plaques.[201-202] The ability of the sHDL product, CSL-112, to reduce the rate of death, myocardial infraction or stroke is currently being tested in a large 17,400 patient phase III clinical trial.[203-204] However, the doses required to produce a clinical effect are 40 mg/kg.[20] Thus, a course of therapy will require approximately 20

grams of protein and treatment for a million of patients—a conservative estimate of the number of patients needing annual treatment—requires 20 tons of protein annually. The recombinant manufacturing process for apoA-I is very expensive due to the hydrophobic nature of this protein, relatively low expression levels and multiple purification steps required to remove protein-bound hydrophobic impurities. The current alternative, a plasma purified version of apoA-I, will likely result in shortages of plasma supply due to high market needs.

Nanomaterials have been shown to mimic the structures and functions of human proteins.[205] Nanoparticles and globular proteins are similar in overall size, charge, and shape, and the exterior surfaces of nanoparticles can be coated with organic functional groups similar to proteins, indicating that nanoparticles could function as protein mimics. Thus, to resolve the cost and scalability dilemma of producing apoA-I, several innovative nanotechnology-based functional mimetics of sHDL have been proposed.[69, 71, 75-76] One such approach describes a HDL biomimetic that is built on a gold nanoparticle core with a functionalized surface via attachment of phospholipids and apoA-I proteins.[69-70] Another approach describes a poly(lactic-co-glycolic) acid (PLGA) core functionalized with lipids and apoA-I mimetic peptides.[75, 77] These HDL nanomimetics accumulate in atherosclerosis plaques and achieve the similar cholesterol efflux capacity as HDL.[78] However, it has not been shown that these HDL nanomimetics are capable of reducing the atheroma area in the standard atherosclerosis animal models.

In this study, we aimed to create a synthetic nanoparticle that mimics the structural and functional properties of sHDL. The main design criteria were: a) nanoparticles of a small HDL-like 10 to 12 nm size to allow endothelial layer penetration and efflux of cholesterol from macrophages through cellular transporters; b) nanoparticles that mimic the amphipathic nature of HDL with a hydrophilic exterior for long circulation time *in vivo* and a hydrophobic interior with the ability to expand in size to allow for cholesterol sequestration in the nanoparticle core. To accomplish this goal, we combined phosphotidylcholine (PC) with polyethylene-glycol modified PC (PEG-PC) to obtain nanoparticles with fatty acids tails in the hydrophobic interior and hydrophilic phosphate head groups and PEG on the exterior at the target particle size of 10 to 15 nm. Two selected HDL mimicking nanostructures of different sizes (NanoMCL-12 and NanoMCL-14) were compared with traditional sHDL composed of PC and apoA-I mimetic peptides. This particular sHDL had previously been tested in single and multiple dose clinical studies as ETC-642, and was found to be safe and capable of cholesterol efflux in patients.[112, 206-

[207] Compared to sHDL, we found that our NanoMCLs have a similar ability to efflux cholesterol, had a 4-14-fold improved ability to inhibit LPS-induced inflammatory response, a 2-fold higher cholesterol mobilization capacity *in vivo*, and a 2-fold superior anti-atherogenic effect in ApoE$^{-/-}$ murine model of the disease.

4.3 Materials and methods

4.3.1 Materials

ApoA-I mimetic peptides 22A (PVLDLFRELLNELLEALKQKLK) and 5A (DWLKAFYDKVAEKLKEAFPDWAKAAYDKAAEKAKEAA) were synthesized by Genscript (Piscataway, NJ). The peptide purities were determined to be over 95% by reserve phase HPLC. 1,2-dipalmitoyl-*sn*-glycero-3-phosphocholine (DPPC) and N-(Carbonyl-methoxypolyethyleneglycol 2000)-1,2-distearoyl-*sn*-glycero-3-phosphoethanolamine (DSPE-PEG2k) were purchased from NOF Corporation (White Plains, NY). Bodipy-labeled cholesterol was purchased from Avanti Polar Lipids, Inc. (Alabaster, AL). Lipopolysaccharide (LPS) (E. coli O111:B4) was purchased from Sigma Aldrich (St. Louis, MO). All other materials were obtained from commercial sources.

4.3.2 Preparation of sHDL and NanoMCL nanoparticles

All investigated particles were prepared using a co-lyophilization method. Briefly, to prepare sHDs, 22A peptide and DPPC were dissolved in glacial acetic acid at a molar ratio of 0.14:1. Micellar nanoparticles (NanoMCLs) were prepared by dissolving DPPC and DSPE-PEG2000 in glacial acetic acid at the molar ratios of 1:0.065, 1:0.131, 1:0.262, 1:0.523, 1:1.05 and 1:2.09. After freeze-drying for over 24 hours, PBS (pH = 7.4) was added to hydrate the powders to a final lipid concentration of 27.24 mM. The mixture was vortexed briefly, heated to 50°C for 10 min. and cooled to 25°C for 10 min. This cycle was repeated three times. sHDL particle and Nano-MCL concentrations are expressed in terms of total lipid concentration throughout this work.

sHDL and micelle particles loaded with DiR fluorescent dye or bodipy-labeled cholesterol were prepared by a freeze-drying method and by dissolving DiR or labelled cholesterol in glacial acidic acid together with all other components. The final concentration of bodipy-cholesterol after hydration of the lyophilized powder was 30 μg/mL.

4.3.3 Characterization of sHDL and Nano-MCL

Particle size distribution of sHDLs and Nano-MCLs was determined by dynamic light scattering (DLS) using a Zetasizer Nano ZSP, Malvern Instruments (Westborough, MA) at

concentration of 2.7 μM. The average size and polydispersity index with standard deviation was reported. The particle morphology was assessed by transmission electron microscopy (TEM). The diluted sample solution was deposited on a carbon film-coated 400 mesh copper grid and dried for 1 minute. Samples were then negatively stained with 1% (w/v) uranyl formate, and the grid was dried before TEM observation. All specimens were imaged on a 100kV Morgagni TEM equipped with a Gatan Orius CCD.

4.3.4 Cholesterol efflux evaluation

RAW 264.7 cells were grown in DMEM medium supplemented with 10% FBS, penicillin (100 units/ml) and streptomycin sulfate (100 mg/ml) in a humidified 5% CO_2 atmosphere. 10^5 cells were then seeded into 24-well plates and grown for 24 hours. Cells were washed with PBS (pH 7.4) once at room temperature and labeled with cholesterol for 24 hours in DMEM/BSA/antibiotic media (0.5 mL) containing 1 μCi of [^{3}H] cholesterol/mL of media. Subsequently, labeled cells were washed twice with PBS (pH 7.4) to remove [^{3}H] cholesterol that was not taken up by cells. Tritium-labeled cholesterol was effluxed from cells for 18 hours, using various lipid complexes at different concentrations in duplicate. Finally, all cell media (0.5 mL) was removed into separate Eppendorf tubes and centrifuged at 10,000 rpm for 5 min. The remained cells were lysed with a 0.1% SDS / 0.1M NaOH solution for 2 hours. Radioactive counts of media and cell fractions were measured separately using a Perkin Elmer liquid scintillation counter. Percent cholesterol effluxed from cells was calculated by dividing media counts by the total sum of media and cell counts and then multiplying this number by 100%.

4.3.5 Liver cell uptake of cholesterol form sHDLs and NanoMCLs

The uptake of bodipy-labeled cholesterol loaded in either sHDLs or NanoMCLs by HepG2 cells was visualized by confocal laser scanning microscopy and quantified by flow cytometry. Briefly, liver hepatocellular carcinoma (HepG2) cells were cultured in Dulbecco's Modified Eagle Medium with 10% FBS and 1% Pen Strep Glutamine and maintained in an incubator at 37°C and 5% CO_2. On day 0, 10^4 to 10^5 cells were seeded in a MatTek 35 mm petri dish in DMEM. The next day, media was aspirated and cells were washed with PBS (pH 7.4). Fresh media containing sHDLs or micelles loaded with bodipy-labeled cholesterol was added at a final lipid concentration of 272.4 μM. After incubation at 37 °C for 2 hours, cells were washed twice with PBS (pH 7.4) followed by fixation with 4% paraformaldehyde in PBS for 15 min at room temperature. 1% Triton-X solution was then added to the dish for 15 min and washed twice with PBS (pH 7.4).

Finally, the cell nuclei were stained with DAPI. The nuclei and bodipy fluorescence images were acquired on a Nikon A-1 Spectral Confocal microscope system (Nikon Corporation, Tokyo), with an excitation wavelength of 495 nm for bodipy. Quantification of the cellular fluorescent signal was performed using a cell sorter (Beckman Coulter FC500 5-colour analyzer) at an excitation wavelength of 495 nm.

4.3.6 Anti-inflammation effect of sHDLs and NanoMCLs in vitro

To evaluate the anti-inflammatory effect of sHDLs and NanoMCLs, RAW 264.7 macrophage cells were seeded in 96-well plate on the first day. After a 24-hour incubation, cytokine release from macrophage cells was stimulated by addition of 2 ng/mL lipopolysaccharides (LPS). Subsequently, nanoparticles were added to the media immediately after the LPS at a 27.2 uM lipid concentration and incubated for 16 hours. The level of pro-inflammatory cytokines, TNF-α and IL-6, in the media were measured with an ELISA kit (Thermo Fisher Scientific, Waltham, MA). HEK-Blue cells purchased from InvivoGen (San Diego, CA) were cultured in DMEM containing 10% low endotoxin FBS and selective antibiotics according to the manufacturer's instructions. Growth medium was discarded, and cells were resuspended in HEK-Blue Detection medium. Cells were seeded at 25,000 cells per well. The cells were treated with sHDLs or NanoMCLs at 0.082 mM in a presence or an absence of 2 ng/ml of LPS and incubated for 18 hours. LPS binding to TLR4 results in activation of NF-κB reporter gene expression, causing the HEK-Blue detection medium to turn blue. The blue color was quantified by measuring absorption at 650 nm using a SpectraMax M3 plate reader from Molecular Devices (San Jose, CA).

4.3.7 Pharmacokinetics and pharmacodynamics evaluation in rats

The sHDL and NanoMCL nanoparticles were prepared at a final lipid concentration of 54.48 μM in PBS (pH 7.4). Eight male Sprague-Dawley rats were randomly assigned to two groups of four rats each, sHDL and NanoMCL-12 (DPPC: DSPE2k = 1:2.09). All rats were fasted overnight before dosing and received different formulations at a dose of 136 μmol/kg based on lipids concentration via tail vein injection. Blood samples of approximately 0.3 mL were collected from the jugular vein in heparinized BD centrifuge tubes (BD, Franklin Lakes, NJ) at pre-dose and 0.25, 0.5, 1, 2, 4, 8, 24 and 48 hours after dosing. Serum samples were separated immediately by centrifugation at 10,000 rpm for 10 minutes at 4°C and stored at -20°C until further analysis.

4.3.8 Quantification of serum lipids

The levels of serum phospholipids (PL), total cholesterol (TC), and unesterified or free cholesterol (FC) were determined by enzymatic analyses using commercially available kits (Wako Chemicals, Richmond, VA). Cholesterol ester levels (CE) were calculated as the difference between TC and FC levels at each time point. Briefly, serum samples were diluted with PBS (pH 7.4) for TC and FC detection, or with Milli Q water for PL detection. Defined amounts of standards or diluted samples were transferred to 96-well plates (50 μL, 60 μL and 20 μL for TC, FC and PL analyses, respectively), and assay reagents were added per manufacturer's instructions. The UV absorbance at 600 nm was measured using a Synergy NEO HTS Multi-Mode Microplate Reader (Bio-Tek).

4.3.9 Pharmacokinetics and pharmacodynamic analyses

A non-compartmental analysis (NCA) was performed to derive basic pharmacokinetic parameters for phospholipids serum concentration versus time profile using Phoenix© WinNonlin® Version 7.3 (Pharsight Corporation, Mountain View, CA). Serum concentration of phospholipids, total cholesterol, free cholesterol and cholesterol ester versus time were plotted. The pharmacokinetics parameters of phospholipids was calculated and the pharmacodynamic effect in each rat was determined as the area under the total effect curve (*AUEC*) from dosing time point to 48 hours after dosing. Secondary pharmacodynamic endpoints (maximal effect [E_{max}] and time to E_{max} [$T_{max,\,E}$]) were also analyzed to compare pharmacodynamic effects. The coefficient of variation was calculated for each parameter.

4.3.10 Cholesterol distribution among lipoproteins

Distribution of mobilized cholesterol between VLDL, LDL and HDL lipoprotein fractions following nanoparticle administration and exchange of cholesterol between lipoprotein throughout the 48-hour elimination process was monitored via lipoprotein analysis. Briefly, rat serum lipoproteins were separated by size using a Waters HPLC system equipped with a Superose 6, 10/300 GL column (GE Healthcare, Piscataway, NJ). Cholesterol distribution among VLDL, LDL, and HDL lipoprotein fractions was determined by post-column enzymatic reactions. Rat serum collected prior to nanoparticle dosing and 0.5, 4, 24 and 48 hours post-injection was analyzed. Serum aliquots (50 μL) were injected and eluted with 154 mM sodium chloride/0.02% sodium azide solution at 0.8 mL/min. The post-column reaction was used to determine cholesterol concentration as described in our previous published work.[208]

4.3.11 Anti-inflammation effect of sHDLs and NanoMCLs in vivo

The anti-inflammatory effects of sHDLs and NanoMCLs were compared in the murine endotoxemia model. 7 to 8 weeks old male C57BL/6 mice were purchased from Jackson Laboratories and randomly divided into four groups , containing 5 mice each: a) PBS, b) LPS, c) LPS and sHDL, and d) LPS and NanoMCL-12. In the first study, 0.05 mg/kg of LPS was mixed with either sHDL or NanoMCL-12 and dosed to mice by intraperitoneal (IP) injection. LPS alone and PBS injections were used as controls. In the second study, 0.05 mg/kg of LPS was dosed initially by intraperitoneal injection. Subsequently, different formulations were dosed at 27.2 μmol/kg (based on the phospholipids concentration) by tail vein injection. All blood samples were collected from the jugular vein in heparinized BD centrifuge tubes (Franklin Lakes, NJ) at 2 hours after LPS dosing. Serum samples were separated immediately by centrifugation at 14,000 rpm for 10 minutes at 4°C and stored at -80°C until further analysis. The concentrations of inflammatory cytokines of TNF-α in the serum were quantified using ELISA (Thermo Fisher Scientific, Waltham, MA) per manufacturer's instruction.

4.3.12 Bio-distribution and accumulation of particles in plaque area in mice

To monitor if sHDL and NanoMCL particles could accumulate in the atheroma, $ApoE^{-/-}$ (knockout) mice were fed a high-fat high-cholesterol diet (21% fat, 34% sucrose, and 0.2% cholesterol; Harlan, T.D. 88137) for 6 weeks to develop atherosclerotic lesions. DiR fluorescent dye was incorporated into sHDLs and NanoMCLs for tracking. The final DiR concentration was 20 μg/ml. The accumulation of sHDLs or micelles in plaque were evaluated by intravenous administration of DiR-labelled particles at a DiR level of 100 μg/kg after 12-weeks of feeding. Aorta were isolated for imaging purpose at 72 hours after dosing using an IVIS Spectrum Imaging System (Caliper, Fullerton, CA).

4.3.13 Anti-atherosclerotic efficacy study

Eight-week-old male ApoE knockout mice purchased from the Jackson Laboratories were fed a high-fat high-cholesterol diet (21% fat, 34% sucrose, and 0.2% cholesterol; Harlan, T.D. 88137) for 6 weeks to develop atherosclerotic lesions. Mice were then randomized into three groups and received an intravenous injection twice a week (Tuesday and Friday) of either sHDLs or NanoMCLs at a lipid dose of 136 μmol/kg or an equivalent volume (200 μl) of PBS as a control for another 6 weeks under the same feeding diet. At 72 hours after the last treatment, whole blood of mice were collected for serum clinical chemistry analysis, and the left ventricle of the heart was

perfused with PBS, followed by a fixative solution (4% paraformaldehyde in PBS). Liver was collected and kept in formalin for histological evaluation. To quantify the extent of the atherosclerotic lesions in the aortic root, the atherosclerotic lesions in the aortic sinus region were examined at three locations, each separated by 80 µm. The largest plaque of the three valve leaflets was used for morphological analysis. The lipid-burden plaque areas at the aortic sinus were determined by Verhoeff's staining. The macrophage cells in plaques were stained using a galectin-3 antibody (Mac-2; SANTA CRUZ Biotechnology, Santa Cruz, CA). To compare the effect of different groups, the area of stained lipid and macrophage were calculated using Image J.

4.3.14 Analysis of serum clinical chemistry and liver histology

As described in section 2.13, whole blood of ApoE knockout mice were collected at 72 hours after the last treatment and serum was separated by centrifuge at 14.000 rpm for 10 min. Serum triglyceride, alanine aminotransferase (ALT) activity and aspartate aminotransferase (AST) activity were measured using kits (TR0100, MAK052, MAK055, Sigma-Aldrich, St. Louis, MO). Liver tissue was collected and fixed in 4% formalin after perfusion of the animals. Then the liver tissue was routinely processed and embedded in paraffin. 8 µm thick sections were cut and stained with hematoxylin and eosin (H&E) for histopathological examination. All sections were investigated using a light microscope.

4.3.15 Lipogenesis study in mice

Normal C57BL/6 mice were divided into three groups (5 animals per group) including a PBS control, sHDL and NanoMCL-12. sHDL or NanoMCL-12 was given at the lipid dose level of 136 µmol/kg through intravenous administration. At 24 hours post-injection, mice were euthanized by CO_2 inhalation. After perfusion using PBS, liver tissues were collected and kept at -80 °C. Total RNA was purified from the liver tissues with TRIzol Reagent (Life technologies. Corp.), followed by reverse transcription with a SuperScript III kit (Invitrogen). qPCR was carried out with iQ SYBR Green Supermix (Bio-Rad). Cholesterol biogenesis related gene expression including Srebp2 and Hmgcr was determined.

4.3.16 Statistical Analysis

For comparisons and analyses between two groups, the significance of differences between data points, calculated pharmacokinetic and pharmacodynamic parameters were determined by the two-tailed unpaired Student's t-test. For comparisons among three groups or more, one-way

ANOVA analysis was performed followed by the Tukey's test. Data are presented as mean ± SEM. A p-value < 0.05 was considered statistically significant.

4.4 Results

4.4.1 Preparation and characterization of nanoparticles

We prepared the model sHDL nanoparticles using 22A apoA-I mimetic peptides and phospholipids (DPPC) combined at a 1:2 w/w (1:7.15 mol/mol) ratio of peptide to lipid. This composition was based on the composition of ETC-642, a peptide-based sHDL that has been previously tested in clinical trials in dyslipidemic patients.[144, 149] The average diameter of sHDLs was determined by dynamic light scattering (DLS) to be 9.2 ± 0.3 nm (Table 4.1, Fig. 4.1A), similar to the reported sHDL size.[152] To match the size of the nano-micelles (NanoMCL) with sHDLs, we combined increasing amounts of pegylated phospholipid (DPSE-PEG2000) with DPPC. We then prepared six NanoMCLs and their compositions and sizes are summarized in Table 4.1. The average particle size of micelles decreased gradually with the increase in DSPE-PEG-2000 to DPPC ratio. We selected two micelles had similar size to sHDL, 14 and 12 nm, and low polydisperse for further investigation and named them NanoMCL-14 and NanoMCL-12, respectively. We further characterized the nanoparticle morphology using transmission electron microscopy (TEM) (Fig. 4.1B). In agreement with our DLS findings, the TEM images showed homogeneous size distribution for all three nanoparticles.

Table 4.1: Characterization of sHDL and NanoMCL particles.

Formulation (molar ratio)	**Particle size (nm)**	**PDI**
22A: DPPC (0.14:1)	9.2 ± 0.3	0.16 ± 0.09
DPPC: DSPE-PEG2k (1:0.0654)	699 ± 51	0.40 ± 0.01
DPPC: DSPE-PEG2k (1:0.131)	403 ± 4.4	0.34 ± 0.03
DPPC: DSPE-PEG2k (1:0.262)	30.9 ± 1.0	0.13 ± 0.01
DPPC: DSPE-PEG2k (1:0.523)	27.8 ± 2.3	0.18 ± 0.01
DPPC: DSPE-PEG2k (1:1.05)	14.2 ± 0.4	0.20 ± 0.01
DPPC: DSPE-PEG2k (1:2.09)	12.2 ± 0.2	0.12 ± 0.01

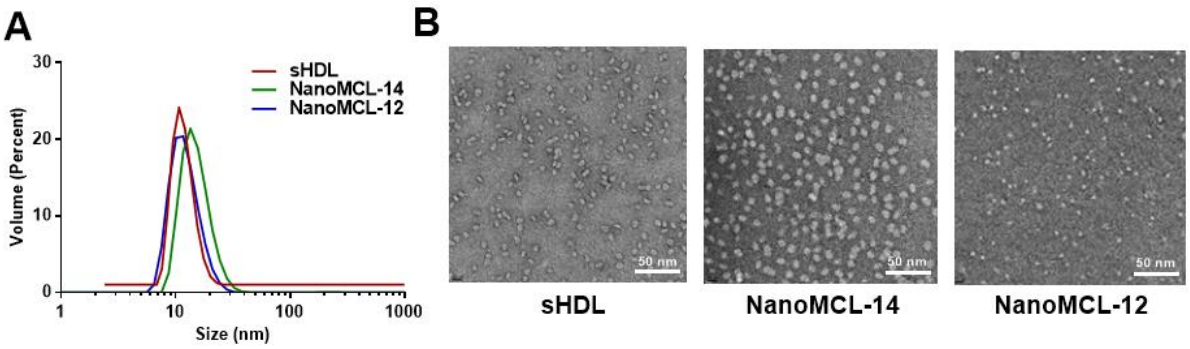

Figure 4.1: Characterization of NanoMCLs and sHDLs. Particle size distribution determined by dynamic light scattering (Panel A) and TEM (Panel B).

4.4.2 Cholesterol efflux capacity of sHDLs and micelles

Cholesterol filled macrophage-derived foam cells in the arterial wall are the hallmark of atherosclerosis. The removal of excess cholesterol from macrophage cells is important for reverse cholesterol transport process and reduction of plaque area.[200] We evaluated the ability of sHDLs and NanoMCLs to facilitate cholesterol efflux using RAW 264.7 macrophages. The cells were loaded with ^{3}H-cholesterol and treated with different concentrations of NanoMCLs and sHDLs to determine cholesterol efflux capacity of the nanoparticles. We determined the percent of cholesterol effluxed into the medium by nanoparticles by counting the radioactivity in the medium relative to combined radioactivity of the medium and lysed cells. All nanoparticles showed a significant ability to efflux cholesterol from the cellular membrane of macrophages (Fig. 4.2A). As the concentration of nanoparticles increased, the amount of effluxed cholesterol also increased and reached saturation at 70 to 80 μM lipid concentrations for all nanoparticles. At low concentration, the sHDLs group had slightly higher cholesterol efflux capacity relative to NanoMCLs groups, while all three groups achieved a similar plateau at high concentrations. Taken together, NanoMCLs have similar cholesterol efflux ability *in vitro* compared to sHDLs.

4.4.3 In vitro anti-inflammation effect of sHDLs and NanoMCLs

The anti-inflammatory properties of sHDLs and NanoMCLs were evaluated in RAW 264.7 macrophages. We induced an inflammatory response by addition of endotoxin (LPS) to stimulate the release of pro-inflammation cytokines such as TNF-α and IL-6.[209] Nanoparticles sHDLs or NanoMCLs were added to cell culture media and we determined cytokine levels by ELISA to assess abilities of the nanoparticles to inhibit the inflammatory response (Fig. 4.2D and E). Both

sHDLs and micelles showed a significant inhibitory effect on the secretion of TNF-α likely due to their abilities to physically bind and neutralize LPS and possibly disrupt toll-like receptor 4 (TLR-4) signaling by altering lipid raft microenvironment through cholesterol efflux.[210] Compared to sHDLs, NanoMCLs had a 4 to 14-fold higher cytokine release inhibitory effect. The difference between the effects of sHDLs and NanoMCLs are potentially due to differences in their LPS binding capacity. The HEK293-derived TLR-4 reporter cells were used to analyze neutralization of the LPS-induced inflammatory response by sHDLs and NanoMCLs. When activated by LPS, TLR4 receptor initiates a downstream signaling cascade resulting in activation of the NF-κB transcription factor, which we monitored in this assay. As shown in Fig. 4.2F, both sHDLs and NanoMCLs interfered with LPS interaction with TLR-4 resulting in the reduced activation of NF-κB. The NanoMCL-12 group exhibited similar activity to sHDLs and appeared to be superior to NanoMCl-14 as measured by this assay.

4.4.4 Cholesterol uptake by liver cells in sHDLs and NanoMCLs

After cholesterol is effluxed from peripheral tissues by sHDLs, it is taken up by scavenger receptors on hepatocytes, metabolized and excreted into the bile.[12] To evaluate cholesterol uptake by hepatocytes, sHDLs and NanoMCL particles were loaded with bodipy-labeled cholesterol and incubated with HepG2 cells for various time intervals. The kinetics of cellular uptake of bodipy-cholesterol was visualized using confocal imaging and quantified by flow cytometry (Fig. 4.2B and 2C). The fluorescence of bodipy appears to distribute throughout the cellular membranes and cytosol for all groups. When bodipy-cholesterol uptake by HepG2 cells was quantified using flow cytometry and compared among different formulations, there were no significant differences observed between the sHDLs and NanoMCLs groups. Thus, we conclude that, similar to delivery of cholesterol by sHDLs, cholesterol can be taken up by hepatocytes when delivered by NanoMCLs.

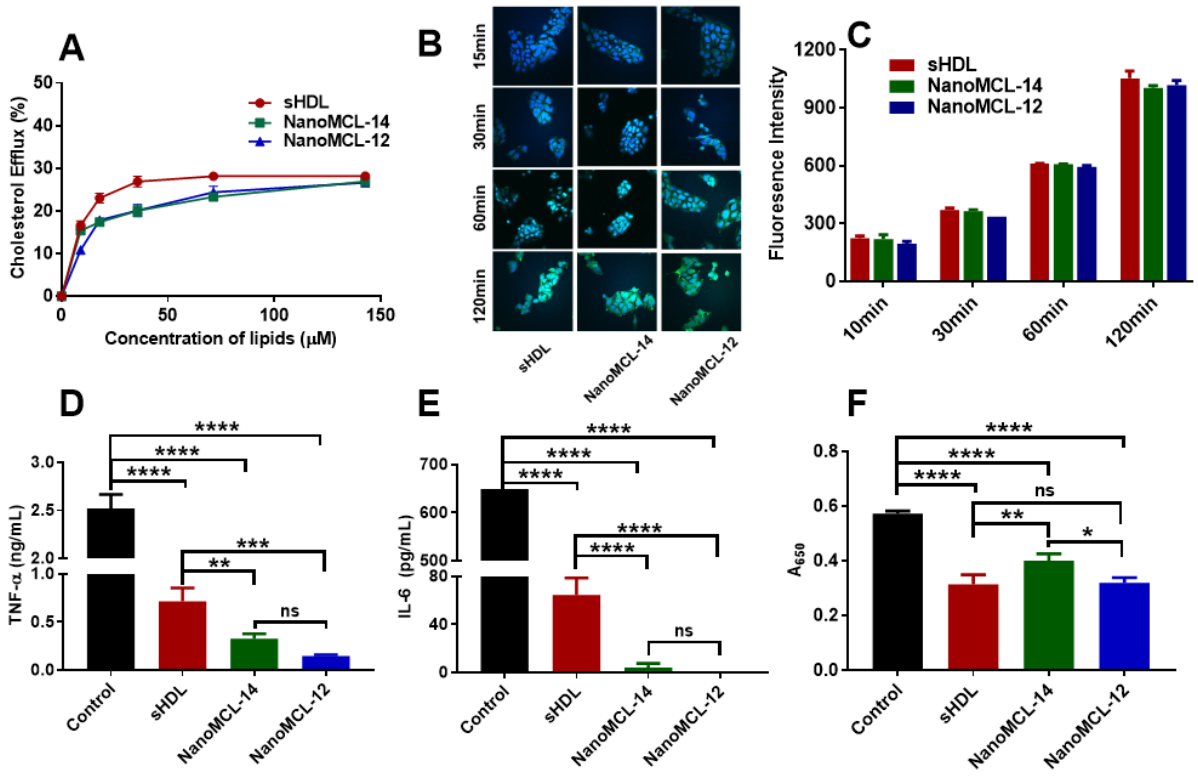

*Figure 4.2: Comparison of in vitro potency of NanoMCLs and sHDL. Cholesterol efflux from RAW 264.7 macrophages (Panel A). Cholesterol uptake kinetics by HepG2 cells following incubation with bodipy-labeled cholesterol-loaded sHDL or NanoMCL nanoparticles imaged with confocal microscopy (Panel B) and quantified by flow cytometry (Panel C). Panel B shows the channel overlay, with nuclei in blue and bodipy-cholesterol in green. Release of inflammatory cytokines TNF-α (Panel D) and IL-6 (Panel E) after incubation of sHDLs or NanoMCLs with RAW 264.7 macrophages for 16 hours with pre-treatment of LPS. LPS-induced NF-kB activation in HEK-blue cells expressing TLR4-NF-kB reporters is reduced by addition of sHDLs and NanoMCLs (Panel F). *p<0.05, **p<0.01, ***p<0.001, ****p<0.0001, ns: no significant difference.*

4.4.5 Pharmacokinetic characterization of sHDLs and NanoMCLs

We selected NanoMCL-12 for further evaluation *in vivo* based on our *in vitro* results showing NanoMCL-12 exhibited higher anti-inflammation efficacy and smaller particle size compared to other micelles analyzed. We compared the pharmacokinetics of sHDLs and NanoMCL-12 and the nanoparticles' abilities to efflux cholesterol from the peripheral cells into blood compartment in the Sprague Dawley (SD) rat. Both nanoparticles were administered at 136 μM of phospholipids/kg dose by an intravenous bolus administration. This phospholipid dose was equivalent to 50 mg/kg dose of apoA-I peptide, the typical dose used in preclinical models.[67, 208] We measured the serum concentrations of the phospholipid components of sHDL and NanoMCL-12 using a plate assay and subtracted the pre-dose levels of lipids (Fig. 4.3A). The

pharmacokinetics data were fitted using a non-compartment analysis (NCA) and pharmacokinetic parameters such as maximum serum concentration (C_{max}), area under the serum concentration-time curve (*AUC*), elimination rate constant (K_{10}), elimination half-life ($T_{1/2}$), total clearance (*CL*) and volume of distribution at steady state (V_{ss}) were derived (Table 4.2).

The PK behavior of sHDL phospholipids was significantly different from that of NanoMCL-12. Though there was no significant difference between the peak concentration C_{max} of phospholipids in sHDL and NanoMCL-12, the peak time of NanoMCL-12 appeared much later than that of sHDL, at 8 hours after administration. The later C_{max} for NanoMCL relative to sHDL may be due to differences in biodistribution of the two nanoparticles.[211] In addition, NanoMCL-12 had a longer lipid serum half-life *in vivo* with value of 16 hours compared to 1.7 hours for sHDL. The *AUC* increased nearly 10-fold from 1063 mg*h/dL for sHDL to 10620 mg*h/dL for NanoMCL-12 resulting from the slower clearance. Thus, packaged in Nano-MCLs, phospholipid appear to have longer residence time *in vivo*, which might result in the ability to efflux and eliminate more cholesterol per injected dose.

Table 4.2: Pharmacokinetic parameters (% CV) of phospholipids after admistration of sHDL and NanoMCL-12 at 136 µmol/kg.

Parameter	**Groups**	
	sHDL	**NanoMCL-12**
C_{max} [a] **(mg/dL)**	383.9 (24.3)	481.8 (36.4)
T_{max} [b] **(h)**	0.38 (33.3)	8.0 (0.00) ****
AUC [c] **(mg*h/dL)**	1603 (26.0)	10620 (31.3) **
K_{10} [d] **(h^{-1})**	0.4776 (41.8)	0.04885 (37.6) **
$T_{1/2}$ [e] **(h)**	1.686 (34.7)	16.07 (32.1) **
CL [f] **(dL/h)**	0.018 (26.9)	0.0027 (30.0) ***
V_{SS} [g] **(dL)**	0.0404 (26.1)	0.0649 (51.8)

[a]C_{max}: the maximum plasma concentration of peptide; [b]*AUC*: the area under the curve in plot of concentration of peptide against time; [c]K_{10}: elimination rate constant; [d]$T_{1/2}$: the half-life of elimination; [e]*CL*: total clearance for peptide; [f]V_{ss}: volume of distribution for peptide at steady state. Data was shown as mean with CV%. Significance:*p<0.05, **p<0.01, ***p<0.001, ****p<0.0001, ns: no significant difference compared with sHDL group.

4.4.6 In vivo pharmacodynamics of sHDLs and NanoMCLs

To examine the impact of increased circulation time of NanoMCLs relative to sHDLs on pharmacological response, we determined the changes in cholesterol metabolism biomarkers following administration of nanoparticles to normal SD rats by IV infusion. sHDLs has been reported to facilitate cholesterol removal from peripheral tissues through RCT, thus, transient increase in serum cholesterol levels reflects cholesterol efflux induced by administration of nanoparticles followed by its elimination by the liver. The levels of plasma total cholesterol (TC) and free cholesterol (FC) were determined directly, while esterified cholesterol level was calculated by subtracting free cholesterol level from total cholesterol level at each time point (CE) (Fig. 4.3D, E and F). Pharmacodynamics parameters were calculated and summarized in Table 2.3. The typical pharmacological response following sHDL infusion is a rapid mobilization of free cholesterol into the plasma compartment, followed by a rise in cholesterol ester due to esterification by lecithin-cholesterol acyltransferase (LCAT) and subsequent elimination of cholesterol by the liver. These expected effects were observed for sHDL infusions with a maximum FC mobilization of 75 mg/dL at 0.5 hours followed by a peak in CE (46 mg/dL) at 4 hours, and elimination of all mobilized cholesterol by 24 hours post-dosing. In line with the improvements in PK, NanoMCL-12 exhibited greater cholesterol mobilization and longer pharmacodynamic effect relative to sHDL with peak time of 7 hours after infusion and maximum free cholesterol increase of 166 mg/dL. The area under the effect curve increased over 10-fold from 422 mg*h/dL (sHDL) to 4387 mg*h/dL (for NanoMCL-12). We observed a similar trend for the total cholesterol and cholesterol ester levels with significantly higher E_{max} and *AUEC* values for NanoMCL-12. However, cholesterol increase in both groups was transient, and the cholesterol level returned back to baseline after 24 hours for sHDLs and 48 h for NanoMCL-12 along with the elimination of particles. Hence, the longer lipid circulation time for NanoMCL-12 resulted in greater levels of mobilized cholesterol and a longer duration of the effect, which, in turn, should lead to a higher amount of cholesterol eliminated from the body and superior anti-atherosclerotic effect of NanoMCLs relative to sHDLs.

Table 4.3: Pharmacodynamic parameters (% CV) of total cholesterol (TC), free cholesterol (FC) and cholesterol ester (CE) after admistration of sHDL and NanoMCL-12 at 136 µmol/kg.

	Parameter	sHDL	NanoMCL-12
TC	$T_{max,E}$[a] (h)	0.75 (33.3)	6.0 (33.3)**
	E_{max}[b](mg/dL)	114.9 (22.0)	237.9 (16.4)**
	AUEC[c] (mg*h/dL)	562.8 (22.4)	6607 (24.1)***
FC	$T_{max,E}$ (h)	0.56 (48.4)	7.0 (24.7)***
	E_{max} (mg/dL)	74.6 (23.2)	165.9 (20.5) **
	AUEC (mg*h/dL)	421.7 (31.6)	4387 (28.9)***
CE	$T_{max,E}$ (h)	1.2 (68.8)	15 (60.7)*
	E_{max} (mg/dL)	46.4 (37.2)	84.7 (17.8)*
	AUEC (mg*h/dL)	372.9 (18.6)	2220 (14.7)****

[a]T_{max}: time at which the E_{max} is observed. [b]E_{max}: the maximum plasma concentration of different cholesterol species. [c]*AUEC*: the area under the effect curve. Data was shown as mean CV%. *p<0.05, **p<0.01, ***p<0.001, ****p<0.0001.

4.4.7 Distribution of mobilized cholesterol and lipoprotein remodeling in vivo

To investigate in greater detail the mechanism of cholesterol mobilization and elimination following administration of sHDLs and NanoMCLs, we determined the relative distribution of mobilized cholesterol in the HDL, LDL, and VLDL fractions by HPLC. The positions of HDL, LDL, and VLDL sized particles containing cholesterol are labeled on Fig. 4.3B and C. The infusion of sHDL caused a rapid mobilization of cholesterol in the HDL fraction, with the maximum increase at 0.5 h postdose (blue line). The increase in HDL-C was accompanied by small increase in VLDL-C, and cholesterol returned to baseline levels by 24 hours post-dosing. The cholesterol profile changes were different when NanoMCL-12 were administered. Because NanoMCL-12s are slightly larger in size than sHDLs, the mobilized cholesterol appeared to elute between the HDL and LDL fractions at 0.5 and 4 hours post-administration. The increase in VLDL-C appeared to be higher for NanoMCL-12s relative to sHDLs. It is possible that DSPE-PEG caused inhibition of lipoprotein lipase or stimulation of liver lipogenesis, which both lead to the transient increase in VLDL-C. However, for both formulations, cholesterol increases were transient. The cholesterol level and its relative lipoprotein distribution returned to pre-dose levels, indicating completion of the RCT process triggered by administered sHDLs and NanoMCL-12s.

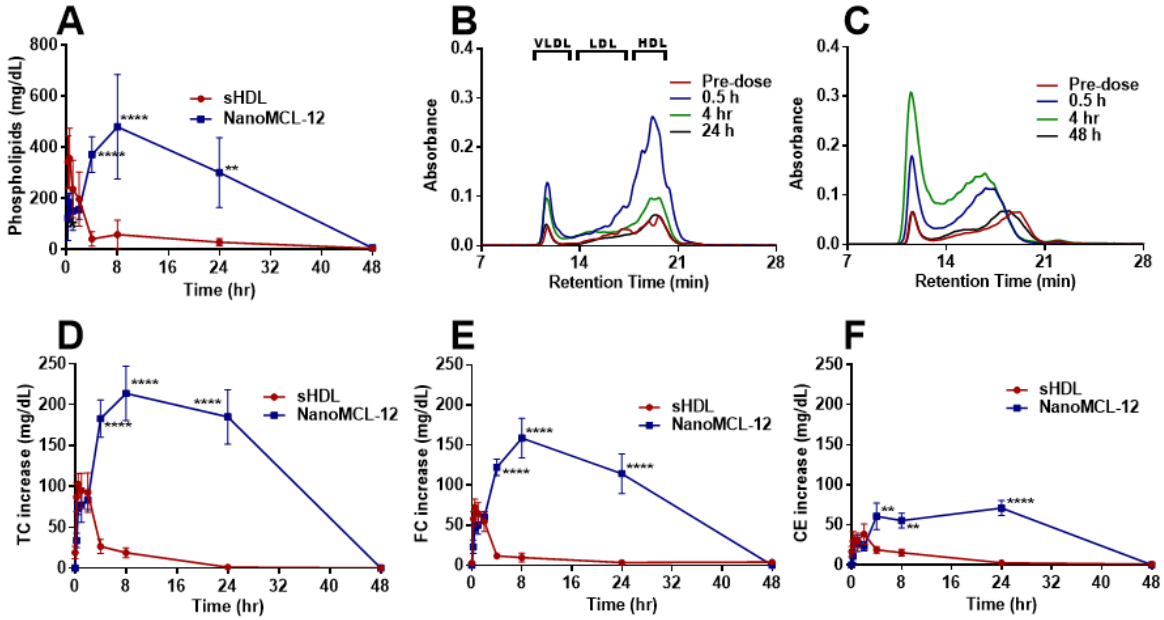

*Figure 4.3: Comparison of sHDL and NanoMCL-12 pharmacokinetics and pharmacodynamics in the rat. Pharmacokinetics of phospholipids after IV bolus administration of 136 µmol/kg of sHDLs or NanoMCL-12s in the Sprague Dawley rat. Change in plasma lipids was measured by choline oxidase assay (Panel A); Distribution of mobilized cholesterol among VLDL, LDL and HDL lipoprotein fractions following administration of sHDLs (Panel B) and NanoMCL-12s (Panel C). Mobilization of cholesterol from prerripheral tissues into blood compartment. The change in levels of total cholesterol (TC, Panel D), free cholesterol (FC, Panel E) and cholesterol ester (CE, Panel F) in rat serum was determined using commercially available kits. *p<0.05, **p<0.01, ***p<0.001, ****p<0.0001, ns: no significant difference.*

4.4.8 In vivo anti-inflammation effect of sHDLs and NanoMCLs

To further examine functional similarities of NanoMCLs and sHDLs, we examined their abilities to inhibit inflammatory cytokine release in a mouse endotoxemia model. In clinical trials, co-administration of endotoxin mixed with sHDLs in health subjects resulted in reduced inflammatory cytokine release, control of blood pressure and a marked decrease of the severity of clinical symptoms relative to administration of endotoxin alone.[79] To simulate this study, we dosed normal C57BL/6 mice with either LPS alone (0.05 mg/kg mixed with PBS) or co-administered either with sHDLs or NanoMCL-12s. When LPS alone was administered to the mice, release of TNF-α was observed at 2 hours post-dosing. In contrast, co-administration of LPS with sHDLs or NanoMCL-12s significantly reduced TNF-α release by 10.7 and 3.7-fold ($p<0.01$, Fig. 4.4A).

To simulate a more realistic scenario of infection-induced sepsis and nanoparticle treatment, we next dosed C57BL/6 mice with LPS by intraperitoneal injection, while sHDLs and NanoMCL-12s were administered subsequently by IV bolus at a 27.2 µmol/kg dose as a rescue treatment.

Two hours later, we collected whole blood and isolated serum to quantify cytokines levels. Both sHDL and NanoMCL-12 groups exhibited notable inhibition of TNF-α release 2 hours post endotoxin challenge (Fig. 4.4B). TNF-a is known a rapid response cytokine elevated shortly after endotoxin challenge, thus, it is logical that we saw functional changes in TNF-a at this time point. Taken together, NanoMCL exhibits both cholesterol efflux and anti-inflammatory functions of sHDL *in vivo*.

4.4.9 Accumulation of sHDLs and NanoMCLs in atherosclerotic plaque

We examined the ability of NanoMCLs and sHDLs to accumulate in atheroma in ApoE$^{-/-}$ mice that were fed a high-fat diet for 12 weeks to develop atherosclerosis. NanoMCL-12s and sHDLs were fluorescently labelled by incorporation of DiR dye and dosed by intravenous administration at a 100 μg/kg DiR dose corresponding to 136 μmole/kg lipid dose. At 72 hours after dosing, the entire aorta was isolated for IVIS imaging (Fig. 4.4C). From the images, both sHDLs and NanoMCL-12s successfully accumulated in the heart and plaque area enabling the potential interaction between sHDLs and micelles with macrophages for cholesterol efflux. The accumulation of both particles can last at least three days after administration due to the hydrophobicity of the particles and the specific distribution can potentially reduce the side effect caused by systemic treatment.

4.4.10 Anti-atherosclerosis efficacy of sHDLs and NanoMCLs

The ability of sHDLs and NanoMCLs to reduce the atherosclerotic burden was evaluated in ApoE$^{-/-}$ mice. ApoE$^{-/-}$ mice were placed on high fat diet for 6 weeks to develop atherosclerosis and were randomly divided into three groups for treatment with either PBS, sHDL or NanoMCL-12s for 6 weeks. We dosed the mice intravenously twice weekly at the dose level of 136 μmol/kg. Following the conclusion of treatment regimens, animals were euthanized and aortic root were excised for plaque area analysis by Verhoeff's staining (Fig. 4.4D) and Mac-2 macrophage staining (Fig. 4.4E).

Compared to PBS control groups, the atheroma area was reduced significantly following the 6-week treatment of either sHDLs or NanoMCL-12s. There was a 21% reduction in plaque area following sHDLs administration and 40% reduction ($p < 0.01$) for NanoMCL-12s compared to the non-treatment group (Fig. 4.4D) suggesting that consistent with a higher efflux capacity *in vivo*, NanMCL-12 sexhibit greater anti-atherosclerotic potency in the ApoE$^{-/-}$ murine model. The Mac-2 staining signal represents the macrophages infiltration in aorta root area, which is a

biomarker for inflammation and plaque formation.[212-213] Compared to the PBS control group, sHDL treatment did not significantly influence the Mac-2 positive macrophage area, while NanoMCL-12 group showed a 36% reduction of macrophage positive plaque burden relative to placebo ($p < 0.05$). By inhibiting the macrophage infiltration into the arterial wall, the induction of an early atherosclerotic lesion development can be prevented.[214] Taken together NanoMCL exhibits superior to sHDL ability to reduce atherosclerotic burden and prevent atherogenesis in murine model of the disease.

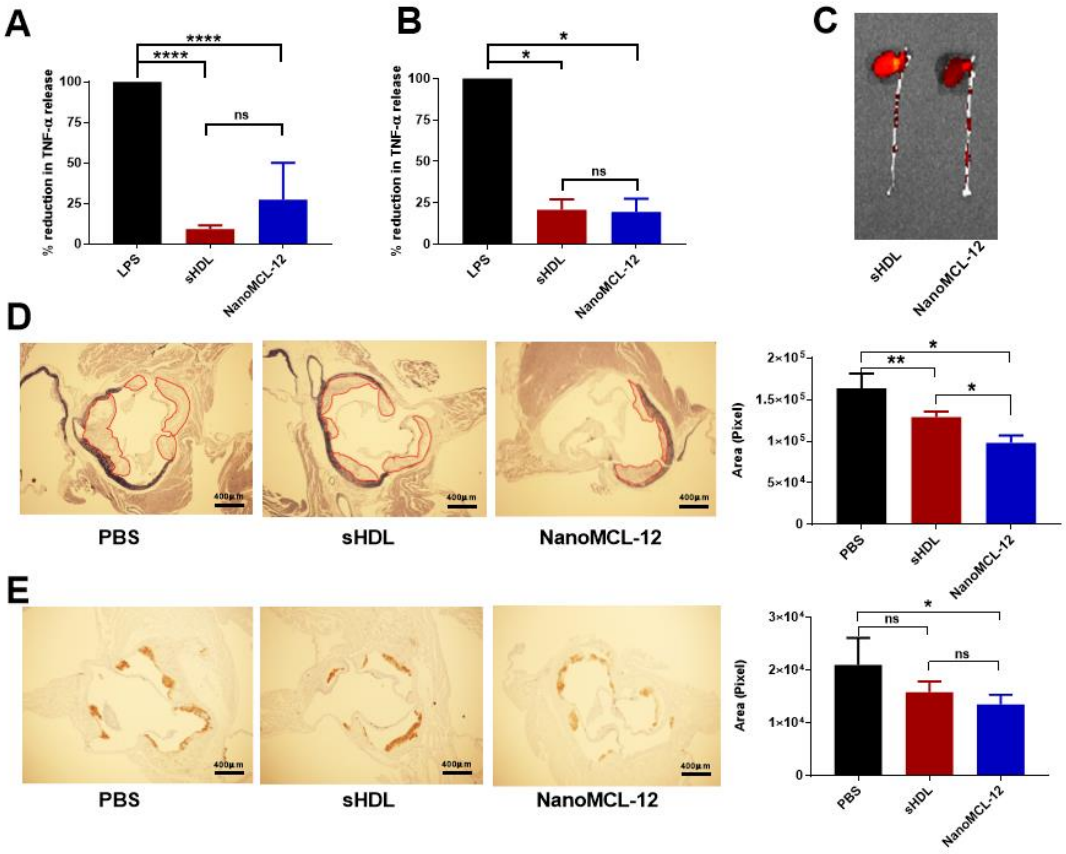

*Figure 4.4: Pharmacological effects of NanoMCL and sHDL in murine models of inflammation and atherosclerosis. Serum concentration of TNF-α in C57BL/6 mice at 2 h after co-administration of sHDLs or NanoMCL-12s (27.2 µmol/kg) with LPS (0.05 mg/kg) by IP route (Panel A) and administration of LPS by IP followed by administration of sHDLs or NanoMLC-12s by IV at the same doses (Panel B). (n=5/group; *p<0.05, **p<0.01, ***p<0.001, ****p<0.0001, ns: no significant difference) Accumulation of DiR-labelled sHDL or NanoMCL-12 particles in plaque in ApoE$^{-/-}$ mice fed a high fat diet for 12 weeks (Panel C). Effect of sHDLs and NanoMCL-12s on atherosclerosis regression in ApoE$^{-/-}$ mice. Mice were fed for 6 weeks, and dosed at 136 µmol/kg on every Tuesday and Friday for 6 weeks. Aortas were dissected and plaque areas were visualized by Verhoeff's staining (Panel D) and macrophage s in aortas sections were visualized by Mac-2 stain (Panet E). Representative lesion images and corresponding quantitative analyses of the aortic root cross-sections are shown. (n=12/group; *p<0.05, **p<0.01, ***p<0.001, ****p<0.0001, ns: no significant difference).*

4.4.11 Safety evaluation after treatment with sHDLs and micelles

We next studied the potential side effects and liver toxicity caused by sHDL or NanoMCL administration in ApoE$^{-/-}$ mice. H&E staining of liver tissues indicated no obvious damage to liver tissues when either sHDLs or NanoMCL-12s were administered (Fig. 4.5A). Plasma AST or ALT levels determined 72 hours following the last dose were similar for all groups indicating no reduction in liver function (Fig. 4.5C and D). In addition, plasma triglycerides level, were identical among the nanoparticle groups (Fig. 4.5E). Then we assessed the effect of sHDL or NanoMCL in C57BL/6 mice at dose level of 136 μmol/kg (Fig. 4.5B). At 24 hours after intravenous administration of nanoparticles cholesterol biosynthesis related genes expression were examined. *Srebp2* expression were not changed while *Hmgcr* expression in the liver was slightly down-regulated in NanoMCL-12 group. The elevation of plasma AST, ALT and triglyceride levels are hallmarks of sHDL nanoparticles toxicity resulting from the need for the liver to metabolize large quantities of mobilized cholesterol. The sHDL nanoparticles used in this ApoE$^{-/-}$ study were found to be safe in dyslipidemic patients at a similar dose level (~ 11.4 μmol/kg peptide) and safe in non-human primates at 2-fold higher doses.[112, 215] Since no significant liver enzymes and triglyceride elevation had been observed for sHDL or NanoMCL at therapeutic doses, we expect that NanoMCL will have comparable safety to that of sHDL in humans.

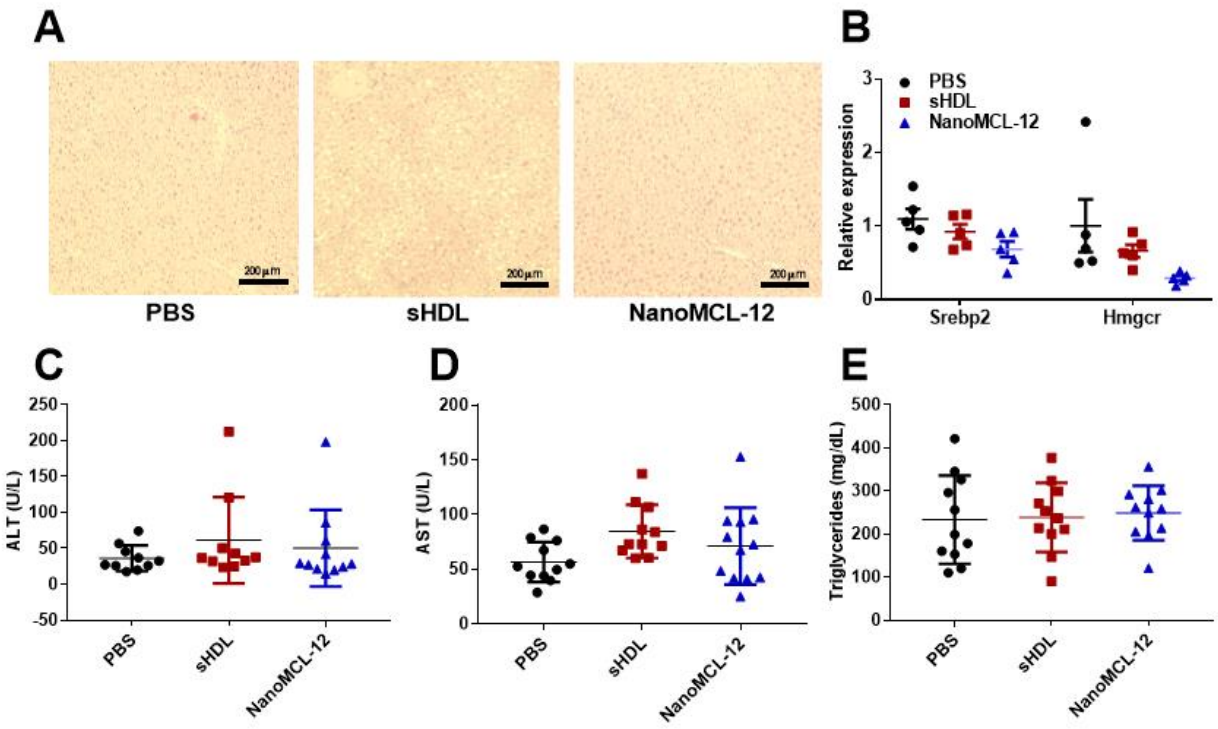

Figure 4.5: Safety comparasion between sHDL and NanoMCL-12. H&E staining of liver tissues after 6-week treatment of either PBS, sHDL or NanoMCL-12 in ApoE$^{-/-}$ mice (scale bar 300 µm) (Panel A). The expression of genes involved in cholesterol biogenesis in the liver at 24 h after administration of sHDLs or NanoMCL-12s at 136 µmol/kg in wildtype mice (Panel B) (n= 5/group). Serum concentration of ALT (Panel C), AST (Panel D) and triglyceride (Panel E) after 6-week treatment with either PBS, sHDLs or NanoMCL-12s in ApoE$^{-/-}$ mice (n=12/group).

4.5 Discussion and conclusion

In this study, we successfully established the NanoMCL system that mimics sHDLs in structure and function. The NanoMCL particles we selected were similar to sHDLs (about 12 nm) with a hydrophobic core and hydrophilic shell. Compared to sHDLs, micelles exhibited similar cholesterol efflux from macrophages (Fig. 4.2A), similar cellular uptake by liver cells (Fig. 4.2B and C), and had a more potent anti-inflammation effect in macrophages (Fig. 4.2D, E and F). Despite a high similarity *in vitro*, the performance of micelles differed when the two different types of nanoparticles were examined in normal rats. Administration of micelles led to greater extent of cholesterol mobilization and a longer duration of cholesterol elevation relative to sHDLs (Fig. 4.3) due to longer NanoMCL circulation *in vivo*. Administration of sHDLs and NanoMCLs led to mobilization of cholesterol into the infused particles and transfer of mobilized cholesterol to larger LDL and VLDL particles, yet all lipoprotein cholesterol levels returned to baseline 48 hours post-dosing (Fig. 4.3B and C). In our therapeutic experiment, both sHDLs and NanoMCLs reached atheroma after IV dosing and achieved a significant reduction of plaque burden following a 6-week treatment of atheroma-bearing ApoE$^{-/-}$ mice. Surprisingly, NanoMCLs showed greater anti-atherosclerosis efficacy relative to sHDLs, with a 40% atheroma area reduction compared to 21% for sHDLs. Following the 6-week treatment, there were no documented histological changes in the liver and no serum safety biomarkers were observed, indicating comparable safety of NanoMCLs and sHDLs at the therapeutic dose levels (Fig. 4.5). Thus, simple NanoMCL nanoparticles appear to function just like sHDL *in vivo*, providing an easy to manufacture and economic alternative to sHDLs as NanoMCLs are prepared without the need for expensive recombinant apoA-I proteins or peptides.

The utility of HDL as a therapeutic target had been challenged in recent years due to failures of several cholesterol ester transfer protein (CETP) inhibitors in large phase III clinical trails.[164, 216] These therapeutic agents inhibit transfer of cholesterol ester from HDL to LDL, resulting in increased levels of circulating HDL cholesterol rather than an increase in the numbers of functional HDL particles. Thus, chronic dosing with CETP inhibitors results in plasma

accumulation of larger, cholesterol ester-loaded HDL particles that have limited capability for additional cholesterol efflux. In contrast, infusion of cholesterol-free sHDL nanoparticles has the proven ability to rapidly efflux an excess of cholesterol from peripheral tissues. After just 5 to 6 infusions, the treatment leads to a drastic reduction in atheroma volume in CVD patients, as seen by intravascular ultrasound imaging in clinical studies.[41, 217-218] Prior studies demonstrated that IVUS imaging studies are capable of detecting significant atheroma reduction in patients with a substantial plaque burden, while it is more difficult to measure atheroma reduction in "healthier" patients due to intrinsic errors in imaging techniques.[219] Still one important clinical question remains: Can acute reduction in atheroma volume lead to a reduction in cardiovascular deaths, heart attacks and strokes. To address this question, a large phase III clinical trial is currently ongoing in 17,400 patients treated with either placebo or an sHDL drug (CSL-112).[203-204] In addition, significant interest in the field remains for the use of sHDL therapeutics for treating systemic inflammatory diseases like sepsis, lupus and rheumatoid arthritis.[79, 220-221] Therefore, the NanoMCLs we describe here could be potentially useful beyond cardiovascular applications.

Several other investigators have developed biomimetic HDLs for either treatment or imaging of atherosclerosis and for drug delivery purposes.[69-77] For example, Marrache *et al.* reported the construction of a synthetic, biodegradable HDL-NP platform for detecting vulnerable plaques by targeting the collapse of the mitochondrial membrane potential that occurs during apoptosis.[77] The particle has an average size of approximately 120 nm and contains a poly(lactide-co-glycolide) polymer, cholesteryl oleate, and phospholipid with triphenylphosphonium (TPP) decorated with apoA-I mimetic peptide 4F. In addition, quantum dots (QDs) have been incorporated into a PLGA matrix for imaging purposes. *In vitro* evaluation of this technique showed a promising detection ability for optimal imaging and therapeutic potential as well as a favorable biodistribution and pharmacokinetics. Sanchez-Gaytan *et al.* developed a hybrid polymer/HDL nanoparticle composed of a lipid/apolipoprotein coating that encapsulates a PLGA core.[75] This PLGA-HDL 30 to 90 nm sized nanoparticle displayed some characteristics of endogenous HDL, including preferential uptake by macrophages and had an effective *in vitro* cholesterol efflux capacity. Presence of a PLGA nanoparticle core also enables incorporation, sustained release and atheroma targeted delivery of therapeutic agents. PLGA-HDL nanoparticles were able to accumulate in atherosclerotic plaques and co-localized with atheroma macrophages in an $ApoE^{-/-}$ mouse model. Thaxton *et al.* synthesized a spherical HDL nanoparticle with an Au

NP core-shell structure, in which the Au NP core serves as a size- and shape-controlling scaffold for constructing an HDL-like particle by surface attachment of phospholipids and apoA-I. The nanoparticles were designed to have a similar size to endogenous HDL and to mimic the general surface composition of HDL to enable physical binding of cholesterol and cellular cholesterol efflux *in vitro*.[69, 78] Biomimetic HDL nanoparticles demonstrated the ability to accumulate in the atheroma and, in some instances, had local anti-inflammatory effects.[79-80] However, to the best of our knowledge, neither the abilities of these biomimetic HDL to reduce atheroma in disease bearing animals have been confirmed and none of these nanoparticles have been compared head to head with the sHDLs that have been tested in clinical trials. In addition, most of biomimetic HDL nanoparticles have a larger particle size and density compared with endogenous HDL likely resulting in differences in biodistribution, HDL receptor interaction and hepatic uptake mechanism of mobilized cholesterol.

With the growing tendency in the field to increase the complexity of nanomedicine designs, our approach to create a simple HDL-mimicking micelle appears to be almost "primitive". Yet, simple ideas often win in clinical translation, as both manufacturing cost and quality of complex products are difficult to control. Both ingredients of NanoMCLs, PC and pegylated-PC, are approved excipients for parenteral administration. Moreover, the process of two-component mixing that results in the formation of nanoparticles with a target size of 12 nm capable of cholesterol efflux as determined by a cell-based bioassay is relatively straight forward. Thus, NanoMCL manufacturing could be established under quality scrutiny required for producing clinical grade material. There are multiple examples of simplistic products advancing to clinical development in the cardiovascular and inflammatory disease fields. For example, ETC-588, a type of blank liposome, has shown efficacy in ischemia patients in a Phase II trial working in combination with[222222222222222] endogenous HDL that would efflux cholesterol from atheroma and deposit in circulating sink of blank liposomes for eventual elimination by the liver.[223] A phospholipid emulsion, GR270773, was developed by GSK as a treatment for sepsis. It works by scavenging endotoxins (lipopolysaccharides) released by bacteria.[222] There have also been micro-emulsions of triglycerides and phospholipids (Intralipid®) that have been tested in clinical studies aiming to treat pharmacotoxicity.[224-225] Synthetic HDL nanoparticles had been shown to bind endotoxins and inhibit inflammatory responses in human studies and able to rapidly regress atheroma in CVD patients.[79, 226] As our simple NanoMCL system appears to have a higher capacity

for binding endotoxin and cholesterol as compared to sHDLs, NanoMCLs likely could provide an exciting translational opportunity for treatment of CVD, sepsis and other diseases involving scavenging hydrophobic molecules.

Chapter 5 : Development of sHDL based drug delivery system for glioma therapy

5.1 Abstract

Glioblastoma multiforme, GBM, is a fast-growing, aggressive type of central nervous system tumor that forms on the supportive tissue of the brain. Docetaxel (DTX) is a chemotherapeutic agent clinically used for treatment of various solid tumors. CpG, oligodeoxynucleotide, is toll-like receptor 9 (TLR9) agonist that can stimulate host immune response to tumor cells. Due to the intrinsic targeting property of sHDL through the interaction with scavenger receptor BI (SR-BI) expressed on GBM cells, DTX-sHDL-CpG nanoparticles were synthesized in this study to deliver chemotherapeutic drug (DTX) together with immune stimulatory molecule (CpG) for tumor inhibition. By determining the expression of SR-BI on various cell lines and through cytotoxicity evaluation, the GL26 cell line was selected to establish the tumor model and DTX was selected as the drug to be loaded in sHDL. Formulation was further optimized based on stability of DTX-loaded sHDL, and apolipoprotein A-I (ApoA-I) mimetic peptide, 22A, and sphingomyelin (SM) were selected for final formulation. *In vitro* studies determined that 30% of sHDL particles could penetrate through blood-brain barrier model and could be successfully taken up by the cancer cells. However, intravenous administration of sHDL didn't show a significant improved therapeutic effect compared to free drug in the murine glioblastoma survival study. For intracranial injection groups, DTX-sHDL-CpG showed 1.17-fold increase of mean survival time (MS) compared to free drug, with 20% of long-term survivors.

5.2 Introduction

Glioblastoma multiforme (GBM) is the most aggressive primary tumor within the central nervous system. [227] Even after performing a surgical excision, chemotherapy, and radiotherapy, the prognosis of patients with GBM remains dismal. GBM commonly recurs, and often results in the death of the patient. Therefore, the development of effective treatment strategies to control the progression and survival of these gliomas is necessary.

Chemotherapy is a commonly used clinical treatment for GBM. Although chemotherapeutic agents are directed to kill cancerous cells, the byproduct of their application

often results in the death of normal cells. Since their cytotoxic effects are not selective for cancerous cells, toxicity is a major issue to consider. Besides, many anti-cancer drugs have poor water solubility and a short half-life *in vivo.* [228] Thus, reduction of possible toxicity requires the delivery of higher specificity chemotherapeutic agents. In addition to chemotherapy, immunotherapy arises to be an attractive alternative strategy to correct the immunosuppressive environment in glioblastomas. CpG oligodeoxynucleotide is a TRL9 ligand expressed by most murine immune cells which can trigger immune rejection and induce long-term immunity against gliomas. [229] CpG loaded products have been explored as an effective treatment for glioma through intracranial injection. [230-232] Co-delivery of chemotherapeutic drugs and CpG can potentially achieve better tumor suppression compared to the individual use.

Ongoing research has demonstrated that nanoparticles (NPs) show the ability to meet the need for targeted delivery of therapeutics and imaging agents (theranostics) into brain tumors. [233-235] They are also widely used in co-delivery of different agents. [231] However, few NPs have met regulatory approval for clinical administration. HDL is a naturally occurring NP that, unlike many engineered NPs, circulates in plasma for long periods of time ($T_{1/2}$ ~ 3-4 days)[20] which allows time for accumulation in hard to reach organs like the brain. It also has a major role in transport of cholesterol and other molecules, such as vitamin E, steroid hormones, signaling lipids, and micro RNAs. It has been found that upon administration multiple drugs bind to HDL and other lipoproteins. [236,237] Several synthetic ApoA-I peptide-based sHDL, which are more cost-effective and easier to produce on a large scale, have been administered to humans in Phase I/II studies and are proven to be well tolerated and safe at high doses. [18, 112, 141]

HDLs are able to interact with the cell surface receptor, scavenger receptor class B-I (SR-BI), which was reported to facilitate the uptake of cholesterol esters and anticancer drugs from HDL-like NPs to the cytosol via a non-endocytic pathway—thus preventing lysosomal degradation of the HDL-like NP payload. [238] SR-BI receptors have been reported to be overexpressed on several cancer cell lines which can facilitate the uptake of HDL by cells. [239] Therefore, HDL has been considered to be a suitable drug-delivery carrier for cancer therapy, capable of overcoming the current challenges within traditional chemotherapy, owing to their structural features, biocompatibility and intrinsic tumor targeting ability via receptor-mediated mechanisms. [141, 240-241] One of the main challenges in achieving therapeutic efficacy in brain tumor patients is the low permeability of the blood brain barrier (BBB) to chemotherapeutic drugs. [242] Various HDL

particles were found to be able to overcome blood-brain barrier through micropinocytosis or SR-BI mediated cell uptake expressed in caveolae. [243-245] Thus, with the unique targeting capabilities HDL particles might be able to facilitate the penetration of drugs through the blood brain barrier by encapsulating molecules in their hydrophobic core. Besides, due to its small size, HDL can diffuse among cancer cells better than other nanoparticles and enhance the accumulation of drugs in tumor cells.

To test our assumptions, synthetic high density lipoprotein (sHDL) NPs were developed to effectively deliver chemotherapeutic agents and CpG to GBM cells in preclinical models. We assessed experimentally whether sHDL NPs will target GBM *in vitro* and *in vivo*, and if sHDL loaded with chemotherapeutic agents and CpG will induce GBM tumor regression and improve the therapeutic effect on tumor-bearing animals after administration through different routes. Several GBM cell lines expressing SR-BI were compared and used for evaluation. We also incorporated near-infrared fluorescent dyes and chemotherapeutic drugs as payloads into sHDL, enabling molecular imaging of invasive GBM cells and targeted drug delivery. A tumor-bearing animal model was established to evaluate the therapeutic effect of drug loaded sHDL.

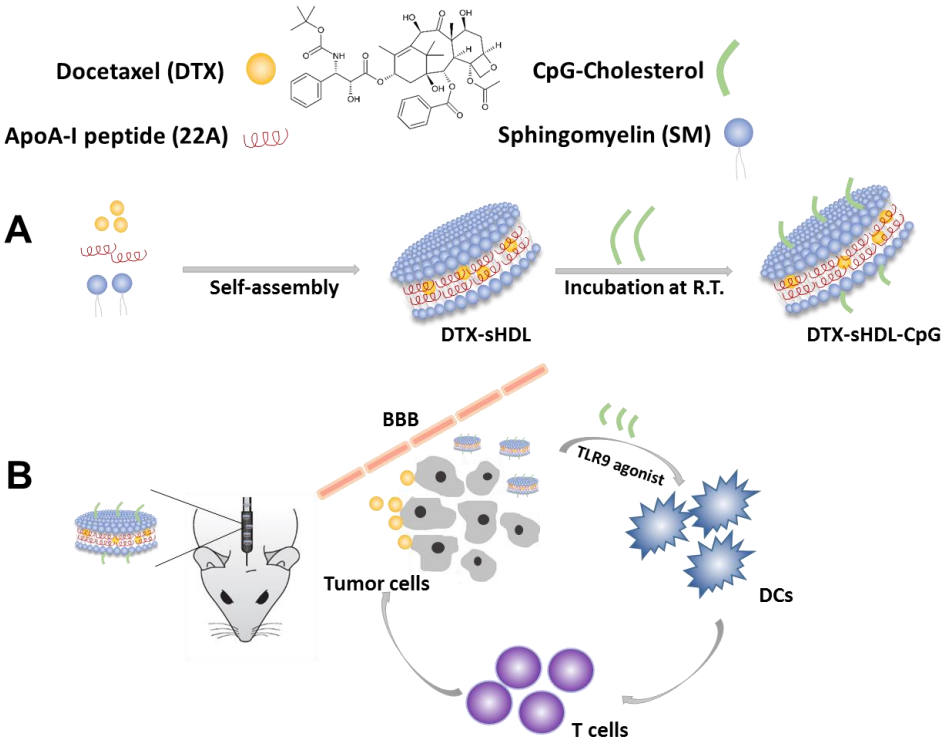

Figure 5.1: Schematic of DTX-sHDL-CpG for chemo-immunotherapy. (A) DTX-sHDL-CpG is formulated by incubation of CpG-cholesterol with preformed sHDL. (B) Intracranial injection of sHDL followed by release of DTX kills tumor cells. Release of CpG trigger DCs recruitment and recognition of tumor cells by T cells.

5.3 Materials and methods

5.3.1 Materials

Paclitaxel (PTX), docetaxel (DTX) and lomustine (CCNU) were purchased from Sigma-Aldrich with purity over 99% (St. Louis, MO). ApoA-I mimetic peptides 22A (PVLDLFRELLNELLEALKQKLK) were synthesized by Genscript Inc. (Piscataway, NJ). The purity of peptide was determined to be over 95% by the reverse phase HPLC. 1-palmitoyl-2-oleoyl-sn-glycero-3-phosphocholine (POPC), 1,2-dipalmitoyl-sn-glycero-3-phosphocholine (DPPC), 1,2-dimyristoyl-sn-glycero-3-phosphocholine (DMPC) and egg sphingomyelin (SM) were purchased from Avanti Polar Lipids (Alabaster, AL). Fluorescent dyes (DiO and DiR) were purchased from Invitrogen (Carlsbad, CA). Additional reagents used were of analytical grade and obtained from commercial suppliers. Preparation and Characterization of drug-loaded sHDL and dye-loaded sHDL

5.3.2 Preparation of drug-loaded sHDL and dye-loaded sHDL

The drug loaded synthetic HDL (sHDL) was prepared by lyophilization method. Briefly, 22A peptide, lipids and anti-cancer drugs with various weight ratios were dissolved and well mixed in glacial acetic acid, which was then removed by freeze-drying method. Lyophilized product was hydrated using 1M phosphate-buffered saline (PBS, pH 7.4) followed by thermal cycling varying from 50°C to 20°C for a minimum of 3 heat and cool cycles (10 minutes each) applying gentle shaking to obtain homogenous sHDL nanoparticles. Fluorescent dye DiD loaded sHDL was prepared by the same process. DTX-sHDL-CpG was prepared by incubating CpG-cholesterol with DTX-sHDL solution at room temperature for 4 hours after DTX-sHDL preparation. Alexa 647 labelled sHDL was prepared by linking Alexa Fluro 647 (Thermo Fisher Scientific, Waltham, MA) per manufacturer's instruction. NBD-labelled sHDL was prepared by mixing NBD-labelled DPPC lipids (Avanti Polar Lipid, Inc. Alabaster, AL) with 22A peptide.

5.3.3 Particle Characterization

Gel permeation chromatography (GPC) was used to separate particles based on their sizes. The purity and homogeneity of prepared sHDL was calculated by dividing area under the curve of sHDL to the total chromatography peaks' area using a Shimadzu HPLC system equipped with a TSKgel G2000SWxl column (7.8 mm ID × 30 cm, Tosoh Bioscience LLC) and the detection wavelengths were set at 220 nm for quantification of ApoA-I mimetic peptide, 22A. The particle

size of drug-sHDL was measured by dynamic light scattering (DLS) on a Malvern Zetasizer (Westborough, MA). The sHDL morphology was assessed by transmission electron microscopy (TEM) after proper dilution of the original samples. The diluted sample solution was deposited on a carbon film-coated 400 mesh copper grid (Electron Microscopy Sciences) and dried for 1 minute. Samples were then negatively stained with 1% (w/v) uranyl formate, and the grid was dried before TEM observation. All specimens were imaged on a 100kV Morgagni TEM equipped with a Gatan Orius CCD.

5.3.4 Western Blot

Cell lysates were prepared by incubating GBM cells in T-75 tissue culture flasks with protease inhibitors and 1.4mL RIPA lysis buffer on ice for 5 minutes. Resulting cell lysates were centrifuged at 13000 RPM at 4°C for 10 minnutes and supernatants were collected to determine protein concertation in comparison to standard bovine serum albumin (BSA) protein concentrations through bicinchonicinc acid (BCA) assay. For electrophoretic separation of protein, twenty-five micrograms of total protein was resuspended in loading buffer (10% sodium dodecyl sulfate, 20% glycerol, and 0.1% bromophenol blue) and incubated for 5 minutes at 95°C for 10 minutes to be loaded onto a 10% polyacrylamide gel. Proteins from the gel were transferred to polyvinylidence difuoride membrane and blocked with 5% nonfat milk in TBS-0.1% Tween-20 to be incubated with primary anti-SR-BI (1:1000) overnight at 4°C. The next day, blots were washed with TBS-0.1% tween-20 and incubated with secondary (1:000) antibody for two hours at room temperature. Blots were washed several times again with TBS-0.1% tween-20 and visualized under Biorad gel imaging software. Band intensities were quantified using ImageJ software.

5.3.5 Cytotoxicity

Human, and mouse glioma cells were plated at 1,000 cells per well in 96-well plate 24 hrs prior to treatment. Cells were then incubated with free-sHDL, free HCPT, CCNU, PTX, DTX; HDLs loaded with HCPT, CCNU, PTX, and DTX for 48hrs. Cell viability was determined with CellTiter-Glo viability assay following manufacture's protocol. IC50 values for each chemotherapeutic reagent were calculated from dose-response curves generated using graphpad prism.

5.3.6 Cell uptake of sHDL

To determine the cellular uptake of sHDL by glioma cells HF2303, CNS1 and GL26-Cit cells were plated onto glass cover slips coated with poly-L lysine in a 24-well plate 12 hours before

treatment. Cells were then treated with 0 ug, 3 ug, 10 ug and 30 ug of DiD-HDL in 0.4 mL of fully supplemented DMEM for 2 hours. Cells were washed three times with PBS and fixed in 4% Paraformaldehyde for 30 minutes and mounted onto slides with Prolong Gold anit-fade solution. DiD-sHDL uptake was imaged with confocal microscopy (instrument info) at 63x with oli-immersion lens and quantified using image J software.

5.3.7 Establishment of BBB model

Co-culture model was used to study the penetration of sHDL through BBB. Briefly, human astrocytes/ tumor cells were seeded on the underside of the 12-well transwell plate insert and incubated with medium overnight. On day 2, human brain membrane endothelial cells were seeded in the transwell insert and were cocultured with astrocytes or tumor cells. Medium was changed every day and the transendothelial electrical resistance (TEER) was measured over time until the value reached plateau. The liquid surface leakage test was conducted by observing the leakage of medium from insert to the bottom well over 24 hours. FITC-Dextran penetration was evaluated to confirm the formation of tight junction.

5.3.8 Penetration of sHDL through BBB

The component of sHDL was labelled with fluorescent dye separately. 22A peptide in sHDL was labelled with Alexa, lipids were labelled with NBD and the core was labelled with DiD. sHDL was added at either high peptide concentration (1mg/mL) or low concentration (0.1 mg/mL) into the insert of transwell plate with established BBB model. The fluorescence in the medium in inset or bottom well was measured to determine the penetration of different component of sHDL at various time points. The percentage of penetrated component was calculated.

5.3.9 Stability Study

In vitro study was performed to quantify the stability of DTX-sHDL particles for formulation screening purpose. Briefly, different formulations of DTX-sHDL were suspended in PBS or human serum and incubated at 37°C with the DTX concentration of 1 mg/ml. At 0, 0.5, 1, 2, 4, 8 and 24 hours after incubation, 100 µl mixture of each sample was collected and filtered through 0.22 µm membrane to separate precipitated drug. After filtration, 50 µl of each sample was mixed with 450 µl acetonitrile to dissolve the all component of nanoparticles and precipitate proteins. After centrifuge, the drug content incorporated in sHDL was determined by UPLC analysis.

5.3.10 Anti-tumor effect in vivo

Syngeneic tumors were established in C57BL/6J mice by stereotactically injecting 20,000 GL26-WT, or GL26-Cit cells into the right striatum using a 22-gauge Hamilton syringe (1uL over 1 minute) with the following coordinates: +1.00 mm anterior, 2.5 mm lateral, and 3 mm deep. Mice were either treated intratumorally with 0.5 mg/kg of free-DTX, DTX-sHDL, sHDL-CpG-DTX, free-HDL NPs or saline 8, 11, 15, 18, 22 and 25 days post tumor implantation. Particles loaded with chemotherapeutic cargo were intratumorally delivered in 4.8 μL volume in three locations to depths of 3.1, 3.0, and 2.9 mm, at the coordinates detailed above. Mice were trascardially perfused when they showed signs of neurological deficits due to tumor burden.

5.3.11 Statistical analysis

Sample sizes were chosen based on preliminary data from pilot experiments and previously published results in the literature. All animal studies were performed after randomization. Data were analyzed by one- or two-way analysis of variance (ANOVA), followed by Tukey's multiple comparisons post-test or log rank (Mantel-Cox) test with Prism 6.0 (GraphPad Software). Data were normally distributed and variance between groups was similar. P values less than 0.05 were considered statistically significant. All values are reported as mean ± SD with the indicated sample size. No samples were excluded from analysis.

5.4 Results

5.4.1 SR-BI expression on glioma cell lines

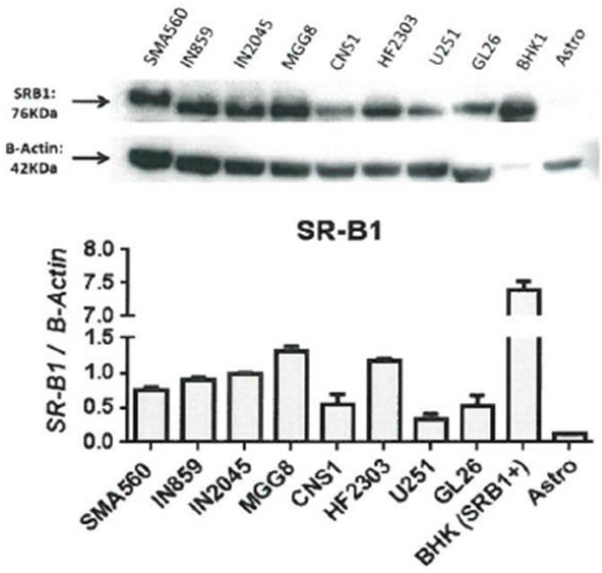

Figure 5.2: Expression of scavenger receptor class B-1 (SR-BI) on rodent and human GBM cell lines and human GBM Stem Cells.

Since sHDL has been reported to be able to interact with SR-BI receptor expressed on macrophage or liver cells to facilitate cellular uptake of sHDL, we would like to confirm the expression level of SR-BI on several glioma or glioma stem cell lines and select the cell line used for tumor model establishment in mouse. Western blot was applied to determine SR-BI levels in cell lysates, and gel image together with quantification of the gel are shown in Fig. 5.2. SMA560 is a murine astrocytoma cell line and GL26 and CNS-1 are murine glioma cells. IN859, IN2045, MGG8, HF2303 and U251 are derived from human. BHK cells transfected with SR-BI was used as the positive control with astrocyte as the negative control. All glioma cells showed manifest expression of SR-BI compared to negative control. Human cells expressed higher level of SR-BI receptors compared to murine cell lines. To establish the mouse glioma model, GL26 was chosen in this study for *in vivo* efficacy assessment since more SR-BI was presented on GL26 cells than U251 cells. HF2303 (human), CNS1 (rat) and GL26 (mouse) cells were used for cell uptake and cytotoxicity studies *in vitro*.

5.4.2 Penetration of sHDL through BBB in vitro

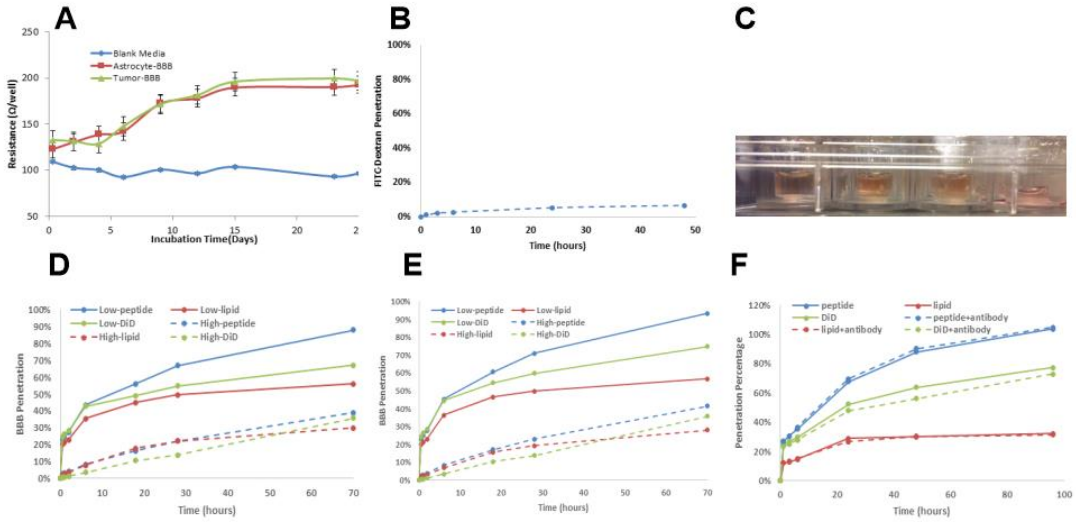

Figure 5.3: Penetration of sHDL through BBB in vitro. Evluation of formation of tight junction and BBB model (PanelA-C); penetation of fluorescence labelled sHDL through BBB (Panel D-F).

The most important factor limiting the application of anti-cancer drug in glioma treatment is the existence of the blood brain barrier, limiting penetration of IV administered chemotherapeutic agents and nanoparticles. Thus, we first examined if sHDL particles can penetrate the BBB *in vitro* using a transwell model. The BBB model was established by co-culture

of human brain microvascular endothelial cells (HBMEC) with either human tumor cells or astrocytes to mimic the biological structure of human BBB under normal and disease condition. It is important to confirm the formation of the BBB and establishment of tight junctions prior to penetration assessment. Normally, the resistance of insert membrane in transwell plate increases as cells numbers increases and reaches plateau. Transepithelial electrical resistance (TEER) was monitored over time after cells were seeded as shown in Fig.5.3A. TEER in both co-culture models kept increasing from day 0 to day 15 until a plateau was achieved at ~ 200 Ω/well indicating formation of a tight junction. In addition, FITC-dextran was added into the insert well and FITC fluorescence intensity in the well was determined to detect the passive diffusion of molecules through BBB. The liquid surface leakage test was conducted by observing the leakage of medium from the insert to the bottom well over 24 hours. As shown in Fig. 5.3B and C, there was only limited FITC-dextran or medium passing across the cell layer confirming formation of tight junctions and establishment of an *in vitro* model of the BBB. sHDL particles were prepared as described in section 5.3.2.

To track the penetration of different components of sHDL, peptide, lipid and hydrophobic core of sHDL were fluorescently labelled with Alexa 647, NBD and DiD, respectively. sHDL particles were added into the insert at either low or high concentration (0.1 mg/mL or 1 mg/mL) to assess the concentration-dependence of BBB penetration and fluorescence in the bottom well was measured over time. In both models, tumor-endothelial model and astrocyte-endothelial model (Fig. 5.3D and E), fluorescence signal increased over time with sHDL incubation, demonstrating that sHDL can penetrate the BBB *in vitro*. The percentage of sHDL passing through the BBB for low concentration of sHDL was higher than high concentration indicating the saturation of, likely, receptor-mediated sHDL transport. Besides, peptide component in sHDL was shown to achieve higher penetration compared to lipid or DiD components, indicating some extent of dissociation of sHDL particles during incubation.

To examine if BBB penetration is mediated by the SR-BI, the cells were pretreated with anti-SR-BI antibody (NB400-113, Novus biological) at 1:100 dilution for 1 h at 37°C. As shown in Fig 5.3F, after incubation with the anti-SR-BI antibody, the penetration of different sHDL components was not reduced, suggesting that BBB penetration is independent of SR-BI-mediated uptake mechanism. Thus, a different mechanism is likely responsible for sHDL penetration through the BBB such as transcellular lipophilic pathway and paracellular pathway.[246]

5.4.3 Cell uptake of sHDL by glioma cells

We next investigated if molecules incorporated in sHDL can be uptaken by glioma cells when incubated together. sHDL particles were loaded with insoluble fluorescent DiD dye to represent hydrophobic drugs and incubated with three types of glioma cells at different concentrations. Following 2 h incubation, cellular uptake of DiD was visualized by confocal imaging and quantified by flow cytometry (Fig. 5.4). The green signal is from cells and blue signal is from DiD. The fluorescence of DiD appears to distribute throughout cellular membranes and cytosol for all groups and increases with higher DiD-sHDL concentration. Thus, the uptake of DiD is dependent on sHDL concentration but it is not clear if DiD first diffused out from sHDL then got taken up by cells or was released after sHDL uptake by cells. When DiD uptake was quantified, GL26 cells exhibits strongest DiD signal at low sHDL concentration while human HF2303 cells achieves highest DiD uptake at high sHDL concentration, which may result from higher SR-BI expression on cells. Based on this observation, the cellular uptake of sHDL is at least partially mediated by SR-BI.

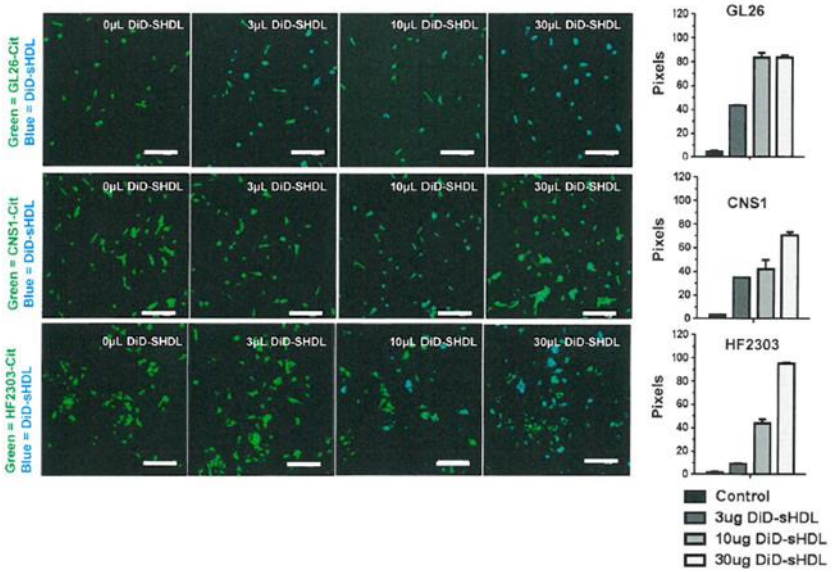

Figure 5.4: Cell uptake of DiD-sHDL by GL26, CNS1 and HF2303 cells.

5.4.4 Preparation and characterization of drug loaded sHDL particles

To screen the ability of various chemotherapeutic agents incorporated in sHDL particles to exert cytotoxic effect in glioma cell lines, PTX, DTX and CCNU were loaded in the nanoparticles using co-lyophilization methodology. We have utilized the same composition of sHDL as was

previously optimized by us for delivery of anticancer agent triacetylated withaferin A, and anti-inflammatory agent, T0901317[247]. DLS and GPC were used to examine particle size, homogeneity and purity. ApoA-I mimetic peptide (22A), phospholipids (DMPC and POPC) and chemotherapeutic agents were combined at 1:1:1:0.06 weight ratio in organic solvent, lyophilized and hydrated with aqueous buffer. The mixture was heated and cooled to facilitate particle assembly. It was demonstrated that homogeneous particles were formed with average size of 10-12 nm and purity >98% (Table 5.1, A-C). As particle size determined by DLS increased, the retention time of GPC running decreased accordingly. All three drugs were shown to be successfully incorporated in sHDL at 2% loading and cytotoxicity of drug loaded sHDL were evaluated to select the most potent drug as model drug in this study.

Table 5.1: The characterization summary of different 22A-sHDL particles.

Group	Formulations (weight ratio)	RT[a] (min)	Particle size (nm)	PDI[b]	Purity
A	22A: DMPC: POPC:PTX (1:1:1:0.06)	7.6	12.1 ± 0.3	0.07 ± 0.01	99.2%
B	22A: DMPC: POPC:DTX (1:1:1:0.06)	7.5	11.2 ± 0.4	0.15 ± 0.01	99.2%
C	22A: DMPC: POPC:CCNU(1:1:1:0.06)	7.4	10.3 ± 0.1	0.05 ± 0.02	98.5%
D	22A: SM (1:2)	7.9	9.5 ± 0.4	0.11 ± 0.01	99.0%
E	22A: SM: DTX (1:2:0.05)	7.9	9.9 ± 0.1	0.07 ± 0.01	97.6%
F	22A: SM: DTX (1:2:0.1)	7.9	9.4 ± 0.2	0.13 ± 0.06	97.2%
G	22A: DPPC: DTX (1:2:0.1)	7.8	8.9 ± 0.1	0.15 ± 0.01	97.3%
H	22A: DPPC: SM:DTX (1:1:1:0.1)	7.8	9.4 ± 0.1	0.14 ± 0.01	98.0%
I	22A: DMPC: POPC: DTX (1:1:1:0.1)	7.4	11.1 ± 0.2	0.14 ± 0.02	99.7%
J	22A: SM: DTX: CpG (1:2:0.05:0.0075)	8.1	8.6 ± 0.1	0.13 ± 0.02	97.9%

5.4.5 Cytotoxicity and selection of model drug

To select the most potent anti-cancer drug as the model drug in this study for glioma suppressing effect evaluation, cell viability of various cell types treated with three formulations were evaluated using the Cell Titer Glo assay method. GL26, HF2303 and U251 cell lines were incubated with either free drug or drug loaded sHDL at various concentrations. Half-maximal inhibitory concentration (IC50) of the different chemotherapeutic agents was obtained from an experimentally derived dose-response curve as plotted in Fig. 5.5.

All drugs were shown to be toxic to all cell lines while blank sHDL achieved little cell killing effect ranging from 0.0001 uM to 1.0uM. For all three molecules, free drug and drug-sHDL have the comparable IC50 values on each cell line. Drug loaded sHDL-NPs did not display differences in the biological properties relative to free drug. The IC50 value for U251 cells is lower

than HF2303 and GL26 cells for all three molecules with or without sHDL formulation indicating that U251 is more sensitive to these three anti-cancer drugs. When different drugs were compared, DTX or DTX-sHDL had the strongest cell killing effect with lowest IC50 values on all cell lines. For example, the IC50 value of DTX-sHDL for GL26 cells is 0.00497 μM which is 5-fold lower than PTX-sHDL and 16,000-fold lower than CCNU-sHDL. Thus, DTX is the most potent agent out of three candidates tested, was selected as the model drug to be delivered by sHDL for brain tumor therapy.

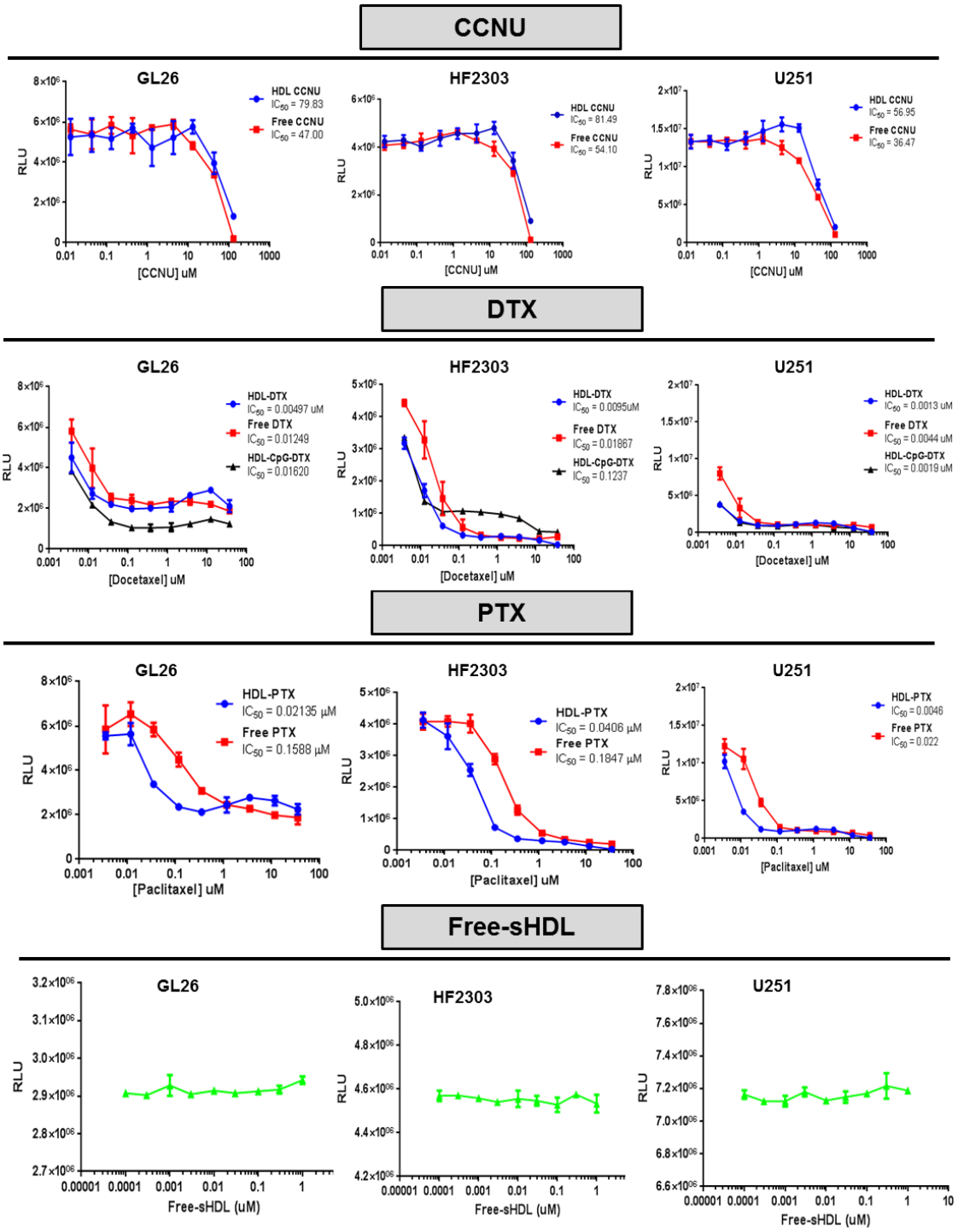

Figure 5.3: Cytoxicity of anti-cancer drugs including CCNU, DTX and PTX on GL26, HF2303 and U251 cells with calculated IC50.

5.4.6 Optimization of DTX-sHDL formulation based on loading and lipid composition

Docetaxel (DTX) was chosen as the model drug in our study based on its lowest IC50 value in *in vitro* cytotoxicity evaluation. To further optimize the DTX-sHDL formulation with sufficient

loading and stability, we prepared DTX-sHDL particles using lipids with different transition temperature and size distribution, and purity of each formulation were summarized in Table 5.1E-I. We first kept the peptide, lipid and drug ratio at 1:2:0.1 (w/w) and varied the lipid composition. *In vitro* stability test in PBS was conducted to select the most stable formulation for DTX retention as shown in Fig. 5.6A. All particles were incubated at 37°C after preparation and drug remained in particles overtime were determined. As gel transition temperature of phospholipids used to prepare sHDL increases (SM > DPPC > DMPC > POPC), lipids become more rigid and stability of DTX-sHDL particles in buffer and plasma increases. Following 24 hours incubation, more than 60% of drug remained encapsulated in SM-based sHDL, while less than 40% of DTX remained in the particles for all other three formulations. Thus, SM was selected to form DTX-sHDL.

In order to investigate the influence of drug loading on DTX retention in sHDL particles during 24hr incubation in either PBS or plasma, two formulations were prepared with changing loading amount of DTX between 1.67% and 3.34% (w/w). From the stability evaluation, DTX-sHDL with low DTX loading resulted in slower drug release with 80% drug remained after 24-h incubation when compared to 60% drug remaining in sHDL with high loading (Fig. 5.6B). This trend was also confirmed in human serum stability evaluation for the same two formulations (Fig. 5.6C). Thus DTX-sHDL with 22A, SM and DTX a weight ratio of 1:1:0.05 was selected as final formulation for *in vivo* efficacy evaluation. sHDL composed of same amount of peptide and lipids without drug was used as blank sHDL control.

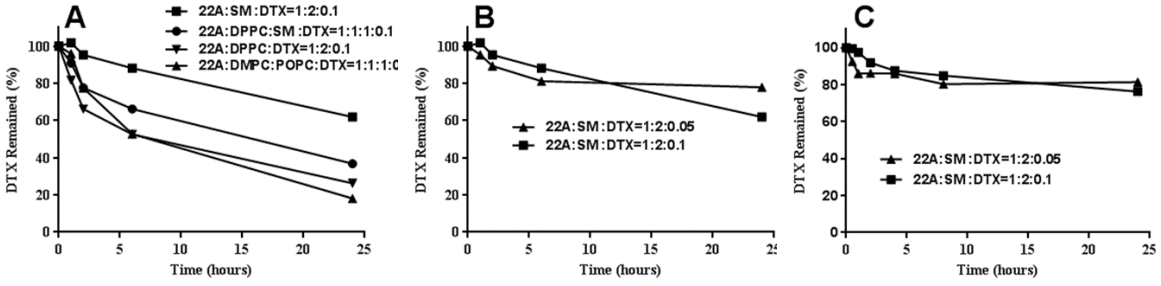

Figure 5.4: Stability of DTX-sHDL in PBS (Panel A and Panel B) and human serum (Panel C).

5.4.7 Analytical characterization of DTX-sHDL and DTX-sHDL-CpG particles

To develop the chemo-immunotherapeutic platform, CpG-cholesterol incorporated in sHDL nanoparticles. CpG-cholesterol was incubated with DTX-sHDL in PBS at room temperature (25°C) allowing the cholesterol moiety to insert into the lipid bilayer of sHDL and form DTX-

sHDL-CpG. The final CpG concentration was 75 µg/mL. The anti-cancer evaluation was conducted in animals for sHDL, DTX-sHDL, DTX-sHDL-CpG. DLS and GPC characterization of the three formulation were summarized in Table 5.1 D, E, and J and Fig. 5.7A and B. Transmission electron microscopy (TEM) was also used to examine morphology of particles (Fig. 5.7C). Both DLS and TEM results showed the homogeneous hydrodynamic size of ~ 10 nm and discoidal shape for "blank" sHDL, DTX-sHDL and DTX-sHDL-CpG, indicating the minimal impact of drug loading on the formation and homogeneity of sHDL particles. GPC curves demonstrated the high purity of sHDL, DTX-sHDL and DTX-sHDL-CpG solution after preparation. The peak of 22A peptide and CpG shifted to sHDL indicated the complete incorporation of 22A and CpG in sHDL.

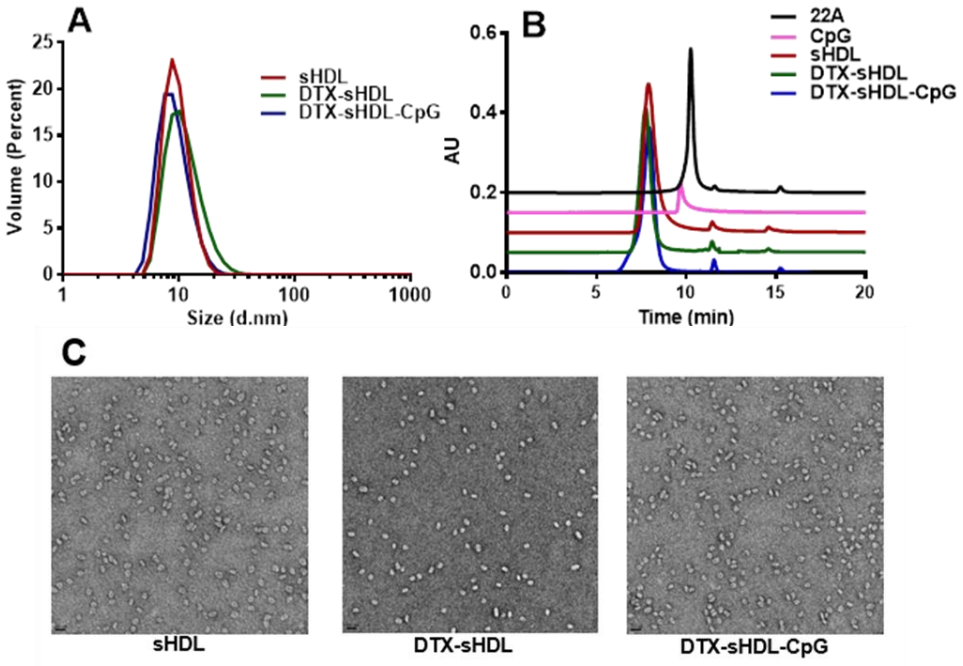

Figure 5.5: Characterization of black sHDL and DTX-sHDL particles with DLS (Panel A), GPC (Panel B) and TEM (Panel C).

5.4.8 In vivo anti-tumor efficacy

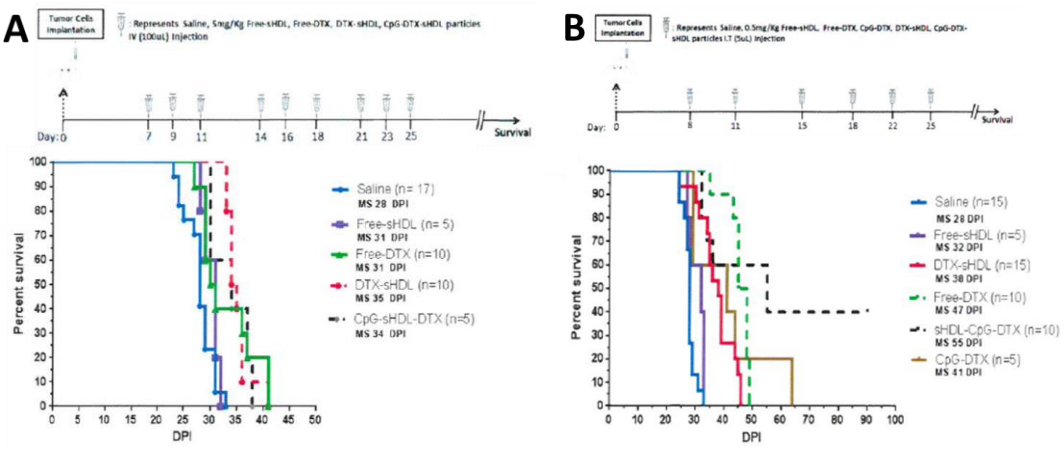

Figure 5.6: Anti-tumor efficacy by DTX-sHDL-CpG chemo-immunotherapy. Animal survival after intravenous administration (Panel A) or intracranial administration (Panel B) of indicated formulations.

Following *in vitro* evaluation of BBB penetration, cell uptake of sHDL, cytotoxity and formulation characterization, *in vivo* therapeutic effect of free DTX, DTX-sHDL, and DTX-sHDL-CpG was evaluated using a brain-tumor bearing mouse model. GL26 tumors were implanted stereotactically into the right striatum of C57BL/6 mice to develop glioma. These mice were then treated intravenously, first with Free-DTX, DTX-sHDL or CpG-sHDL-DTX with Free-HDL as vehicle control twice per week for three weeks starting 8d-post implantation. The survival Kaplan-Meier curve was plotted in Fig. 5.8A. Administration of free DTX, DTX-sHDL and DTX-sHDL-CpG all extend the mean survival (MS) time of animals significantly compared to saline group from 28 days to 31, 35, 34 days. However, there was no difference between the three treatment groups and neither sHDL formulation nor addition of CpG improved anti-tumor efficacy of DTX. This is possibly due to limited penetration of sHDL particles through BBB or instability of sHDL with immediate particle dissociation and drug release after administration.

We next dosed the animals by intracranial injection using the same tumor model to bypass the BBB. As shown in Fig. 5.8B, DTX-sHDL and mixing of CpG and DTX didn't lead to better therapeutic outcome relative to free DTX with no increase in MS values. However, when DTX-sHDL-CpG was given intratumorally, a notable increase in median survival of mice (MS: 55 DPI) compared to the free DTX (MS: 47 DPI), DTX-sHDL (MS: 38 DPI) and CpG-DTX (MS: 41 DPI) groups was observed, demonstrating the chemo-immunotherapy achieved the highest survival advantage because CpG incited immune response to tumor cells. Remarkably, there were two long-

term survivors in DTX-sHDL-CpG group which enable intracranial administration of DTX-sHDL-CpG a promising therapy for glioma.

5.5 Discussion and conclusion

In this study, we constructed the DTX-sHDL-CpG delivery platform for glioma chemo-immunotherapy with *in vitro* and *in vivo* evaluations. The cell lines we selected all highly expressed the SR-BI receptor, which can interact with sHDL. sHDL was shown to be taken up by glioma cells after 2 hr incubation and pass through the BBB monolayer in Transwell cell models. During the course of this project we optimized the use of a number of sHDL-NPs of varied formulations. We constructed sHDL-NPs loaded with chemotherapeutic agents DTX that are known to be active against brain tumors. It was identified that intratumoral delivery of the sHDL-NPs results in a significant increase in median survival with less systemic toxicity. Modifying the sHDL-NPs with immune stimulatory molecules such as CpG resulted in immune mediated anti-glioma activity.

Systemic administration of DTX-sHDL-CpG didn't demonstrate an improved tumor inhibitory effect as we hypothesized. This could be caused by lack of particle distribution in brain or instability of sHDL system with fast dissociation of particles and release of incorporated drugs. Though *in vitro* studies showed obvious penetration of sHDL using cell co-culture model, it still does not fully symbolize the biological structure and function of the BBB in body. The formed tight junction in cell models can be leakier with TEER value of 200 Ω versus physiological value of more than 1,500 Ω/cm^2, which has been measured in capillaries of rats. [248] To facilitate effective delivery of sHDL particles loaded with drugs, modifications of sHDL with targeting molecules or cell penetrating peptide or stabilization of the system by future optimization are alternative strategies, which can be tested later.[233, 235] In the intracranial injection study, simple mixture of CpG and DTX didn't perform better than free DTX drug which can be due to restricted exposure of CpG to dendritic cells which prevent the following activation of TLR9 regulated immune response. [229] By inserting CpG into sHDL, CpG can be stabilized and recognized by DC more readily, which may results from sHDL ultrasmall particle size (~10 nm), extended pharmacokinetics, and extensive uptake by metabolically highly active cancer cells that require a large amount of lipids and cholesterol for proliferation.[249-250] In addition, DTX and CpG can be presented to the glioma microenvironment at the same time to achieve a synergic killing effect with different mechanisms. Although other conventional nanoformulations may also be applicable

to this approach, we believe that the sHDL system is particularly attractive for translation because of the ease of synthesis, established large-scale manufacturing, proven human safety, and nonimmunogenicity of the blank sHDL, as demonstrated in a number of clinical trials.[11]

In conclusion, we have produced a new, generalizable framework for chemoimmunotherapy. By delivering chemotherapeutic agents together with immune activating molecules via nanocarriers in a manner that sensitizes tumor cells to immune activation, we have achieved potent antitumor efficacy, leading to elimination of established tumors in 40% of animals. Our approach may be readily applied to other hydrophobic chemotherapeutic agents known to induce tumor cell death. [251-252] Because there is intense interest in improving the patient response rate and therapeutic efficacy of immunotherapy combined with chemotherapy or radiation, our strategy presented here may have a wide-ranging impact in the field of drug delivery, nanotechnology, and cancer immunotherapy.

Chapter 6 : Conclusion, implications and future directions

The work presented in this thesis has shown that both the route of administration and the formulation of apoA-I peptide significantly affect its pharmacokinetics and pharmacodynamics. To address the problem of short half-life of sHDL, sHDL-PEG nanoparticles were developed. By increasing the stability of sHDL particles, sHDL-PEG was shown to achieve longer circulation of phospholipids component and more cholesterol mobilization or efflux, this effect is dependent on PEG density and molecular weight. The results have broad impact on the field of sHDL design and nanoparticle drug delivery. In addition, NanoMCL, a structural and functional mimetic of the sHDL nanoparticle, was developed for the first time and proved to be more effective in relevant animal models compared to sHDL and also exhibited similar safety properties as sHDL. Due to the intrinsic targeting effect and amphipathic, bilayer structure, DTX-sHDL-CpG achieved a promising anti-tumor effect in animal model and sHDL can be applied as a drug delivery system for treatment of glioma or other cancer types.

This research has important implications for thorough understanding of components of sHDL on cholesterol efflux and future development of sHDL-like nanoparticles for either atherosclerosis or other disease therapy. Despite that PEGylation has been investigated for years and researchers have modified apoA-I with PEG, this is the first time to modify the lipid component in sHDL with PEG and study the impact of PEG density and molecular weight on corresponding effects. The study in Chapter 3 underlines the importance of sHDL remodeling by endogenous lipoproteins *in vivo* in regards to sHDL's PK and pharmacological effect. Hence, strategies for minimizing sHDL *in vivo* remodeling, such as crosslinking ApoA-I or lipid components, could potentially improve sHDL PK properties and efficacy. Thus, understanding the forces driving lipoprotein remodeling *in vivo* and developing strategies to minimize it could lead to the design of more stable and efficacious sHDL based nanomedicines. In addtion, because of the simplicity and ease of preparation, NanoMCL could prove to be a valuable alternative to sHDL in treatment of ACS and other inflammatory diseases. Significant interest in the field remains for the use of sHDL therapeutics for treating systemic inflammatory diseases like sepsis, lupus and

rheumatoid arthritis. Therefore, the NanoMCLs we describe here could be potentially useful beyond cardiovascular applications. As our simple NanoMCL system appears to have a higher capacity for binding endotoxin and cholesterol as compared to sHDLs, NanoMCLs likely could provide an exciting translational opportunity for treatment of CVD, sepsis and other diseases involving scavenging hydrophobic molecules.

In this study, serum cholesterol levels were detected to indicate the cholesterol efflux effect of sHDL from peripheral tissues, but it is unknown where exactly the cholesterol is from and future studies may include the determination of cholesterol levels in different tissues or organs to investigate how much of the cholesterol accumulated in the plaque or macrophages get removed. Since NanoMCLs were administered systemically through IV injection without specific targeting to plaque, modification of NanoMCL with targeting molecules to macrophage or artery plaque can potentially improve the anti-atherosclerosis effect of NanoMCL following this study. This can be another direction for future investigation. As mentioned above, we have not examined the impact of pegylation of sHDL or the constructed NanoMCL system on the anti-inflammatory and anti-thrombotic properties, thus evaluations in other disease areas are suggested.

This thesis figures out the importance of lipid component in sHDL in relation to its efficacy and provides the possible strategies to improve the cholesterol mobilization ability of sHDL. Future stuties built on the research presented will lead to expanded application and benefit of sHDL systems.

Bibliography

1. McMahon, K. M.; Foit, L.; Angeloni, N. L.; Giles, F. J.; Gordon, L. I.; Thaxton, C. S., Synthetic high-density lipoprotein-like nanoparticles as cancer therapy. *Cancer treatment and research* **2015,** *166*, 129-50.

2. Graf, G. A.; Connell, P. M.; van der Westhuyzen, D. R.; Smart, E. J., The class B, type I scavenger receptor promotes the selective uptake of high density lipoprotein cholesterol ethers into caveolae. *J Biol Chem* **1999,** *274* (17), 12043-8.

3. Favari, E.; Chroni, A.; Tietge, U. F.; Zanotti, I.; Escolà-Gil, J.; Bernini, F., Cholesterol Efflux and Reverse Cholesterol Transport. In *High Density Lipoproteins*, von Eckardstein, A.; Kardassis, D., Eds. Springer International Publishing: 2015; Vol. 224, pp 181-206.

4. Lund-Katz, S.; Phillips, M., High Density Lipoprotein Structure–Function and Role in Reverse Cholesterol Transport. In *Cholesterol Binding and Cholesterol Transport Proteins:*, Harris, J. R., Ed. Springer Netherlands: 2010; Vol. 51, pp 183-227.

5. Camont, L.; Chapman, M. J.; Kontush, A., Biological activities of HDL subpopulations and their relevance to cardiovascular disease. *Trends Mol Med* **2011,** *17* (10), 594-603.

6. Joy, T.; Hegele, R. A., Is raising HDL a futile strategy for atheroprotection? *Nature reviews. Drug discovery* **2008,** *7* (2), 143-55.

7. Kontush, A.; Lhomme, M.; Chapman, M. J., Unraveling the complexities of the HDL lipidome. *Journal of Lipid Research* **2013,** *54* (11), 2950-2963.

8. Rye, K. A.; Hime, N. J.; Barter, P. J., The influence of sphingomyelin on the structure and function of reconstituted high density lipoproteins. *J Biol Chem* **1996,** *271* (8), 4243-50.

9. Kontush, A.; Therond, P.; Zerrad, A.; Couturier, M.; Negre-Salvayre, A.; de Souza, J. A.; Chantepie, S.; Chapman, M. J., Preferential sphingosine-1-phosphate enrichment and sphingomyelin depletion are key features of small dense HDL3 particles: relevance to antiapoptotic and antioxidative activities. *Arteriosclerosis, thrombosis, and vascular biology* **2007,** *27* (8), 1843-9.

10. Kontush, A.; Lhomme, M.; Chapman, M. J., Unraveling the complexities of the HDL lipidome. *Journal of lipid research* **2013,** *54* (11), 2950-63.

11. Kingwell, B. A.; Chapman, M. J.; Kontush, A.; Miller, N. E., HDL-targeted therapies: progress, failures and future. *Nat Rev Drug Discov* **2014,** *13* (6), 445-64.

12. Linsel-Nitschke, P.; Tall, A. R., HDL as a target in the treatment of atherosclerotic cardiovascular disease. *Nature reviews. Drug discovery* **2005,** *4* (3), 193-205.

13. Tabet, F.; Rye, K. A., High-density lipoproteins, inflammation and oxidative stress. *Clinical science* **2009,** *116* (2), 87-98.

14. Weber, C.; Noels, H., Atherosclerosis: current pathogenesis and therapeutic options. *Nature Medicine* **2011,** *17* (11), 1410-1422.

15. Zhang, W.; He, H.; Liu, J.; Wang, J.; Zhang, S.; Zhang, S.; Wu, Z., Pharmacokinetics and atherosclerotic lesions targeting effects of tanshinone IIA discoidal and spherical biomimetic high density lipoproteins. *Biomaterials* **2013,** *34* (1), 306-19.

16. Tran-Dinh, A.; Diallo, D.; Delbosc, S.; Varela-Perez, L. M.; Dang, Q. B.; Lapergue, B.; Burillo, E.; Michel, J. B.; Levoye, A.; Martin-Ventura, J. L.; Meilhac, O., HDL and endothelial protection. *British journal of pharmacology* **2013,** *169* (3), 493-511.

17. Yuhanna, I. S.; Zhu, Y.; Cox, B. E.; Hahner, L. D.; Osborne-Lawrence, S.; Lu, P.; Marcel, Y. L.; Anderson, R. G.; Mendelsohn, M. E.; Hobbs, H. H.; Shaul, P. W., High-density lipoprotein binding to scavenger receptor-BI activates endothelial nitric oxide synthase. *Nature medicine* **2001,** *7* (7), 853-7.

18. Krause, B. R.; Remaley, A. T., Reconstituted HDL for the acute treatment of acute coronary syndrome. *Current opinion in lipidology* **2013,** *24* (6), 480-6.

19. Kootte, R. S.; Smits, L. P.; van der Valk, F. M.; Dasseux, J. L.; Keyserling, C. H.; Barbaras, R.; Paolini, J. F.; Santos, R. D.; van Dijk, T. H.; Dallinga-van Thie, G. M.; Nederveen, A. J.; Mulder, W. J.; Hovingh, G. K.; Kastelein, J. J.; Groen, A. K.; Stroes, E. S., Effect of open-label infusion of an apoA-I-containing particle (CER-001) on RCT and artery wall thickness in patients with FHA. *J Lipid Res* **2015,** *56* (3), 703-12.

20. Gille, A.; Easton, R.; D'Andrea, D.; Wright, S. D.; Shear, C. L., CSL112 enhances biomarkers of reverse cholesterol transport after single and multiple infusions in healthy subjects. *Arteriosclerosis, thrombosis, and vascular biology* **2014,** *34* (9), 2106-14.

21. Nanjee, M. N.; Doran, J. E.; Lerch, P. G.; Miller, N. E., Acute effects of intravenous infusion of ApoA1/phosphatidylcholine discs on plasma lipoproteins in humans. *Arterioscler. Thromb. Vasc. Biol.* **1999,** *19* (4), 979-89.

22. Lerch, P. G.; Fortsch, V.; Hodler, G.; Bolli, R., Production and characterization of a reconstituted high density lipoprotein for therapeutic applications. *Vox sanguinis* **1996,** *71* (3), 155-64.

23. Spieker, L. E.; Sudano, I.; Hurlimann, D.; Lerch, P. G.; Lang, M. G.; Binggeli, C.; Corti, R.; Ruschitzka, F.; Luscher, T. F.; Noll, G., High-density lipoprotein restores endothelial function in hypercholesterolemic men. *Circulation* **2002,** *105* (12), 1399-402.

24. Bisoendial, R. J.; Hovingh, G. K.; Levels, J. H.; Lerch, P. G.; Andresen, I.; Hayden, M. R.; Kastelein, J. J.; Stroes, E. S., Restoration of endothelial function by increasing high-density lipoprotein in subjects with isolated low high-density lipoprotein. *Circulation* **2003,** *107* (23), 2944-8.

25. van Oostrom, O.; Nieuwdorp, M.; Westerweel, P. E.; Hoefer, I. E.; Basser, R.; Stroes, E. S.; Verhaar, M. C., Reconstituted HDL increases circulating endothelial progenitor cells in patients with type 2 diabetes. *Arteriosclerosis, thrombosis, and vascular biology* **2007,** *27* (8), 1864-5.

26. Shaw, J. A.; Bobik, A.; Murphy, A.; Kanellakis, P.; Blombery, P.; Mukhamedova, N.; Woollard, K.; Lyon, S.; Sviridov, D.; Dart, A. M., Infusion of reconstituted high-density

lipoprotein leads to acute changes in human atherosclerotic plaque. *Circ. Res.* **2008,** *103* (10), 1084-91.

27. Calkin, A. C.; Drew, B. G.; Ono, A.; Duffy, S. J.; Gordon, M. V.; Schoenwaelder, S. M.; Sviridov, D.; Cooper, M. E.; Kingwell, B. A.; Jackson, S. P., Reconstituted high-density lipoprotein attenuates platelet function in individuals with type 2 diabetes mellitus by promoting cholesterol efflux. *Circulation* **2009,** *120* (21), 2095-104.

28. Tardif, J. C.; Gregoire, J.; L'Allier, P. L.; Ibrahim, R.; Lesperance, J.; Heinonen, T. M.; Kouz, S.; Berry, C.; Basser, R.; Lavoie, M. A.; Guertin, M. C.; Rodes-Cabau, J.; Effect of r, H. D. L. o. A.-S.; Efficacy, I., Effects of reconstituted high-density lipoprotein infusions on coronary atherosclerosis: a randomized controlled trial. *JAMA* **2007,** *297* (15), 1675-82.

29. Safety, Tolerability and Pharmacokinetics of CSL112 in Healthy Volunteers. https://clinicaltrials.gov/ct2/show/study/NCT01129661?term=CSL112&rank=4.

30. A Multiple Ascending Dose Study of CSL112 in Healthy Volunteers. https://clinicaltrials.gov/ct2/show/NCT01281774?term=CSL112&rank=3.

31. Easton, R.; Gille, A.; D'Andrea, D.; Davis, R.; Wright, S. D.; Shear, C., A multiple ascending dose study of CSL112, an infused formulation of ApoA-I. *J Clin Pharmacol* **2014,** *54* (3), 301-10.

32. A Single Ascending Dose Study Examining the Safety and Pharmacokinetic Profile of Reconstituted High Density Lipoprotein (CSL112) Administered to Patients. https://clinicaltrials.gov/ct2/show/NCT01499420?term=CSL112&rank=5.

33. Michael Gibson, C.; Korjian, S.; Tricoci, P.; Daaboul, Y.; Yee, M.; Jain, P.; Alexander, J. H.; Steg, P. G.; Lincoff, A. M.; Kastelein, J. J.; Mehran, R.; D'Andrea, D. M.; Deckelbaum, L. I.; Merkely, B.; Zarebinski, M.; Ophuis, T. O.; Harrington, R. A., Safety and Tolerability of CSL112, a Reconstituted, Infusible, Plasma-Derived Apolipoprotein A-I, After Acute Myocardial Infarction: The AEGIS-I Trial (ApoA-I Event Reducing in Ischemic Syndromes I). *Circulation* **2016,** *134* (24), 1918-1930.

34. Gibson, C. M.; Korjian, S.; Tricoci, P.; Daaboul, Y.; Alexander, J. H.; Steg, P. G.; Lincoff, A. M.; Kastelein, J. J.; Mehran, R.; D'Andrea, D.; Merkely, B.; Zarebinski, M.; Ophius, T. O.; Harrington, R. A., Rationale and design of Apo-I Event Reduction in Ischemic Syndromes I (AEGIS-I): A phase 2b, randomized, placebo-controlled, dose-ranging trial to investigate the safety and tolerability of CSL112, a reconstituted, infusible, human apoA-I, after acute myocardial infarction. *Am Heart J* **2016,** *180*, 22-8.

35. CSL Behring Advances to Phase 3 Cardiovascular Outcomes Trial for CSL112, its Novel Apolipoprotein A-I (Human) Infusion Therapy. http://markets.businessinsider.com/news/stocks/csl-behring-advances-to-phase-3-cardiovascular-outcomes-trial-for-csl112-its-novel-apolipoprotein-a-i-human-infusion-therapy-1002240360.

36. Carlson, L. A., Effect of a Single Infusion of Recombinant Human Proapolipoprotein a-I Liposomes (Synthetic HDL) on Plasma-Lipoproteins in Patients with Low High-Density-Lipoprotein Cholesterol. *Nutr. Metab. Cardiovasc. Dis.* **1995,** *5* (2), 85-91.

37. Eriksson, M.; Carlson, L. A.; Miettinen, T. A.; Angelin, B., Stimulation of fecal steroid excretion after infusion of recombinant proapolipoprotein A-I - Potential reverse cholesterol transport in humans. *Circulation* **1999,** *100* (6), 594-598.

38. Bisgaier, C. L. R., W. V.; Lalwani, N. D.; Hartman, D.; Johansson, J. Pharmaceutical formulations, methods and dosing regimens for the treatment and prevention of acute coronary syndromes. CA2542726 C.

39. Nissen, S. E.; Tsunoda, T.; Tuzcu, E. M.; Schoenhagen, P.; Cooper, C. J.; Yasin, M.; Eaton, G. M.; Lauer, M. A.; Sheldon, W. S.; Grines, C. L.; Halpern, S.; Crowe, T.; Blankenship, J. C.; Kerensky, R., Effect of recombinant ApoA-I Milano on coronary atherosclerosis in patients with acute coronary syndromes: a randomized controlled trial. *JAMA* **2003,** *290* (17), 2292-300.

40. Dasseux, J.-L. O., D. C.; Ackermann, R Lipoprotein complexes and manufacturing and uses thereof. US 20120232005 A1, 2012.

41. Keyserling, C. H.; Hunt, T. L.; Klepp, H. M.; Scott, R. A.; Barbaras, R.; Schwendeman, A.; Lalwani, N.; Dasseux, J. L., CER-001, a Synthetic HDL-Mimetic, Safely Mobilizes Cholesterol in Healthy Dyslipidemic Volunteers. *Circulation* **2011,** *124* (21).

42. Tardif, J. C.; Ballantyne, C. M.; Barter, P.; Dasseux, J. L.; Fayad, Z. A.; Guertin, M. C.; Kastelein, J. J. P.; Keyserling, C.; Klepp, H.; Koenig, W.; L'Allier, P. L.; Lesperance, J.; Luscher, T. F.; Paolini, J. F.; Tawakol, A.; Waters, D. D.; Significantly, C. H. I., Effects of the high-density lipoprotein mimetic agent CER-001 on coronary atherosclerosis in patients with acute coronary syndromes: a randomized trial. *Eur. Heart J.* **2014,** *35* (46), 3277-3286.

43. Effect of CER-001 on Atherosclerosis in Acute Coronary Syndrome (ACS) Patients - Efficacy and Safety: The CHI SQUARE Trial. https://clinicaltrials.gov/ct2/show/NCT01201837?term=CER001&rank=2.

44. Effect of CER-001 on Plaque Volume in Homozygous Familial Hypercholesterolemia (HoFH) Subjects (MODE). https://clinicaltrials.gov/ct2/show/NCT01412034?term=CER001&rank=1.

45. Hovingh, G. K.; Smits, L. P.; Stefanutti, C.; Soran, H.; Kwok, S.; de Graaf, J.; Gaudet, D.; Keyserling, C. H.; Klepp, H.; Frick, J.; Paolini, J. F.; Dasseux, J. L.; Kastelein, J. J. P.; Stroes, E. S., The effect of an apolipoprotein A-I-containing high-density lipoprotein-mimetic particle (CER-001) on carotid artery wall thickness in patients with homozygous familial hypercholesterolemia: The Modifying Orphan Disease Evaluation (MODE) study. *Am. Heart J.* **2015,** *169* (5), 736-U196.

46. Exploratory Study of Plaque Regression (EXPRESS). https://clinicaltrials.gov/ct2/show/NCT01515241?term=CER001&rank=3.

47. Rawat, A.; Bhardwaj, U.; Burgess, D. J., Comparison of in vitro-in vivo release of Risperdal (R) Consta (R) microspheres. *Int. J. Pharm.* **2012,** *434* (1-2), 115-121.

48. Khan, M. L., N. D.; Drake, S. L.; Crockatt, J. G.; Dasseux, J. L. H., Single-dose intravenous infusion of ETC-642, a 22-mer ApoA-I analogue and phospholipids complex, elevates HDL-C in atherosclerosis patients. *Circulation* **2003,** *108*, 563-564.

49. Di Bartolo, B. A.; Nicholls, S. J.; Bao, S.; Rye, K. A.; Heather, A. K.; Barter, P. J.; Bursill, C., The apolipoprotein A-I mimetic peptide ETC-642 exhibits anti-inflammatory properties that are comparable to high density lipoproteins. *Atherosclerosis* **2011,** *217* (2), 395-400.

50. Miles, J., et al. , Single-dose tolerability, pharmacokinetics, and cholesterol mobilization in HDL-C fraction following intravenous administration of ETC-642, a 22-mer ApoA-I analogue

and phospholipids complex, in atherosclerosis patients. *Proceedings of Arteriosclerosis Thrombosis and Vascular Biology* **2004,** *24*, E19-E19.

51. Davidson, W.; Silva, R.; Chantepie, S.; Lagor, W.; Chapman, M.; Kontush, A., Proteomic Analysis of Defined Hdl Subpopulations Reveals Particle-Specific Protein Clusters: Relevance to Antioxidative Function. *Atherosclerosis Supplements* **2009,** *10* (2).

52. Moguilevsky, N.; Varsalona, F.; Guillaume, J. P.; Gilles, P.; Bollen, A.; Roobol, K., Production of Authentic Human Proapolipoprotein-a-I in Escherichia-Coli - Strategies for the Removal of the Amino-Terminal Methionine. *J. Biotechnol.* **1993,** *27* (2), 159-172.

53. Kempen, H. J.; Schranz, D. B.; Asztalos, B. F.; Otvos, J.; Jeyarajah, E.; Drazul-Schrader, D.; Collins, H. L.; Adelman, S. J.; Wijngaard, P. L., Incubation of MDCO-216 (ApoA-IMilano/POPC) with Human Serum Potentiates ABCA1-Mediated Cholesterol Efflux Capacity, Generates New Prebeta-1 HDL, and Causes an Increase in HDL Size. *J. Lipids* **2014,** *2014*, 923903.

54. Anantharamaiah, G. M.; Jones, J. L.; Brouillette, C. G.; Schmidt, C. F.; Chung, B. H.; Hughes, T. A.; Bhown, A. S.; Segrest, J. P., Studies of synthetic peptide analogs of the amphipathic helix. Structure of complexes with dimyristoyl phosphatidylcholine. *Journal of Biological Chemistry* **1985,** *260* (18), 10248-55.

55. Navab, M.; Anantharamaiah, G. M.; Reddy, S. T.; Fogelman, A. M., Apolipoprotein A-I mimetic peptides and their role in atherosclerosis prevention. *Nat Clin Pract Cardiovasc Med* **2006,** *3* (10), 540-547.

56. Di Bartolo, B. A.; Nicholls, S. J.; Bao, S.; Rye, K.-A.; Heather, A. K.; Barter, P. J.; Bursill, C., The apolipoprotein A-I mimetic peptide ETC-642 exhibits anti-inflammatory properties that are comparable to high density lipoproteins. *Atherosclerosis* **2011,** *217* (2), 395-400.

57. Amar, M. J. A.; D'Souza, W.; Turner, S.; Demosky, S.; Sviridov, D.; Stonik, J.; Luchoomun, J.; Voogt, J.; Hellerstein, M.; Sviridov, D.; Remaley, A. T., 5A Apolipoprotein Mimetic Peptide Promotes Cholesterol Efflux and Reduces Atherosclerosis in Mice. *Journal of Pharmacology and Experimental Therapeutics* **2010,** *334* (2), 634-641.

58. Navab, M.; Anantharamaiah, G. M.; Reddy, S. T.; Hama, S.; Hough, G.; Grijalva, V. R.; Yu, N.; Ansell, B. J.; Datta, G.; Garber, D. W.; Fogelman, A. M., Apolipoprotein A-I Mimetic Peptides. *Arteriosclerosis, Thrombosis, and Vascular Biology* **2005,** *25* (7), 1325-1331.

59. Bloedon, L. T.; Dunbar, R.; Duffy, D.; Pinell-Salles, P.; Norris, R.; DeGroot, B. J.; Movva, R.; Navab, M.; Fogelman, A. M.; Rader, D. J., Safety, pharmacokinetics, and pharmacodynamics of oral apoA-I mimetic peptide D-4F in high-risk cardiovascular patients. *Journal of Lipid Research* **2008,** *49* (6), 1344-1352.

60. Watson, C. E.; Weissbach, N.; Kjems, L.; Ayalasomayajula, S.; Zhang, Y.; Chang, I.; Navab, M.; Hama, S.; Hough, G.; Reddy, S. T.; Soffer, D.; Rader, D. J.; Fogelman, A. M.; Schecter, A., Treatment of patients with cardiovascular disease with L-4F, an apo-A1 mimetic, did not improve select biomarkers of HDL function. *Journal of Lipid Research* **2011,** *52* (2), 361-373.

61. van de Steeg, E.; van Esch, A.; Wagenaar, E.; van der Kruijssen, C. M.; van Tellingen, O.; Kenworthy, K. E.; Schinkel, A. H., High impact of Oatp1a/1b transporters on in vivo disposition of the hydrophobic anticancer drug paclitaxel. *Clinical cancer research : an official journal of the American Association for Cancer Research* **2011,** *17* (2), 294-301.

62. Desseux, J. L.; Schwendeman, A. S.; Zhu, L. Apolipoprotein A-I mimics. 8,378,068, 2013.

63. Wool, G. D.; Reardon, C. A.; Getz, G. S., Apolipoprotein A-I mimetic peptide helix number and helix linker influence potentially anti-atherogenic properties. *Journal of Lipid Research* **2008,** *49* (6), 1268-1283.

64. Bielicki, J. K.; Zhang, H.; Cortez, Y.; Zheng, Y.; Narayanaswami, V.; Patel, A.; Johansson, J.; Azhar, S., A new HDL mimetic peptide that stimulates cellular cholesterol efflux with high efficiency greatly reduces atherosclerosis in mice. *J. Lipid Res.* **2010,** *51* (6), 1496-1503.

65. Zhang, Z. H.; Chen, J.; Ding, L. L.; Jin, H. L.; Lovell, J. F.; Corbin, I. R.; Cao, W. G.; Lo, P. C.; Yang, M.; Tsao, M. S.; Luo, Q. M.; Zheng, G., HDL-Mimicking Peptide-Lipid Nanoparticles with Improved Tumor Targeting. *Small* **2010,** *6* (3), 430-437.

66. Dasseux, J. L. Peptide/lipid complex formation by co-lyophilization. 6,287,590, 2001.

67. Schwendeman, A.; Sviridov, D. O.; Yuan, W.; Guo, Y.; Morin, E. E.; Yuan, Y.; Stonik, J.; Freeman, L.; Ossoli, A.; Thacker, S.; Killion, S.; Pryor, M.; Chen, Y. E.; Turner, S.; Remaley, A. T., The effect of phospholipid composition of reconstituted HDL on its cholesterol efflux and anti-inflammatory properties. *J Lipid Res* **2015,** *56* (9), 1727-37.

68. Vllasaliu, D.; Fowler, R.; Stolnik, S., PEGylated Nanomedicines: Recent Progress and Remaining Concerns. *Expert opinion on drug delivery* **2014,** *11* (1), 139-54.

69. Thaxton, C. S.; Daniel, W. L.; Giljohann, D. A.; Thomas, A. D.; Mirkin, C. A., Templated spherical high density lipoprotein nanoparticles. *J Am Chem Soc* **2009,** *131* (4), 1384-5.

70. Luthi, A. J.; Zhang, H.; Kim, D.; Giljohann, D. A.; Mirkin, C. A.; Thaxton, C. S., Tailoring of biomimetic high-density lipoprotein nanostructures changes cholesterol binding and efflux. *ACS Nano* **2012,** *6* (1), 276-85.

71. Duivenvoorden, R.; Tang, J.; Cormode, D. P.; Mieszawska, A. J.; Izquierdo-Garcia, D.; Ozcan, C.; Otten, M. J.; Zaidi, N.; Lobatto, M. E.; van Rijs, S. M.; Priem, B.; Kuan, E. L.; Martel, C.; Hewing, B.; Sager, H.; Nahrendorf, M.; Randolph, G. J.; Stroes, E. S.; Fuster, V.; Fisher, E. A.; Fayad, Z. A.; Mulder, W. J., A statin-loaded reconstituted high-density lipoprotein nanoparticle inhibits atherosclerotic plaque inflammation. *Nat Commun* **2014,** *5*, 3065.

72. Cormode, D. P.; Skajaa, T.; van Schooneveld, M. M.; Koole, R.; Jarzyna, P.; Lobatto, M. E.; Calcagno, C.; Barazza, A.; Gordon, R. E.; Zanzonico, P.; Fisher, E. A.; Fayad, Z. A.; Mulder, W. J. M., Nanocrystal Core High-Density Lipoproteins: A Multimodality Contrast Agent Platform. *Nano Letters* **2008,** *8* (11), 3715-3723.

73. Tang, J.; Lobatto, M. E.; Hassing, L.; van der Staay, S.; van Rijs, S. M.; Calcagno, C.; Braza, M. S.; Baxter, S.; Fay, F.; Sanchez-Gaytan, B. L.; Duivenvoorden, R.; Sager, H.; Astudillo, Y. M.; Leong, W.; Ramachandran, S.; Storm, G.; Perez-Medina, C.; Reiner, T.; Cormode, D. P.; Strijkers, G. J.; Stroes, E. S.; Swirski, F. K.; Nahrendorf, M.; Fisher, E. A.; Fayad, Z. A.; Mulder, W. J., Inhibiting macrophage proliferation suppresses atherosclerotic plaque inflammation. *Sci Adv* **2015,** *1* (3).

74. Perez-Medina, C.; Binderup, T.; Lobatto, M. E.; Tang, J.; Calcagno, C.; Giesen, L.; Wessel, C. H.; Witjes, J.; Ishino, S.; Baxter, S.; Zhao, Y.; Ramachandran, S.; Eldib, M.; Sanchez-Gaytan, B. L.; Robson, P. M.; Bini, J.; Granada, J. F.; Fish, K. M.; Stroes, E. S.; Duivenvoorden, R.; Tsimikas, S.; Lewis, J. S.; Reiner, T.; Fuster, V.; Kjaer, A.; Fisher, E. A.; Fayad, Z. A.; Mulder,

W. J., In Vivo PET Imaging of HDL in Multiple Atherosclerosis Models. *JACC Cardiovasc Imaging* **2016,** *9* (8), 950-61.

75. Sanchez-Gaytan, B. L.; Fay, F.; Lobatto, M. E.; Tang, J.; Ouimet, M.; Kim, Y.; van der Staay, S. E.; van Rijs, S. M.; Priem, B.; Zhang, L.; Fisher, E. A.; Moore, K. J.; Langer, R.; Fayad, Z. A.; Mulder, W. J., HDL-mimetic PLGA nanoparticle to target atherosclerosis plaque macrophages. *Bioconjug Chem* **2015,** *26* (3), 443-51.

76. McMahon, K. M.; Mutharasan, R. K.; Tripathy, S.; Veliceasa, D.; Bobeica, M.; Shumaker, D. K.; Luthi, A. J.; Helfand, B. T.; Ardehali, H.; Mirkin, C. A.; Volpert, O.; Thaxton, C. S., Biomimetic high density lipoprotein nanoparticles for nucleic acid delivery. *Nano Lett* **2011,** *11* (3), 1208-14.

77. Marrache, S.; Dhar, S., Biodegradable synthetic high-density lipoprotein nanoparticles for atherosclerosis. *Proc Natl Acad Sci U S A* **2013,** *110* (23), 9445-50.

78. Luthi, A. J.; Lyssenko, N. N.; Quach, D.; McMahon, K. M.; Millar, J. S.; Vickers, K. C.; Rader, D. J.; Phillips, M. C.; Mirkin, C. A.; Thaxton, C. S., Robust passive and active efflux of cellular cholesterol to a designer functional mimic of high density lipoprotein. *J Lipid Res* **2015,** *56* (5), 972-85.

79. Pajkrt, D.; Doran, J. E.; Koster, F.; Lerch, P. G.; Arnet, B.; van der Poll, T.; ten Cate, J. W.; van Deventer, S. J., Antiinflammatory effects of reconstituted high-density lipoprotein during human endotoxemia. *J Exp Med* **1996,** *184* (5), 1601-8.

80. Barter, P. J.; Nicholls, S.; Rye, K. A.; Anantharamaiah, G. M.; Navab, M.; Fogelman, A. M., Antiinflammatory properties of HDL. *Circ Res* **2004,** *95* (8), 764-72.

81. Eisenberg, S.; Windmueller, H. G.; Levy, R. I., Metabolic fate of rat and human lipoprotein apoproteins in the rat. *J Lipid Res* **1973,** *14* (4), 446-58.

82. Rensen, P. C.; de Vrueh, R. L.; Kuiper, J.; Bijsterbosch, M. K.; Biessen, E. A.; van Berkel, T. J., Recombinant lipoproteins: lipoprotein-like lipid particles for drug targeting. *Advanced drug delivery reviews* **2001,** *47* (2-3), 251-76.

83. Ng, K. K.; Lovell, J. F.; Zheng, G., Lipoprotein-Inspired Nanoparticles for Cancer Theranostics. *Accounts of Chemical Research* **2011,** *44* (10), 1105-1113.

84. Moskal, J. R.; Sinnett, M.; Kornblith, P. L.; LaSala, P.; Levine, D. M.; Parker, T. S.; Lander, H., The effect of lipoproteins on human glioblastoma growth in vitro. *Molecular and chemical neuropathology / sponsored by the International Society for Neurochemistry and the World Federation of Neurology and research groups on neurochemistry and cerebrospinal fluid* **1992,** *17* (2), 169-81.

85. Damiano, M. G.; Mutharasan, R. K.; Tripathy, S.; McMahon, K. M.; Thaxton, C. S., Templated high density lipoprotein nanoparticles as potential therapies and for molecular delivery. *Advanced drug delivery reviews* **2013,** *65* (5), 649-62.

86. Shahzad, M. M. K.; Mangala, L. S.; Han, H. D.; Lu, C.; Bottsford-Miller, J.; Nishimura, M.; Mora, E. M.; Lee, J.-W.; Stone, R. L.; Pecot, C. V.; Thanapprapasr, D.; Roh, J.-W.; Gaur, P.; Nair, M. P.; Park, Y.-Y.; Sabnis, N.; Deavers, M. T.; Lee, J.-S.; Ellis, L. M.; Lopez-Berestein, G.; McConathy, W. J.; Prokai, L.; Lacko, A. G.; Sood, A. K., Targeted Delivery of Small Interfering

RNA Using Reconstituted High-Density Lipoprotein Nanoparticles. *Neoplasia* **2011,** *13* (4), 309-IN8.

87. Leon, C. G.; Locke, J. A.; Adomat, H. H.; Etinger, S. L.; Twiddy, A. L.; Neumann, R. D.; Nelson, C. C.; Guns, E. S.; Wasan, K. M., Alterations in cholesterol regulation contribute to the production of intratumoral androgens during progression to castration-resistant prostate cancer in a mouse xenograft model. *The Prostate* **2010,** *70* (4), 390-400.

88. Liadaki, K. N.; Liu, T.; Xu, S.; Ishida, B. Y.; Duchateaux, P. N.; Krieger, J. P.; Kane, J.; Krieger, M.; Zannis, V. I., Binding of high density lipoprotein (HDL) and discoidal reconstituted HDL to the HDL receptor scavenger receptor class B type I. Effect of lipid association and APOA-I mutations on receptor binding. *The Journal of biological chemistry* **2000,** *275* (28), 21262-71.

89. Zhang, Z.; Chen, J.; Ding, L.; Jin, H.; Lovell, J. F.; Corbin, I. R.; Cao, W.; Lo, P.-C.; Yang, M.; Tsao, M.-S.; Luo, Q.; Zheng, G., HDL-Mimicking Peptide-Lipid Nanoparticles with Improved Tumor Targeting. *Small* **2010,** *6* (3), 430-437.

90. Chen, W.; Jarzyna, P. A.; van Tilborg, G. A. F.; Nguyen, V. A.; Cormode, D. P.; Klink, A.; Griffioen, A. W.; Randolph, G. J.; Fisher, E. A.; Mulder, W. J. M.; Fayad, Z. A., RGD peptide functionalized and reconstituted high-density lipoprotein nanoparticles as a versatile and multimodal tumor targeting molecular imaging probe. *Faseb Journal* **2010,** *24* (6), 1689-1699.

91. Corbin, I. R.; Ng, K. K.; Ding, L.; Jurisicova, A.; Zheng, G., Near-infrared fluorescent imaging of metastatic ovarian cancer using folate receptor-targeted high-density lipoprotein nanocarriers. *Nanomedicine* **2013,** *8* (6), 875-890.

92. Corbin, I. R.; Chen, J.; Cao, W.; Li, H.; Lund-Katz, S.; Zheng, G., Enhanced cancer-targeted delivery using engineered high-density lipoprotein-based nanocarriers. *Journal of Biomedical Nanotechnology* **2007,** *3* (4), 367-376.

93. Smith, J. D., Apolipoprotein AI and its mimetics for the treatment of atherosclerosis. *Curr. Opin. Investig. Drug* **2010,** *11* (9), 989.

94. van Capelleveen, J. C.; Brewer, H. B.; Kastelein, J. J.; Hovingh, G. K., Novel therapies focused on the high-density lipoprotein particle. *Circ. Res.* **2014,** *114* (1), 193-204.

95. Nanjee, M.; Crouse, J.; King, J.; Hovorka, R.; Rees, S.; Carson, E.; Morgenthaler, J.-J.; Lerch, P.; Miller, N., Effects of intravenous infusion of lipid-free apo AI in humans. *Arterioscler. Thromb. Vasc. Biol.* **1996,** *16* (9), 1203-1214.

96. Kuai, R.; Li, D.; Chen, Y. E.; Moon, J. J.; Schwendeman, A., High-density lipoproteins: nature's multifunctional nanoparticles. *ACS Nano.* **2016,** *10* (3), 3015-3041.

97. Nissen, S. E.; Tsunoda, T.; Tuzcu, E. M.; Schoenhagen, P.; Cooper, C. J.; Yasin, M.; Eaton, G. M.; Lauer, M. A.; Sheldon, W. S.; Grines, C. L., Effect of recombinant ApoA-I Milano on coronary atherosclerosis in patients with acute coronary syndromes: a randomized controlled trial. *Jama.* **2003,** *290* (17), 2292-2300.

98. Osei-Hwedieh, D. O.; Amar, M.; Sviridov, D.; Remaley, A. T., Apolipoprotein mimetic peptides: Mechanisms of action as anti-atherogenic agents. *Pharmacol. Ther.* **2011,** *130* (1), 83-91.

99. Favari, E.; Calabresi, L.; Adorni, M. P.; Jessup, W.; Simonelli, S.; Franceschini, G.; Bernini, F., Small discoidal pre-β1 HDL particles are efficient acceptors of cell cholesterol via ABCA1 and ABCG1. *Biochemistry.* **2009,** *48* (46), 11067-11074.

100. Duong, P. T.; Weibel, G. L.; Lund-Katz, S.; Rothblat, G. H.; Phillips, M. C., Characterization and properties of preβ-HDL particles formed by ABCA1-mediated cellular lipid efflux to apoA-I. *J. Lipid Res.* **2008,** *49* (5), 1006-1014.

101. Kee, P.; Rye, K.-A.; Taylor, J. L.; Barrett, P. H. R.; Barter, P. J., Metabolism of apoA-I as lipid-free protein or as component of discoidal and spherical reconstituted HDLs: studies in wild-type and hepatic lipase transgenic rabbits. *Arterioscler. Thromb. Vasc. Biol.* **2002,** *22* (11), 1912-1917.

102. Patel, S.; Di Bartolo, B. A.; Nakhla, S.; Heather, A. K.; Mitchell, T. W.; Jessup, W.; Celermajer, D. S.; Barter, P. J.; Rye, K.-A., Anti-inflammatory effects of apolipoprotein AI in the rabbit. *Atherosclerosis.* **2010,** *212* (2), 392-397.

103. Wu, B. J.; Ong, K. L.; Shrestha, S.; Chen, K.; Tabet, F.; Barter, P. J.; Rye, K.-A., Inhibition of arthritis in the Lewis rat by apolipoprotein AI and reconstituted high-density lipoproteins. *Arterioscler. Thromb. Vasc. Biol.* **2014,** *34* (3), 543-551.

104. Nicholls, S. J.; Dusting, G. J.; Cutri, B.; Bao, S.; Drummond, G. R.; Rye, K.-A.; Barter, P. J., Reconstituted high-density lipoproteins inhibit the acute pro-oxidant and proinflammatory vascular changes induced by a periarterial collar in normocholesterolemic rabbits. *Circulation.* **2005,** *111* (12), 1543-1550.

105. Peterson, S. J.; Husney, D.; Kruger, A. L.; Olszanecki, R.; Ricci, F.; Rodella, L. F.; Stacchiotti, A.; Rezzani, R.; McClung, J. A.; Aronow, W. S., Long-term treatment with the apolipoprotein A1 mimetic peptide increases antioxidants and vascular repair in type I diabetic rats. *J. Pharm. Exp. Ther.* **2007,** *322* (2), 514-520.

106. Shah, P. K.; Yano, J.; Reyes, O.; Chyu, K.-Y.; Kaul, S.; Bisgaier, C. L.; Drake, S.; Cercek, B., High-dose recombinant apolipoprotein a-imilano mobilizes tissue cholesterol and rapidly reduces plaque lipid and macrophage content in apolipoprotein e–deficient mice potential implications for acute plaque stabilization. *Circulation.* **2001,** *103* (25), 3047-3050.

107. Nanjee, M.; Doran, J.; Lerch, P.; Miller, N., Acute effects of intravenous infusion of ApoA1/phosphatidylcholine discs on plasma lipoproteins in humans. *Arterioscler. Thromb. Vasc. Biol.* **1999,** *19* (4), 979-989.

108. Remaley, A. T.; Amar, M.; Sviridov, D., HDL-replacement therapy: mechanism of action, types of agents and potential clinical indications. *Expert Rev. Cardiovasc. Ther.* **2008,** *6* (9), 1203-1215.

109. Sharifov, O. F.; Xu, X.; Gaggar, A.; Grizzle, W. E.; Mishra, V. K.; Honavar, J.; Litovsky, S. H.; Palgunachari, M. N.; White, C. R.; Anantharamaiah, G., Anti-inflammatory mechanisms of apolipoprotein AI mimetic peptide in acute respiratory distress syndrome secondary to sepsis. *PLoS One* **2013,** *8* (5), e64486.

110. Meibohm, B.; Derendorf, H., Pharmacokinetic/pharmacodynamic studies in drug product development. *J. Pharm. Sci.* **2002,** *91* (1), 18-31.

111. Olsen, C. K.; Brennum, L. T.; Kreilgaard, M., Using pharmacokinetic-pharmacodynamic modelling as a tool for prediction of therapeutic effective plasma levels of antipsychotics. *Eur. J. Pharmacol.* **2008,** *584* (2-3), 318-27.

112. Li, D.; Gordon, S.; Schwendeman, A.; Remaley, A. T., Apolipoprotein Mimetic Peptides for Stimulating Cholesterol Efflux. In *Apolipoprotein Mimetics in the Management of Human Disease*, Anantharamaiah, G. M.; Goldberg, D., Eds. Springer International Publishing: Cham, 2015; pp 29-42.

113. Miles, J., Single-dose tolerability, pharmacokinetics, and cholesterol mobilization in HDL-C fraction following intravenous administration of ETC-642, a 22-mer ApoA-I analogue and phospholipids complex, in atherosclerosis patients. *Arterioscler. Thromb. Vasc. Biol.* **2004,** *24* (5), E19.

114. Dayneka, N. L.; Garg, V.; Jusko, W. J., Comparison of four basic models of indirect pharmacodynamic responses. *J. Pharmacokinet. Biopharm.* **1993,** *21* (4), 457-478.

115. Garber, D. W.; Kulkarni, K. R.; Anantharamaiah, G. M., A sensitive and convenient method for lipoprotein profile analysis of individual mouse plasma samples. *J. Lipid Res.* **2000,** *41* (6), 1020-1026.

116. Freeman, L. A., Native–native 2D gel electrophoresis for HDL subpopulation analysis. *Lipoproteins and Cardiovascular Disease: Methods and Protocols* **2013**, 353-367.

117. Stoekenbroek, R.; Stroes, E.; Hovingh, G., ApoA-I mimetics. In *High Density Lipoproteins*, Springer: 2015; pp 631-648.

118. Subbaiah, P.; Liu, M., Role of sphingomyelin in the regulation of cholesterol esterification in the plasma lipoproteins. Inhibition of lecithin-cholesterol acyltransferase reaction. *J. Biol. Chem.* **1993,** *268* (27), 20156-20163.

119. Dasseux, J.-L.; Schwendeman, A. S.; Zhu, L., Apolipoprotein ai mimics. Google Patents: 2015; p EP2396017 A4.

120. Anderson, D. W.; Nichols, A. V.; Forte, T. M.; Lindgren, F. T., Particle distribution of human serum high density lipoproteins. *Biochim. Biophys. Acta* **1977,** *493* (1), 55-68.

121. Tamvakopoulos, C., Mass spectrometry for the quantification of bioactive peptides in biological fluids. *Mass Spectrom. Rev.* **2007,** *26* (3), 389-402.

122. Spady, D. K.; Woollett, L. A.; Meidell, R. S.; Hobbs, H. H., Kinetic characteristics and regulation of HDL cholesteryl ester and apolipoprotein transport in the apoA-I-/-mouse. *J. Lipid Res.* **1998,** *39* (7), 1483-1492.

123. Horowitz, B.; Goldberg, I.; Merab, J.; Vanni, T.; Ramakrishnan, R.; Ginsberg, H., Increased plasma and renal clearance of an exchangeable pool of apolipoprotein AI in subjects with low levels of high density lipoprotein cholesterol. *J. Clin. Invest.* **1993,** *91* (4), 1743.

124. Lu, S.-C.; Atangan, L.; Kim, K. W.; Chen, M. M.; Komorowski, R.; Chu, C.; Han, J.; Hu, S.; Gu, W.; Véniant, M., An apoA-I mimetic peptibody generates HDL-like particles and increases alpha-1 HDL subfraction in mice. *J. Lipid Res.* **2012,** *53* (4), 643-652.

125. Dasseux, J.-L.; Ackermann, R., Lipoprotein complexes and manufacturing and uses thereof. Google Patents: 2015; p US9187551 B2.

126. Kootte, R. S.; Smits, L. P.; van der Valk, F. M.; Dasseux, J.-L.; Keyserling, C. H.; Barbaras, R.; Paolini, J. F.; Santos, R. D.; van Dijk, T. H.; Dallinga-van Thie, G. M., Effect of open-label infusion of an apoA-I-containing particle (CER-001) on RCT and artery wall thickness in patients with FHA. *J. Lipid Res.* **2015,** *56* (3), 703-712.

127. Bisgaier, C. L.; Ackermann, R.; Rea, T.; Rodrigueza, W. V.; Hartman, D., ApoA-IMilano phospholipid complex (ETC-216) infusion in human volunteers. Insights into the phenotypic characteristics of ApoA-IMilano carriers. *Pharmacol. Res.* **2016,** *111*, 86-99.

128. Cuchel, M.; Lund-Katz, S.; de la Llera-Moya, M.; Millar, J. S.; Chang, D.; Fuki, I.; Rothblat, G. H.; Phillips, M. C.; Rader, D. J., Pathways by which reconstituted high-density lipoprotein mobilizes free cholesterol from whole body and from macrophages. *Arterioscler. Thromb. Vasc. Biol.* **2010,** *30* (3), 526-532.

129. Herzog, E.; Pragst, I.; Waelchli, M.; Gille, A.; Schenk, S.; Mueller‐Cohrs, J.; Diditchenko, S.; Zanoni, P.; Cuchel, M.; Seubert, A., Reconstituted high‐density lipoprotein can elevate plasma alanine aminotransferase by transient depletion of hepatic cholesterol: role of the phospholipid component. *J. Appl. Toxicol.* **2016,** *36*, 1038-1047.

130. Gille, A.; Easton, R.; D'Andrea, D.; Wright, S. D.; Shear, C. L., CSL112 enhances biomarkers of reverse cholesterol transport after single and multiple infusions in healthy subjects. *Arterioscler. Thromb. Vasc. Biol.* **2014,** *34* (9), 2106-2114.

131. Yancey, P. G.; Bielicki, J. K.; Johnson, W. J.; Lund-Katz, S.; Palgunachari, M. N.; Anantharamaiah, G.; Segrest, J. P.; Phillips, M. C.; Rothblat, G. H., Efflux of cellular cholesterol and phospholipid to lipid-free apolipoproteins and class A amphipathic peptides. *Biochemistry.* **1995,** *34* (24), 7955-7965.

132. Schwendeman, A.; Sviridov, D. O.; Yuan, W. M.; Guo, Y. H.; Morin, E. E.; Yuan, Y.; Stonik, J.; Freeman, L.; Ossoli, A.; Thacker, S.; Killion, S.; Pryor, M.; Chen, Y. E.; Turner, S.; Remaley, A. T., The effect of phospholipid composition of reconstituted HDL on its cholesterol efflux and anti-inflammatory properties. *J. Lipid Res.* **2015,** *56* (9), 1727-1737.

133. Di Bartolo, B. A.; Nicholls, S. J.; Bao, S.; Rye, K.-A.; Heather, A. K.; Barter, P. J.; Bursill, C., The apolipoprotein AI mimetic peptide ETC-642 exhibits anti-inflammatory properties that are comparable to high density lipoproteins. *Atherosclerosis.* **2011,** *217* (2), 395-400.

134. Iwata, A.; Miura, S.-i.; Zhang, B.; Imaizumi, S.; Uehara, Y.; Shiomi, M.; Saku, K., Antiatherogenic effects of newly developed apolipoprotein AI mimetic peptide/phospholipid complexes against aortic plaque burden in Watanabe-heritable hyperlipidemic rabbits. *Atherosclerosis.* **2011,** *218* (2), 300-307.

135. Heidenreich, P. A.; Trogdon, J. G.; Khavjou, O. A.; Butler, J.; Dracup, K.; Ezekowitz, M. D.; Finkelstein, E. A.; Hong, Y.; Johnston, S. C.; Khera, A.; Lloyd-Jones, D. M.; Nelson, S. A.; Nichol, G.; Orenstein, D.; Wilson, P. W.; Woo, Y. J., Forecasting The Future of Cardiovascular Disease in the United States: A Policy Statement From the American Heart Association. *Circulation* **2011,** *123* (8), 933-44.

136. Rosenson, R. S.; Brewer, H. B., Jr.; Ansell, B. J.; Barter, P.; Chapman, M. J.; Heinecke, J. W.; Kontush, A.; Tall, A. R.; Webb, N. R., Dysfunctional HDL and Atherosclerotic Cardiovascular Disease. *Nature reviews. Cardiology* **2015**.

137. Remaley, A. T.; Amar, M.; Sviridov, D., HDL-Replacement Therapy: Mechanism of Action, Types of Agents and Potential Clinical Indications. *Expert review of cardiovascular therapy* **2008,** *6* (9), 1203-15.

138. Iwata, A.; Miura, S.; Zhang, B.; Imaizumi, S.; Uehara, Y.; Shiomi, M.; Saku, K., Antiatherogenic effects of newly developed apolipoprotein A-I mimetic peptide/phospholipid complexes against aortic plaque burden in Watanabe-heritable hyperlipidemic rabbits. *Atherosclerosis* **2011,** *218* (2), 300-7.

139. Hafiane, A.; Genest, J., HDL, Atherosclerosis, and Emerging Therapies. *Cholesterol* **2013,** *2013*, 891403.

140. Darabi, M.; Guillas-Baudouin, I.; Le Goff, W.; Chapman, M. J.; Kontush, A., Therapeutic Applications of Reconstituted HDL: When Structure Meets Function. *Pharmacology & therapeutics* **2016,** *157*, 28-42.

141. Kuai, R.; Li, D.; Chen, Y. E.; Moon, J. J.; Schwendeman, A., High-Density Lipoproteins: Nature's Multifunctional Nanoparticles. *ACS Nano* **2016,** *10* (3), 3015-41.

142. Charlton-Menys, V.; Durrington, P. N., Human cholesterol metabolism and therapeutic molecules. *Experimental physiology* **2008,** *93* (1), 27-42.

143. Hovorka, R.; Nanjee, M. N.; Cooke, C. J.; Miller, I. P.; Olszewski, W. L.; Miller, N. E., Mass Kinetics of Apolipoprotein a-I in Interstitial Fluid after Administration of Intravenous Apolipoprotein a-I/Lecithin Discs in Humans. *Journal of lipid research* **2006,** *47* (5), 975-81.

144. Khan, M.; Lalwani, N.; Drake, S.; Crockatt, J.; Dasseux, J., Single-Dose Intravenous Infusion of ETC-642, a 22-Mer ApoA-I Analogue and Phospholipids Complex, Elevates HDL-C in Atherosclerosis Patients. *Circulation* **2003,** *108* (17), 563-564.

145. Zundorf, I.; Dingermann, T., PEGylation--a Well-Proven Strategy for the Improvement of Recombinant Drugs. *Die Pharmazie* **2014,** *69* (5), 323-6.

146. Weissig, V.; Pettinger, T. K.; Murdock, N., Nanopharmaceuticals (Part 1): Products on the Market. *International journal of nanomedicine* **2014,** *9*, 4357-73.

147. Murphy, A. J.; Funt, S.; Gorman, D.; Tall, A. R.; Wang, N., Pegylation of High-Density Lipoprotein Decreases Plasma Clearance and Enhances Antiatherogenic Activity. *Circulation research* **2013,** *113* (1), e1-9.

148. Suk, J. S.; Xu, Q.; Kim, N.; Hanes, J.; Ensign, L. M., PEGylation as a Strategy for Improving Nanoparticle-Based Drug and Gene Delivery. *Advanced drug delivery reviews* **2015**.

149. Miles, J.; Khan, M.; Painchaud, C.; Lalwani, N.; Drake, S.; Dasseux, J., Single-Dose Tolerability, Pharmacokinetics, and Cholesterol Mobilization in HDL-C Fraction Following Intravenous Administration of ETC-642, a 22-mer ApoA-I Analogue and Phospholipids Complex, in Atherosclerosis Patients. *Arterioscler Thromb Vasc Biol* **2004,** *24* (5), E19-E19.

150. Patel, S.; Drew, B. G.; Nakhla, S.; Duffy, S. J.; Murphy, A. J.; Barter, P. J.; Rye, K. A.; Chin-Dusting, J.; Hoang, A.; Sviridov, D.; Celermajer, D. S.; Kingwell, B. A., Reconstituted high-density lipoprotein increases plasma high-density lipoprotein anti-inflammatory properties and cholesterol efflux capacity in patients with type 2 diabetes. *J Am Coll Cardiol* **2009,** *53* (11), 962-71.

151. Garber, D. W.; Kulkarni, K. R.; Anantharamaiah, G. M., A Sensitive and Convenient Method for Lipoprotein Profile Analysis of Individual Mouse Plasma Samples. *Journal of lipid research* **2000,** *41* (6), 1020-6.

152. Tang, J.; Li, D.; Drake, L.; Yuan, W.; Deshaine, S.; Morin, E. E.; Ackermann, R.; Olsen, K.; Smith, D. E.; Schwendeman, A., Influence of Route of Administration and Lipidation of Apolipoprotein A-I Peptide on Pharmacokinetics and Cholesterol Mobilization. *Journal of lipid research* **2016**.

153. Didichenko, S. A.; Navdaev, A. V.; Cukier, A. M. O.; Gille, A.; Schuetz, P.; Spycher, M. O.; Therond, P.; Chapman, M. J.; Kontush, A.; Wright, S. D., Enhanced HDL Functionality in Small HDL Species Produced Upon Remodeling of HDL by Reconstituted HDL, CSL112: Effects on Cholesterol Efflux, Anti-Inflammatory and Antioxidative Activity. *Circulation research* **2016,** *119* (6), 751-763.

154. Heinecke, J. W., Small HDL Promotes Cholesterol Efflux by the ABCA1 Pathway in Macrophages: Implications for Therapies Targeted to HDL. *Circulation research* **2015,** *116* (7), 1101-3.

155. Ng, K. K.; Lovell, J. F.; Zheng, G., Lipoprotein-Inspired Nanoparticles for Cancer Theranostics. *Accounts of chemical research* **2011,** *44* (10), 1105-13.

156. Murphy, A. J.; Hoang, A.; Aprico, A.; Sviridov, D.; Chin-Dusting, J., Anti-Inflammatory Functions of Apolipoprotein A-I and High-Density Lipoprotein Are Preserved in Trimeric Apolipoprotein A-I. *The Journal of pharmacology and experimental therapeutics* **2013,** *344* (1), 41-9.

157. Lin, Q.; Chen, J.; Zhang, Z.; Zheng, G., Lipid-Based Nanoparticles in the Systemic Delivery of siRNA. *Nanomedicine* **2014,** *9* (1), 105-20.

158. Bisgaier, C. L.; Ackermann, R.; Rea, T.; Rodrigueza, W. V.; Hartman, D., ApoA-IMilano Phospholipid Complex (ETC-216) Infusion in Human Volunteers. Insights into the Phenotypic Characteristics of ApoA-IMilano Carriers. *Pharmacol Res* **2016,** *111*, 86-99.

159. Tricoci, P.; D'Andrea, D. M.; Gurbel, P. A.; Yao, Z. L.; Cuchel, M.; Winston, B.; Schott, R.; Weiss, R.; Blazing, M. A.; Cannon, L.; Bailey, A.; Angiolillo, D. J.; Gille, A.; Shear, C. L.; Wright, S. D.; Alexander, J. H., Infusion of Reconstituted High-Density Lipoprotein, CSL112, in Patients With Atherosclerosis: Safety and Pharmacokinetic Results From a Phase 2a Randomized Clinical Trial. *J Am Heart Assoc* **2015,** *4* (8).

160. Barbaras, R., Non-clinical development of CER-001. *Front Pharmacol* **2015,** *6*, 220.

161. Eyvazian, V. A.; Frishman, W. H., Evacetrapib: Another CETP Inhibitor for Dyslipidemia With No Clinical Benefit. *Cardiology in review* **2017,** *25* (2), 43-52.

162. Mullard, A., CETP inhibitors stumble on. *Nature reviews. Drug discovery* **2017,** *16* (10), 669.

163. CETP inhibitor class finally dies as Merck abandons anacetrapib. http://www.pmlive.com/pharma_news/cetp_inhibitor_class_finally_dies_as_merck_abandons_anacetrapib_1208239.

164. Kosmas, C. E.; DeJesus, E.; Rosario, D.; Vittorio, T. J., CETP Inhibition: Past Failures and Future Hopes. *Clin Med Insights Cardiol* **2016,** *10*, 37-42.

165. Learning lessons from Pfizer's $800 million failure. *Nature reviews. Drug discovery* **2011,** *10* (3), 163-4.

166. Filippatos, T. D.; Kei, A.; Elisaf, M. S., Anacetrapib, a New CETP Inhibitor: The New Tool for the Management of Dyslipidemias? *Diseases* **2017,** *5* (4).

167. Tall, A. R.; Rader, D. J., The Trials and Tribulations of CETP Inhibitors. *Circulation research* **2017**.

168. Bloedon, L. T.; Dunbar, R.; Duffy, D.; Pinell-Salles, P.; Norris, R.; DeGroot, B. J.; Movva, R.; Navab, M.; Fogelman, A. M.; Rader, D. J., Safety, Pharmacokinetics, and Pharmacodynamics of Oral ApoA-I Mimetic Peptide D-4F in High-risk Cardiovascular Patients. *Journal of lipid research* **2008,** *49* (6), 1344-52.

169. Nanjee, M. N.; Crouse, J. R.; King, J. M.; Hovorka, R.; Rees, S. E.; Carson, E. R.; Morgenthaler, J. J.; Lerch, P.; Miller, N. E., Effects of Intravenous Infusion of Lipid-free Apo A-I in Humans. *Arterioscler Thromb Vasc Biol* **1996,** *16* (9), 1203-14.

170. Watson, C. E.; Weissbach, N.; Kjems, L.; Ayalasomayajula, S.; Zhang, Y. M.; Chang, I.; Navab, M.; Hama, S.; Hough, G.; Reddy, S. T.; Soffer, D.; Rader, D. J.; Fogelman, A. M.; Schecter, A., Treatment of Patients with Cardiovascular Disease with L-4F, an Apo-A1 Mimetic, Did not Improve Select Biomarkers of HDL Function. *Journal of lipid research* **2011,** *52* (2), 361-373.

171. Van Lenten, B. J.; Wagner, A. C.; Jung, C. L.; Ruchala, P.; Waring, A. J.; Lehrer, R. I.; Watson, A. D.; Hama, S.; Navab, M.; Anantharamaiah, G. M.; Fogelman, A. M., Anti-inflammatory ApoA-I-Mimetic Peptides Bind Oxidized Lipids with Much Higher Affinity than Human ApoA-I *Journal of lipid research* **2008,** *49* (12), 2698-2698.

172. Getz, G. S.; Wool, G. D.; Reardon, C. A., Biological Properties of Apolipoprotein a-I Mimetic Peptides. *Curr Atheroscler Rep* **2010,** *12* (2), 96-104.

173. Navab, M.; Shechter, I.; Anantharamaiah, G. M.; Reddy, S. T.; Van Lenten, B. J.; Fogelman, A. M., Structure and Function of HDL Mimetics. *Arterioscler Thromb Vasc Biol* **2010,** *30* (2), 164-168.

174. Tabet, F.; Remaley, A. T.; Segaliny, A. I.; Millet, J.; Yan, L.; Nakhla, S.; Barter, P. J.; Rye, K. A.; Lambert, G., The 5A apolipoprotein A-I mimetic peptide displays antiinflammatory and antioxidant properties in vivo and in vitro. *Arterioscler Thromb Vasc Biol* **2010,** *30* (2), 246-52.

175. Van Lenten, B. J.; Wagner, A. C.; Anantharamaiah, G. M.; Navab, M.; Reddy, S. T.; Buga, G. M.; Fogelman, A. M., Apolipoprotein A-I mimetic peptides. *Curr Atheroscler Rep* **2009,** *11* (1), 52-7.

176. Liu, Y.; Hu, Y.; Huang, L., Influence of Polyethylene Glycol Density and Surface Lipid on Pharmacokinetics and Biodistribution of Lipid-Calcium-Phosphate Nanoparticles. *Biomaterials* **2014,** *35* (9), 3027-34.

177. Tang, J.; Kuai, R.; Yuan, W.; Drake, L.; Moon, J. J.; Schwendeman, A., Effect of Size and Pegylation of Liposomes and Peptide-Based Synthetic Lipoproteins on Tumor Targeting. In *AAPS 2016*, Denver, CO, 2016.

178. Zhang, Z.; Chen, J.; Ding, L.; Jin, H.; Lovell, J. F.; Corbin, I. R.; Cao, W.; Lo, P. C.; Yang, M.; Tsao, M. S.; Luo, Q.; Zheng, G., HDL-Mimicking Peptide-Lipid Nanoparticles with Improved Tumor Targeting. *Small* **2010,** *6* (3), 430-7.

179. Keyserling, C. H.; Hunt, T. L.; Klepp, H. M.; Scott, R. A.; Barbaras, R.; Schwendeman, A.; Lalwani, N.; Dasseux, J.-L., Abstract 15525: CER-001, a Synthetic HDL-Mimetic, Safely Mobilizes Cholesterol in Healthy Dyslipidemic Volunteers. *Circulation* **2011,** *124* (Suppl 21), A15525-A15525.

180. Agassandian, M.; Mallampalli, R. K., Surfactant Phospholipid Metabolism. *Biochimica et biophysica acta* **2013,** *1831* (3), 612-25.

181. Graversen, J. H.; Laurberg, J. M.; Andersen, M. H.; Falk, E.; Nieland, J.; Christensen, J.; Etzerodt, M.; Thogersen, H. C.; Moestrup, S. K., Trimerization of Apolipoprotein A-I Retards Plasma Clearance and Preserves Antiatherosclerotic Properties. *Journal of cardiovascular pharmacology* **2008,** *51* (2), 170-7.

182. Ohnsorg, P. M.; Mary, J. L.; Rohrer, L.; Pech, M.; Fingerle, J.; von Eckardstein, A., Trimerized Apolipoprotein A-I (TripA) Forms Lipoproteins, Activates Lecithin:Cholesterol Acyltransferase, Elicits Lipid Efflux, and Is Transported Through Aortic endothelial Cells. *Bba-Mol Cell Biol L* **2011,** *1811* (12), 1115-1123.

183. Zhao, Y.; Imura, T.; Leman, L. J.; Curtiss, L. K.; Maryanoff, B. E.; Ghadiri, M. R., Mimicry of High-Density Lipoprotein: Functional Peptide-Lipid Nanoparticles Based on Multivalent Peptide Constructs. *Journal of the American Chemical Society* **2013,** *135* (36), 13414-24.

184. Sviridov, D. O.; Ikpot, I. Z.; Stonik, J.; Drake, S. K.; Amar, M.; Osei-Hwedieh, D. O.; Piszczek, G.; Turner, S.; Remaley, A. T., Helix Stabilization of Amphipathic Peptides by Hydrocarbon Stapling Increases Cholesterol Efflux by the Abca1 Transporter. *Biochemical and biophysical research communications* **2011,** *410* (3), 446-51.

185. Gessner, A.; Lieske, A.; Paulke, B. R.; Muller, R. H., Functional Groups on Polystyrene Model Nanoparticles: Influence on Protein Adsorption. *J Biomed Mater Res A* **2003,** *65A* (3), 319-326.

186. Lundqvist, M.; Stigler, J.; Elia, G.; Lynch, I.; Cedervall, T.; Dawson, K. A., Nanoparticle Size and Surface Properties Determine the Protein Corona with Possible Implications for Biological Impacts. *Proceedings of the National Academy of Sciences of the United States of America* **2008,** *105* (38), 14265-70.

187. Tenzer, S.; Docter, D.; Kuharev, J.; Musyanovych, A.; Fetz, V.; Hecht, R.; Schlenk, F.; Fischer, D.; Kiouptsi, K.; Reinhardt, C.; Landfester, K.; Schild, H.; Maskos, M.; Knauer, S. K.; Stauber, R. H., Rapid Formation of Plasma Protein Corona Critically Affects Nanoparticle Pathophysiology. *Nat Nanotechnol* **2013,** *8* (10), 772-U1000.

188. Cedervall, T.; Lynch, I.; Foy, M.; Berggard, T.; Donnelly, S. C.; Cagney, G.; Linse, S.; Dawson, K. A., Detailed Identification of Plasma Proteins Adsorbed on Copolymer Nanoparticles. *Angewandte Chemie* **2007,** *46* (30), 5754-6.

189. Aggarwal, P.; Hall, J. B.; McLeland, C. B.; Dobrovolskaia, M. A.; McNeil, S. E., Nanoparticle Interaction with Plasma Proteins as It Relates to Particle Biodistribution,

Biocompatibility and Therapeutic Efficacy. *Advanced drug delivery reviews* **2009,** *61* (6), 428-437.

190. Corbo, C.; Molinaro, R.; Parodi, A.; Toledano Furman, N. E.; Salvatore, F.; Tasciotti, E., The Impact of Nanoparticle Protein Corona on Cytotoxicity, Immunotoxicity and Target Drug Delivery. *Nanomedicine* **2016,** *11* (1), 81-100.

191. Moore, K. J.; Sheedy, F. J.; Fisher, E. A., Macrophages in atherosclerosis: a dynamic balance. *Nat Rev Immunol* **2013,** *13* (10), 709-21.

192. van der Wal, A. C.; Becker, A. E., Atherosclerotic plaque rupture--pathologic basis of plaque stability and instability. *Cardiovasc Res* **1999,** *41* (2), 334-44.

193. Ibanez, B.; Vilahur, G.; Badimon, J. J., Plaque progression and regression in atherothrombosis. *J Thromb Haemost* **2007,** *5 Suppl 1*, 292-9.

194. Jamkhande, P. G.; Chandak, P. G.; Dhawale, S. C.; Barde, S. R.; Tidke, P. S.; Sakhare, R. S., Therapeutic approaches to drug targets in atherosclerosis. *Saudi Pharm J* **2014,** *22* (3), 179-90.

195. Bittencourt, M. S.; Cerci, R. J., Statin effects on atherosclerotic plaques: regression or healing? *BMC Med* **2015,** *13*, 260.

196. Rockberg, J.; Jorgensen, L.; Taylor, B.; Sobocki, P.; Johansson, G., Risk of mortality and recurrent cardiovascular events in patients with acute coronary syndromes on high intensity statin treatment. *Prev Med Rep* **2017,** *6*, 203-209.

197. van der Heijden, A. A.; Van't Riet, E.; Bot, S. D.; Cannegieter, S. C.; Stehouwer, C. D.; Baan, C. A.; Dekker, J. M.; Nijpels, G., Risk of a recurrent cardiovascular event in individuals with type 2 diabetes or intermediate hyperglycemia: the Hoorn Study. *Diabetes Care* **2013,** *36* (11), 3498-502.

198. Lewis, G. F.; Rader, D. J., New insights into the regulation of HDL metabolism and reverse cholesterol transport. *Circulation Research* **2005,** *96* (12), 1221-1232.

199. Phillips, M. C., Molecular mechanisms of cellular cholesterol efflux. *J Biol Chem* **2014,** *289* (35), 24020-9.

200. Hutchins, P. M.; Heinecke, J. W., Cholesterol efflux capacity, macrophage reverse cholesterol transport and cardioprotective HDL. *Curr Opin Lipidol* **2015,** *26* (5), 388-93.

201. Gille, A.; D'Andrea, D.; Tortorici, M. A.; Hartel, G.; Wright, S. D., CSL112 (Apolipoprotein A-I [Human]) Enhances Cholesterol Efflux Similarly in Healthy Individuals and Stable Atherosclerotic Disease Patients. *Arterioscler Thromb Vasc Biol* **2018,** *38* (4), 953-963.

202. Tardif, J. C.; Ballantyne, C. M.; Barter, P.; Dasseux, J. L.; Fayad, Z. A.; Guertin, M. C.; Kastelein, J. J.; Keyserling, C.; Klepp, H.; Koenig, W.; L'Allier, P. L.; Lesperance, J.; Luscher, T. F.; Paolini, J. F.; Tawakol, A.; Waters, D. D.; Can, H. D. L. I. S. Q. A. R. I., Effects of the high-density lipoprotein mimetic agent CER-001 on coronary atherosclerosis in patients with acute coronary syndromes: a randomized trial. *Eur Heart J* **2014,** *35* (46), 3277-86.

203. CSL Behring Announces First Patient Enrollment in Phase 3 Clinical Trial of CSL112 to Assess Reduction of Early Recurrent Cardiovascular Events in Heart Attack Survivors. https://www.cslbehring.com/vita/newsroom/20180322-csl112-phase3.

204. CSL Confirms Phase 3 Clinical Trial of New Therapy for Heart Attack Survivors. **2017**.

205. Kotov, N. A., Inorganic Nanoparticles as Protein Mimics. *Science* **2010,** *330* (6001), 188-189.

206. Khan, M.; Lalwani, N. D.; Drake, S. L.; Crockatt, J. G.; Dasseux, J. L. H., Single-dose intravenous infusion of ETC-642, a 22-mer ApoA-I analogue and phospholipids complex, elevates HDL-C in atherosclerosis patients. *Circulation* **2003,** *108* (17), 563-564.

207. Miles, J.; Khan, M.; Painchaud, C.; Lalwani, N.; Drake, S.; Dasseux, J. L., Single-dose tolerability, pharmacokinetics, and cholesterol mobilization in HDL-C fraction following intravenous administration of ETC-642, a 22-mer ApoA-I analogue and phospholipids complex, in atherosclerosis patients. *Arterioscl Throm Vas* **2004,** *24* (5), E19-E19.

208. Tang, J.; Li, D.; Drake, L.; Yuan, W.; Deschaine, S.; Morin, E. E.; Ackermann, R.; Olsen, K.; Smith, D. E.; Schwendeman, A., Influence of route of administration and lipidation of apolipoprotein A-I peptide on pharmacokinetics and cholesterol mobilization. *J Lipid Res* **2017,** *58* (1), 124-136.

209. Tessaro, F. H. G.; Ayala, T. S.; Nolasco, E. L.; Bella, L. M.; Martins, J. O., Insulin Influences LPS-Induced TNF-alpha and IL-6 Release Through Distinct Pathways in Mouse Macrophages from Different Compartments. *Cellular physiology and biochemistry : international journal of experimental cellular physiology, biochemistry, and pharmacology* **2017,** *42* (5), 2093-2104.

210. Wang, S. H.; Yuan, S. G.; Peng, D. Q.; Zhao, S. P., High-density lipoprotein affects antigen presentation by interfering with lipid raft: a promising anti-atherogenic strategy. *Clin Exp Immunol* **2010,** *160* (2), 137-42.

211. Kudgus, R. A.; Walden, C. A.; McGovern, R. M.; Reid, J. M.; Robertson, J. D.; Mukherjee, P., Tuning Pharmacokinetics and Biodistribution of a Targeted Drug Delivery System Through Incorporation of a Passive Targeting Component. *Scientific reports* **2014,** *4*.

212. Li, Q.; Park, K.; Xia, Y.; Matsumoto, M.; Qi, W.; Fu, J.; Yokomizo, H.; Khamaisi, M.; Wang, X.; Rask-Madsen, C.; King, G. L., Regulation of Macrophage Apoptosis and Atherosclerosis by Lipid-Induced PKCdelta Isoform Activation. *Circ Res* **2017,** *121* (10), 1153-1167.

213. Menu, P.; Pellegrin, M.; Aubert, J. F.; Bouzourene, K.; Tardivel, A.; Mazzolai, L.; Tschopp, J., Atherosclerosis in ApoE-deficient mice progresses independently of the NLRP3 inflammasome. *Cell Death Dis* **2011,** *2*, e137.

214. Ye, D.; Zhao, Y.; Hildebrand, R. B.; Singaraja, R. R.; Hayden, M. R.; Van Berkel, T. J. C.; Van Eck, M., The Dynamics of Macrophage Infiltration into the Arterial Wall during Atherosclerotic Lesion Development in Low-Density Lipoprotein Receptor Knockout Mice. *Am J Pathol* **2011,** *178* (1), 413-422.

215. Jean-Louis Dasseux, A. S. S., Lingyu Zhu Apolipoprotein A-I mimics. US8378068 B2, Feb 19, 2013, 2013.

216. Tall, A. R.; Rader, D. J., Trials and Tribulations of CETP Inhibitors. *Circ Res* **2018,** *122* (1), 106-112.

217. Nissen, S. E.; Tsunoda, T.; Tuzcu, E. M.; Schoenhagen, P.; Cooper, C. J.; Yasin, M.; Eaton, G. M.; Lauer, M. A.; Sheldon, W. S.; Grines, C. L.; Halpern, S.; Crowe, T.; Blankenship, J. C.;

Kerensky, R., Effect of recombinant ApoA-I Milano on coronary atherosclerosis in patients with acute coronary syndromes - A randomized controlled trial. *Jama-J Am Med Assoc* **2003,** *290* (17), 2292-2300.

218. Tardif, J. C.; Gregoire, J.; L'Allier, P. L.; Ibrahim, R.; Lesperance, J.; Heinonen, T. M.; Kouz, S.; Berry, C.; Basser, R.; Lavoie, M. A.; Guertin, M. C.; Rodes-Cabau, J., Effects of reconstituted high-density lipoprotein infusions on coronary atherosclerosis - A randomized controlled trial. *Jama-J Am Med Assoc* **2007,** *297* (15), 1675-1682.

219. Honda, S.; Kataoka, Y.; Kanaya, T.; Noguchi, T.; Ogawa, H.; Yasuda, S., Characterization of coronary atherosclerosis by intravascular imaging modalities. *Cardiovasc Diagn Ther* **2016,** *6* (4), 368-81.

220. McMahon, M.; Grossman, J.; FitzGerald, J.; Dahlin-Lee, E.; Wallace, D. J.; Thong, B. Y.; Badsha, H.; Kalunian, K.; Charles, C.; Navab, M.; Fogelman, A. M.; Hahn, B. H., Proinflammatory high-density lipoprotein as a biomarker for atherosclerosis in patients with systemic lupus erythematosus and rheumatoid arthritis. *Arthritis Rheum* **2006,** *54* (8), 2541-2549.

221. Wu, B. J.; Ong, K. L.; Shrestha, S.; Chen, K.; Tabet, F.; Barter, P. J.; Rye, K. A., Inhibition of Arthritis in the Lewis Rat by Apolipoprotein A-I and Reconstituted High-Density Lipoproteins. *Arterioscl Throm Vas* **2014,** *34* (3), 543-551.

222. Dellinger, R. P.; Tomayko, J. F.; Angus, D. C.; Opal, S.; Cupo, M. A.; McDermott, S.; Ducher, A.; Calandra, T.; Cohen, J.; Lipid, I.; Patient Outcomes in Sepsis, I., Efficacy and safety of a phospholipid emulsion (GR270773) in Gram-negative severe sepsis: results of a phase II multicenter, randomized, placebo-controlled, dose-finding clinical trial. *Crit Care Med* **2009,** *37* (11), 2929-38.

223. Doggrell, S. A., ETC-588 (Pfizer). *Curr Opin Investig Drugs* **2004,** *5* (9), 993-9.

224. Cave, G.; Harvey, M., Intravenous Lipid Emulsion as Antidote Beyond Local Anesthetic Toxicity: A Systematic Review. *Acad Emerg Med* **2009,** *16* (9), 815-824.

225. Cave, G.; Harvey, M.; Willers, J.; Uncles, D.; Meek, T.; Picard, J.; Weinberg, G., LIPAEMIC Report: Results of Clinical Use of Intravenous Lipid Emulsion in Drug Toxicity Reported to an Online Lipid Registry. *Journal of Medical Toxicology* **2014,** *10* (2), 133-142.

226. Tricoci, P.; D'Andrea, D. M.; Gurbel, P. A.; Yao, Z.; Cuchel, M.; Winston, B.; Schott, R.; Weiss, R.; Blazing, M. A.; Cannon, L.; Bailey, A.; Angiolillo, D. J.; Gille, A.; Shear, C. L.; Wright, S. D.; Alexander, J. H., Infusion of Reconstituted High-Density Lipoprotein, CSL112, in Patients With Atherosclerosis: Safety and Pharmacokinetic Results From a Phase 2a Randomized Clinical Trial. *J Am Heart Assoc* **2015,** *4* (8), e002171.

227. Bondy, M. L.; Scheurer, M. E.; Malmer, B.; Barnholtz-Sloan, J. S.; Davis, F. G.; Il'yasova, D.; Kruchko, C.; McCarthy, B. J.; Rajaraman, P.; Schwartzbaum, J. A.; Sadetzki, S.; Schlehofer, B.; Tihan, T.; Wiemels, J. L.; Wrensch, M.; Buffler, P. A.; Brain Tumor Epidemiology, C., Brain tumor epidemiology: consensus from the Brain Tumor Epidemiology Consortium. *Cancer* **2008,** *113* (7 Suppl), 1953-68.

228. Kalepu, S.; Nekkanti, V., Insoluble drug delivery strategies: review of recent advances and business prospects. *Acta Pharm Sin B* **2015,** *5* (5), 442-53.

229. Carpentier, A. F.; Auf, G.; Delattre, J. Y., CpG-oligonucleotides for cancer immunotherapy : review of the literature and potential applications in malignant glioma. *Front Biosci* **2003,** *8*, e115-27.

230. Fan, H.; Zhang, I.; Chen, X.; Zhang, L.; Wang, H.; Da Fonseca, A.; Manuel, E. R.; Diamond, D. J.; Raubitschek, A.; Badie, B., Intracerebral CpG immunotherapy with carbon nanotubes abrogates growth of subcutaneous melanomas in mice. *Clin Cancer Res* **2012,** *18* (20), 5628-38.

231. Lollo, G.; Vincent, M.; Ullio-Gamboa, G.; Lemaire, L.; Franconi, F.; Couez, D.; Benoit, J. P., Development of multifunctional lipid nanocapsules for the co-delivery of paclitaxel and CpG-ODN in the treatment of glioblastoma. *Int J Pharm* **2015,** *495* (2), 972-80.

232. Zhao, D.; Alizadeh, D.; Zhang, L.; Liu, W.; Farrukh, O.; Manuel, E.; Diamond, D. J.; Badie, B., Carbon nanotubes enhance CpG uptake and potentiate antiglioma immunity. *Clin Cancer Res* **2011,** *17* (4), 771-82.

233. Parrish, K. E.; Sarkaria, J. N.; Elmquist, W. F., Improving drug delivery to primary and metastatic brain tumors: strategies to overcome the blood-brain barrier. *Clin Pharmacol Ther* **2015,** *97* (4), 336-46.

234. van Tellingen, O.; Yetkin-Arik, B.; de Gooijer, M. C.; Wesseling, P.; Wurdinger, T.; de Vries, H. E., Overcoming the blood-brain tumor barrier for effective glioblastoma treatment. *Drug resistance updates : reviews and commentaries in antimicrobial and anticancer chemotherapy* **2015,** *19*, 1-12.

235. Zhang, F.; Xu, C. L.; Liu, C. M., Drug delivery strategies to enhance the permeability of the blood-brain barrier for treatment of glioma. *Drug Des Devel Ther* **2015,** *9*, 2089-2100.

236. Weiss, H. M.; Fresneau, M.; Moenius, T.; Stuetz, A.; Billich, A., Binding of pimecrolimus and tacrolimus to skin and plasma proteins: implications for systemic exposure after topical application. *Drug Metab Dispos* **2008,** *36* (9), 1812-8.

237. Sykes, E.; Woodburn, K.; Decker, D.; Kessel, D., Effects of Cremophor EL on distribution of Taxol to serum lipoproteins. *Br J Cancer* **1994,** *70* (3), 401-4.

238. Lin, Q. Y.; Chen, J.; Ng, K. K.; Cao, W. G.; Zhang, Z. H.; Zheng, G., Imaging the Cytosolic Drug Delivery Mechanism of HDL-Like Nanoparticles. *Pharmaceutical Research* **2014,** *31* (6), 1438-1449.

239. Mooberry, L. K.; Nair, M.; Paranjape, S.; McConathy, W. J.; Lacko, A. G., Receptor mediated uptake of paclitaxel from a synthetic high density lipoprotein nanocarrier. *Journal of Drug Targeting* **2010,** *18* (1), 53-58.

240. Glickson, J. D.; Lund-Katz, S.; Zhou, R.; Choi, H.; Chen, I. W.; Li, H.; Corbin, I.; Popov, A. V.; Cao, W.; Song, L.; Qi, C.; Marotta, D.; Nelson, D. S.; Chen, J.; Chance, B.; Zheng, G., Lipoprotein nanoplatform for targeted delivery of diagnostic and therapeutic agents. *Molecular Imaging* **2008,** *7* (2), 101-110.

241. Yuan, Y.; Wen, J.; Tang, J.; Kan, Q.; Ackermann, R.; Olsen, K.; Schwendeman, A., Synthetic high-density lipoproteins for delivery of 10-hydroxycamptothecin. *Int J Nanomedicine* **2016,** *11*, 6229-6238.

242. Banks, W. A., From blood-brain barrier to blood-brain interface: new opportunities for CNS drug delivery. *Nat Rev Drug Discov* **2016,** *15* (4), 275-92.

243. Balazs, Z.; Panzenboeck, U.; Hammer, A.; Sovic, A.; Quehenberger, O.; Malle, E.; Sattler, W., Uptake and transport of high-density lipoprotein (HDL) and HDL-associated alpha-tocopherol by an in vitro blood-brain barrier model. *Journal of neurochemistry* **2004,** *89* (4), 939-50.

244. Huang, J. L.; Jiang, G.; Song, Q. X.; Gu, X.; Hu, M.; Wang, X. L.; Song, H. H.; Chen, L. P.; Lin, Y. Y.; Jiang, D.; Chen, J.; Feng, J. F.; Qiu, Y. M.; Jiang, J. Y.; Jiang, X. G.; Chen, H. Z.; Gao, X. L., Lipoprotein-biomimetic nanostructure enables efficient targeting delivery of siRNA to Ras-activated glioblastoma cells via macropinocytosis. *Nat Commun* **2017,** *8*, 15144.

245. Song, Q.; Huang, M.; Yao, L.; Wang, X.; Gu, X.; Chen, J.; Chen, J.; Huang, J.; Hu, Q.; Kang, T.; Rong, Z.; Qi, H.; Zheng, G.; Chen, H.; Gao, X., Lipoprotein-based nanoparticles rescue the memory loss of mice with Alzheimer's disease by accelerating the clearance of amyloid-beta. *ACS Nano* **2014,** *8* (3), 2345-59.

246. Chen, Y.; Liu, L., Modern methods for delivery of drugs across the blood-brain barrier. *Adv Drug Deliv Rev* **2012,** *64* (7), 640-65.

247. Guo, Y.; Yuan, W.; Yu, B.; Kuai, R.; Hu, W.; Morin, E. E.; Garcia-Barrio, M. T.; Zhang, J.; Moon, J. J.; Schwendeman, A.; Eugene Chen, Y., Synthetic High-Density Lipoprotein-Mediated Targeted Delivery of Liver X Receptors Agonist Promotes Atherosclerosis Regression. *EBioMedicine* **2018,** *28*, 225-233.

248. Appelt-Menzel, A.; Cubukova, A.; Gunther, K.; Edenhofer, F.; Piontek, J.; Krause, G.; Stuber, T.; Walles, H.; Neuhaus, W.; Metzger, M., Establishment of a Human Blood-Brain Barrier Co-culture Model Mimicking the Neurovascular Unit Using Induced Pluri- and Multipotent Stem Cells. *Stem Cell Reports* **2017,** *8* (4), 894-906.

249. Cui, L.; Lin, Q.; Jin, C. S.; Jiang, W.; Huang, H.; Ding, L.; Muhanna, N.; Irish, J. C.; Wang, F.; Chen, J.; Zheng, G., A PEGylation-Free Biomimetic Porphyrin Nanoplatform for Personalized Cancer Theranostics. *ACS Nano* **2015,** *9* (4), 4484-95.

250. Tang, J.; Kuai, R.; Yuan, W.; Drake, L.; Moon, J. J.; Schwendeman, A., Effect of size and pegylation of liposomes and peptide-based synthetic lipoproteins on tumor targeting. *Nanomedicine* **2017,** *13* (6), 1869-1878.

251. Manatunga, D. C.; de Silva, R. M.; de Silva, K. M. N.; Malavige, G. N.; Wijeratne, D. T.; Williams, G. R.; Jayasinghe, C. D.; Udagama, P. V., Effective delivery of hydrophobic drugs to breast and liver cancer cells using a hybrid inorganic nanocarrier: A detailed investigation using cytotoxicity assays, fluorescence imaging and flow cytometry. *Eur J Pharm Biopharm* **2018,** *128*, 18-26.

252. Manatunga, D. C.; de Silva, R. M.; de Silva, K. M. N.; de Silva, N.; Bhandari, S.; Yap, Y. K.; Costha, N. P., pH responsive controlled release of anti-cancer hydrophobic drugs from sodium alginate and hydroxyapatite bi-coated iron oxide nanoparticles. *Eur J Pharm Biopharm* **2017,** *117*, 29-38.